EFFECT OF DEFECTS AND TEMPERATURE ON THE MECHANICAL AND ELECTRONIC PROPERTIES OF NbC AND NbN: A FIRST-PRINCIPLES STUDY

PERPETUA WANJIRU MUCHIRI

B.Sc. (UoE)

SPPU/04244P/2019

A Thesis Submitted in Partial Fulfillment of the Requirements for the Award of the Degree of Master of Science in Physics

in

School of Physics and Earth Sciences

of

The Technical University of Kenya

(2023)

DECLARATION

This thesis is my original work and has not been presented in any other institution for a degree award or other qualification.

Signature:.....Date .....

PERPETUA WANJIRU MUCHIRI

SPPU/04244P/2019

Declaration by Supervisors

This thesis has been submitted with our approval as supervisors:

Signature.....Date.....

DR. MICHAEL ATAMBO

DEPARTMENT OF TECHNICAL AND APPLIED PHYSICS

THE TECHNICAL UNIVERSITY OF KENYA

NAIROBI, KENYA

Signature.....Date.....

DR. KORIR KIPTIEMOI

DEPARTMENT OF MATHEMATICS, PHYSICS & COMPUTING

MOI UNIVERSITY

ELDORET, KENYA

Signature.....Date.....

DR. NICHOLAS W. MAKAU

DEPARTMENT OF PHYSICS

UNIVERSITY OF ELDORET

ELDORET, KENYA

DEDICATION

I dedicate this work to my lovely family for their support in my academic journey and my daughter Patricia Murugi

ACKNOWLEDGEMENT

I wish to express my heartfelt appreciation to my supervisors, Dr. M. O. Atambo, Dr. N. W. Makau and Dr. K. K Korir as well as my mentor Prof. G. O. Amolo for their endless support as well as their time that has made the work to be how it is. I feel sincere gratitude to them for offering fully excellent professional guidance to me during the research period. I also wish to appreciate the entire staff of the Department of Technical and Applied Physics, Technical University of Kenya for their support which promoted a friendly environment for my research. Many thanks to members of Computational Material Science group for your ideas that helped me shape the discussion in my write-up. Thanks to Dr. M. Chepkoech, C. Bakasa, J. Sifuna, Dr. P. Egbele among others. I really appreciate your support. Above all I thank Almighty God for life and good health during my study comprising the research time. Special thanks to my family for being there for me always. I also wish to thank the CHPC lengau cluster in South Africa for provision of computing resources. May God bless all who made contributions towards the success of this study. Infrastructural assistance from the Technical University of Kenya is also acknowledged and appreciated.

TABLE OF CONTENTS

LIST OF TABLES

LIST OF FIGURES

LIST OF ABBREVIATIONS AND ACRONYMS

B_0	Bulk modulus
BO	Born-Oppenheimer
BZ	Brillouin Zone
DFT	Density Functional Theory
E	Energy
Ecut	Kinetic energy cut-off of the plane wave
Ecutrho	Charge density cut-off of the plane wave
EOS	Equation of State
GGA	Generalized Gradient Approximation
GPa	Giga Pascal
LDA	Local Density Approximation
MD	Molecular dynamics
MEP	Minimum energy path
N	Number of particles
NbC	Niobium Carbide
NbN	Niobium Nitride
NEB	Nudged Elastic Band
PAW	Projector augmented waves
PBE	Perdew Burke and Ernzerhof
PW	plane wave
PWscf	Plane wave self-consistent field
QE	opEn Source Package for Research in Electronic Structure, Simulation and Optimization.
RS	Rocksalt
T	Temperature
TMCNs	Transition metal carbides and nitrides
V	Volume
VASP	Vienna Ab-*initio* Simulation Package
V_{ex}	Exchange-correlation potential
WZ	Wurzite
ZB	Zinc blende

DEFINITIONS OF TERMS USED

Brillouin zone is the Wigner-Seitz cell of the reciprocal lattice.

Bulk modulus It is a measure of the resistance of a system to uniform compression whereby the hydrostatic pressure is expected to result into reduction of volume.

Exchange correlation expresses the interaction occurring between electrons in a system.

Functional it is a function expressed in terms of another function.

Hardness It is the resistance of a material to either indentation or scratch by another material.

Lattice parameter gives the dimensions of a unit cell.

Phonons A phonon is a quanta of lattice vibration.

Pseudo-potentials this is a weak potential compared to the true potential that mimics the strong Coulomb potential as well as core electrons which play minimal role in determining the properties of a given system.

Shear modulus this gives the resistance to change in shape when shear stress is applied on a material during twisting and other related processes.

Superhard materials have values of hardness that surpasses 40 GPa upon Vickers hardness examination. Their bulk modulus is also more than 350 GPa.

ABSTRACT

Transition metal carbides and nitrides (TMCNs) are materials that have attracted a lot of attention for both theoretical and experimental studies. This is largely attributed to their excellent physical and electronic properties that makes them ideal candidates for technological and industrial applications. This study focuses on the structural, mechanical and electronic properties of Niobium carbide (NbC) and Niobium Nitride (NbN). Also, owing to their fascinating properties, this study investigated the effects of defects and temperature on the mechanical properties of NbC and NbN from first-principles. The study also investigated the effects of defects on the properties of the two materials with concentration ranging between (1.56% − 12.5%) and temperature ranging between 300 K – 1500 K. This is crucial since there exist no perfect materials in nature and the materials are used under extreme conditions such as high temperatures and high pressure. The calculations are performed on the rocksalt (RS), zinc blende (ZB) and wurzite (WZ) structures of the two compounds through the density functional theory formalism using generalized gradient functional approximation for the exchange correlation potential. The obtained results show that the pristine NbC and NbN have high values of elastic constants and mechanical properties in the range of 71 GPa – 815 GPa. The values of the mechanical properties among them bulk moduli, shear moduli, Vicker's hardness as well as Young's modulus decrease with increasing defect concentration (1.56 % - 12.5 %) and temperature (300 K - 1500 K). The results obtained show that defect concentration of up to 12.5 % does not compromise the structural properties of the materials and hence, they can still be used in various industrial applications. Further, the temperature range of 300 K – 1500 K considered show that the materials are still mechanically stable and can be suitable candidates in harsh environments of high temperature. Consequently, control of defects and temperature especially during synthesis of these materials is important in evaluating their mechanical response that can drive them to be ideal for super-hard and other related applications.

CHAPTER ONE
INTRODUCTION

1.1 BACKGROUND OF THE STUDY

One of the noble driving force behind theoretical modelling in the 21st century is the need to develop novel materials with excellent properties. Many researchers aim to design materials which suit specific industrial and technological applications, Matthias (1953), Wang et al. (1999), Benkahoul et al. (2004), Jhi et al. (1999). This dream has been realised by use of first principles calculations whereby key laws of Physics are applied to determine the properties of materials, Yuji (2014). The electronic structure calculations are used to predict the properties of materials since electrons are used as the building blocks of a crystal. Also, the exponential development in computer technology has significantly accelerated the studies as the research can be done faster and accurately. The predictions made by first principles calculations have become more useful especially with the backing up of experimental analysis.

1.1.1 Traditional hard materials

Currently, machining as well as cutting industries have witnessed some technological developments which require wear resistant tools that can be used for cutting, drilling and polishing surfaces, Upadhyaya (1996). These developments have emerged to replace the traditionally used hard materials which include diamond and cubic boron nitride, Zhang et al. (2014). For instance, diamond is used in abrasive tools as a result of its fascinating properties among them high heat conductivity, high electron and holes mobility together with high hardness, Kurakevych (2009). The high values of hardness are some of the properties of these materials treated as a fundamental mechanical aspects of different materials. At a macroscopic level, hardness defines the ability of materials resisting indentation by another material or a scratch. Both diamond and cubic boron nitride are termed as superhard materials with their hardness exceeding 40 Giga Pascal when tested using Vickers hardness test, Tian & Zhao (2012). According to the Vicker's hardness test, diamond and cubic boron nitride have hardness of 115 GPa and 62 GPa, respectively.

Other materials used in the hard metal industry even though with lower values of hardness include silicon carbide (31 GPa), Šimůnek & Vackář (2006) and tungsten carbide (24 GPa). The hardness of these materials is as a result of both strong directional as well as covalent bonds present in their crystal structures of materials. These are largely responsible for the resistance to compression and bending of the bonds. These type of materials are known as intrinsic superhard materials, Veprek (1999). On the other hand, the extrinsic superhard materials have micro-structure responsible for their hardness which hinder both creation together with movement of dislocations, for example, carbon nanorods, Dubrovinskaia et al. (2005).

1.1.2 Hardness

In order for any material to be suitable in any industrial application, a variety of its properties have to be investigated thoroughly. One of these characteristics which is of great importance is its hardness. For a material to be considered hard, it has to be resistant to any form of local deformations which may be dependent on pressure, temperature together with extended defects such as dislocation. The deformation can be demonstrated by exposing the material under consideration to some physical activities which need application of force such as cutting, scratching, twisting and bending. Hardness is an important mechanical property in the hard metal industry, Smith and Sandly (1922). It can be investigated through several processes. One of the oldest methods is Mohs Hardness which was developed in 1812 by a German mineralogist Friedrich Mohs, Staples (1964). The property was investigated by observing if a material would be scratched by another, Tabor (1954). The Brinell Hardness Test is also used. For this case, a desktop machine is used in the application of definite load to a selected hardened sphere with a specific diameter, Hill et al. (1989). Another hardness test is the Rockwell method. Here, machine is used to apply a load with specified magnitude and then the depth of indentation is recorded. For this to be realized, an indenter is used which would be a steel ball with known diameter. Alternatively, a diamond-tipped cone which is spherical in shape of 0.2mm tip radius, Hill et al. (1989) can be used. In addition to these, the Vickers and Knoop Micro-hardness tests are also used to measure

hardness. A small square diamond pyramid is used as the indenter as it is pressed into a material under load, although this is prone to crack brittle materials, Smith and Sandly (1922). However, there are theoretical methods that are appropriate when determining the hardness and strength of a material. They include bulk moduli, shear moduli as well as the elastic constants. The first method has already been performed in a previous study by Korir et al. (2011) involving the 4d transition metal carbides and nitrides. The bulk moduli generally illustrates the opposition to the variation of volume for a given material. Similarly, the shear modulus shows the resistance to reversible deformation due to change in shape. On the other hand, an elastic constant expresses the intensity of elasticity of any given material.

1.2 TRANSITION METAL CARBIDES AND NITRIDES (TMCNS)

Transition Metal carbides and Nitrides are important and promising materials to be used as alternatives to the traditional hard materials. These materials can be used in the production of industrial items such as machining parts which involve shaping and forming behaviors. For instance, according to, Amriou et al. (2003), TMCNs possess both scientifically interesting as well as technologically important properties. These compounds display various different types of bonding characteristics namely; metallic, ionic and covalent. As a result, their unusual combination of bonding mechanisms is manifested in various macroscopic properties such as ultra high hardness, high melting points, wear resistance, resistance to corrosion as well as high bulk modulus. For instance, a range of binary carbides are associated with micro hardness values lying between 2000 and 3000 kg/mm^2 values which lie within the range of those of Al_2O_3 and diamond, Toth (1971). For instance, Al_2O_3 has a Vicker's hardness of 22 GPa, Nicholls et al. (1994) while diamond has a higher value of 79.7 GPa, Dub et al. (2017). Other oxides with known hardness include Fe_2O_3, FeO, $Cr_2O_3$with values of 3.27 GPa Yefei et al. (2011), 1.67 GPa, Yefei et al. (2011), 15 GPa, Nicholls et al. (1994), respectively. As a result of this property, metal carbides and nitrides are used extensively as cutting tools together with wear-resistant surfaces. Due to their excellent properties TMCNs can be used as thin

films as utilized as diffusion barriers in either microelectronics or wear-resistant coatings on engine components and cutting tools, Oyama (1996). The presence of these coatings on materials usually increases their lifetime, thus reducing the cost of wear and tear and replacement. Apart from the exciting physical properties, the TMCNs adopt a number of crystal structures since they can crystallize in various crystal lattices to form various structures. This occurs if the ratio of atomic radii of the nonmetallic to that of the metallic atom is less than 0.59, Hägg (1931). Some of the resultant structures are cubic if the ratio of metal to nonmetal is one. The first scenario results in the formation of Face-Centered cubic sub-lattice whereby the atoms of the nonmetal occupy the interstitial position resulting to NaCl-structure, for example, NbC and NbN, Isaev et al. (2007) as shown in Figure 1.2.1 where the big balls represent the Niobium element while C/N are represented by the small balls. Moreover, the zinc blende structure can be formed as illustrated in Figure 1.2.2 with Nb being the red balls and green balls are the C/N atoms. Lastly, hexagonal crystal structures can be formed as illustrated in Figure 1.2.3. The grey balls are the Niobium atoms and yellow balls are the C/N atoms.

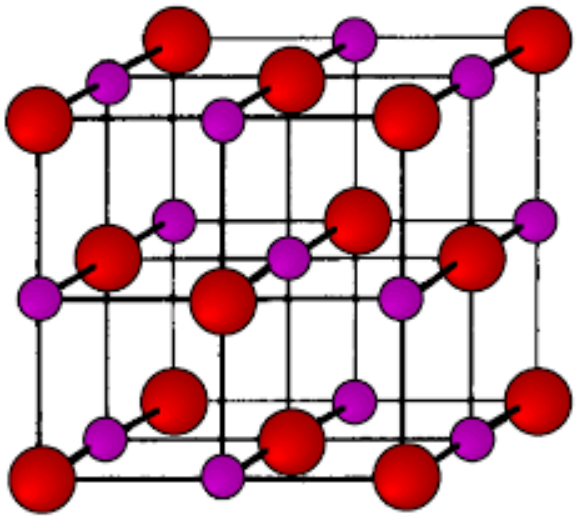

Figure 1.2.1: An illustration of rock salt crystal structure where the red and purple balls represent Niobium and C/N, respectively, Raja & Barron (2022)

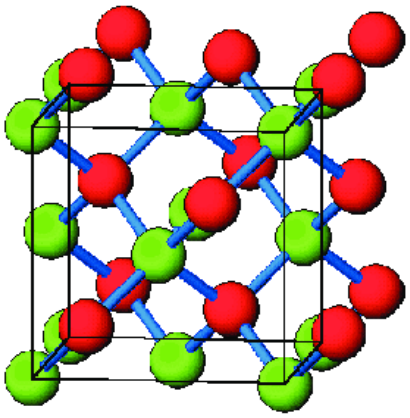

Figure 1.2.2: An illustration of zinc blende crystal structure where the red and green balls represent Niobium and C/N, respectively, Mlinar (2007)

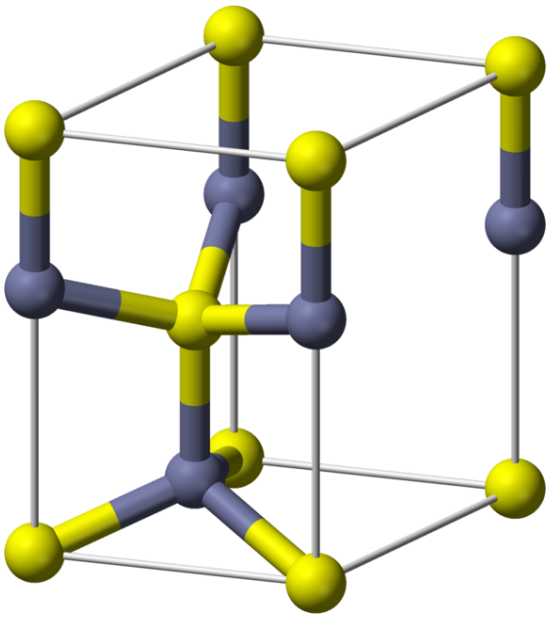

Figure 1.2.3: An illustration of wurzite crystal structure where the grey and yellow balls represent Niobium and C/N, respectively, Desai (2008)

1.3 NIOBIUM NITRIDE

Group IV_b as well as V_b together with carbon and nitrogen as light nonmetallic materials make strong solids which exist in different crystal structures such as rocksalt, zinc blende and wurzite structures Toth (1971). For instance, Niobium Nitride is formed from a Niobium metal and nitrogen as the nonmetallic element. Transition metal nitrides are some of the group of compounds formed by these elements and these have captivated

alot of attention from many researchers as a result of their properties together with applications. These nitrides have distinct applications such as in areas where hardness is a requirement, Koseki et al. (2015), Hones et al. (1999), Musil (2000) and Polcar et al. (2008) due to their excellent mechanical properties which include high values of bulk modulus as well as large hardness. For instance, the bulk modulus of NbN, HfN and ZrN are 354, 306, 285 GPa, respectively while the hardness values of these systems are 20.0, 19.5, and 17.4 GPa Xiao-Jia et al. (2005). These materials are also applied as protective coatings, Polcar & Cavaleiro (2010) and Samano et al. (2010). They have excellent thermal stability and are resistant to corrosion as well as having high melting point, Koseki et al. (2015), Musil (2000), Zhang et al. (2015) as well as Seo et al. (2004). Other applications include hard coatings which is associated with their excellent mechanical properties such as NbN, Benkahoul et al. (2004).

Early transition metals form stoichiometric nitrides which crystallize in different structures, for instance, the rocksalt, Zhang et al. (2016), zinc blende as well as hexagonal structures, Wen et al. (2009) and Benkahoul et al. (2004). Early trnasition metals are elements sitting on the left hand side of the periodic table and form the first half of the transition series. They include elements from group 3 to group 7. However, the compounds exist with substantial levels of vacancies, Toth (1971), Holleck (1986) and thus, studying defects is crucial. This study reports on the three crystal structures of NbN indicating that temperature as well as defects which are some of the growth conditions have significant influence on the crystal structure. The crystal structure is defined by the arrangement of atoms in a crystal whereby the arrangement of the atoms which is the basis is associated with each lattice point. However, the nitrides exist in the rock-salt structure over large composition range. This is supported by performing simulations with defects. For instance, TiNx in the rocksalt structure has been synthesized for a range of values of x from 0.67 to 1.3, Balasubramanian et al. (2018a). This study showed that point defect concentration of certain ranges results in compositional variation of the nitrides, Shin et al. (2003), Shin et al. (2004), Lee et al. (2005) and G. Smith et al. (1999). Although NbN exist in stoichiometric structures and the presence of vacancies is

inevitable, the nonmetal deficiency tend to be the source of nonstoichiometry in these materials. The control of the stoichiometry by these deficiencies as well as effects of the vacancies on the mechanical properties are important especially when designing hard materials based on NbN, Balasubramanian et al. (2018a).

Cubic δ- NbN which exists in the sodium chloride structure has been a highly studied structure of the nitrides since it gives rise to superconducting materials. During superconductivity process the transition temperature (T_c) of the solid solution of either NbN or NbC reaches a value of 17.8 K, Matthias (1953). Regardless of the value of (T_c) of the nitride being a lower value, the system has high hardness as mentioned earlier which makes it possible for the compound to be used in specific electronic applications. For example, the superconducting behaviour of NbN is applicable in low temperature superconducting electrons which include tunnel junctions, Zhen et al. (1999) as well as nano-structured single photon detectors as illustrated in Figure 1.3.1 , Wen et al. (2008).

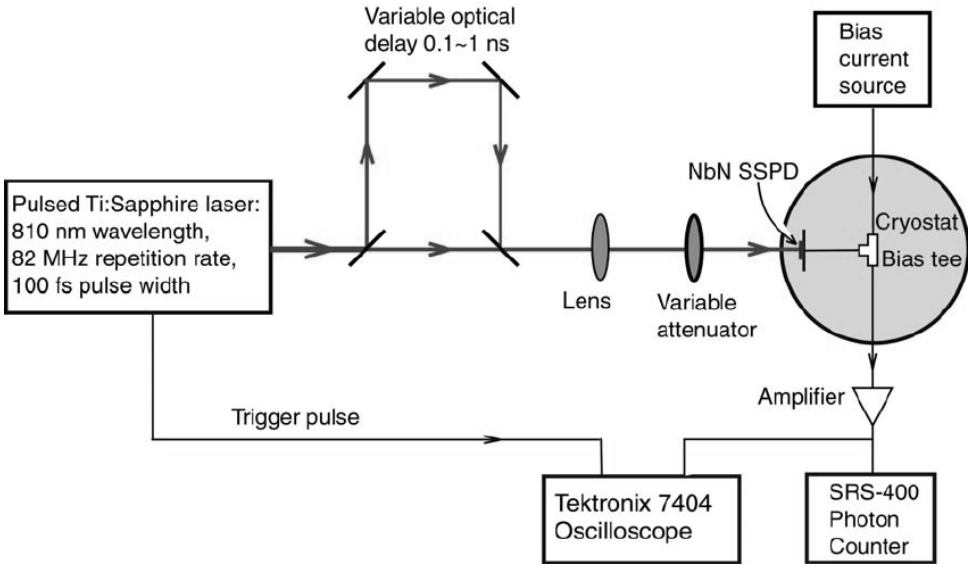

Figure 1.3.1: Experimental set up of single photon detector made using NbN, Yefei et al. (2011)

1.4 NIOBIUM CARBIDE

Apart from nitrides, carbides are also of great interest. Niobium carbide is a system composed of metallic Niobium and carbon as the nonmetal. The system exist in both cubic and hexagonal crystal structures which include rocksalt, zinc blende and wurzite

structures. The latter is the hexagonal while the first two are the cubic structures, Cuppari & Santos (2016). Several research works have paid attention to several IV_b and V_b TMCs among them NbC due to their outstanding properties that include mechanical, high thermal and chemical properties, Seung-Hoon et al. (2001), Kral et al. (1998) together with Conklin et al. (1968). Here group IV_b and V_b refers to the group of the transition metal that combines with a non metal to for the TMC. These materials are also known as refractory materials due to their high values of melting points and metallic in nature. Following these excellent properties, NbC has found various applications such as in cutting tools as well as grinding tools which is a major industrial application of this material. Moreover, due to high value of melting point (3610 °C), high values of hardness due to their mixed covalent-metallic-ionic bonding and resistance to chemical attack, Sen (2004), Nedfors et al. (2011), NbC is used as reinforced phase as applied in iron matrix as well as hard coating for wear resistant materials. The materials are also used as diffusion-resistant thin-film coatings especially in microcircuit devices, Williams (1998). Altogether, the above named properties ensure that these materials are suited for structural applications even at high and extreme temperatures where strength is required.

The TMCs are characterised by complex chemical bonding formed by the metal and the carbon elements which is evident in the combination of their physical properties. However the carbides have simple crystalline structures. For instance, NbC exist in substoichiometry form in different structures such as rocksalt, zinc blende, hexagonal among others. At near equal parts of TM and the carbon, the system exist in rocksalt structure. The rocksalt structure is stable, Yu et al. (2015). However, these substoichiometry forms are achieved if there is presence of carbon vacancy. For group VB materials such as NbC and TaC, the FCC structure is maintained when the carbon loss does not exceed approximately 25 % at elevated temperatures. On the other hand, at low temperatures carbon loss can result into precipitation of the Me_4C_3. Incase of further carbon loss, precipitation of faulted metal-rich carbide occurs and several phases such as Me_4C_3 as well as Me_2C form. These metal-rich carbides do not maintain the

FCC metal ordering. Thus, the study of defects is very crucial when understanding the properties of these TMCs. This has been confirmed through different approaches used to prepare NbC. The major methods include magnetic-controlled sputtering, Nedfors et al. (2011), self-propagating reaction, Yangsheng & Gregory (1995), atomic layer depositing, Klug et al. (2011) among others.

According to Cuppari & Santos (2016), a lot of work has been done on metal carbides whereby researchers have studied the systems extensively since 1960s. This work noted that both crystal structures as well as chemical bonding have been used to explain the main characteristics of these systems. However, there are phenomena that are still not well understood and need some attention. For example, TiC together with WC have found technological relevance and are some of the carbides widely used in the industry. On the other hand, the technological relevance and use of some TMC such as NbC has been neglected. This is regardless of the material influencing the microstructural evolution of steels and cast irons during their processing and on the final properties of these materials.

1.4.1 Applications and challenges of traditional hard materials

Technology development is one of the aspects that has been on a rapid rise recently due to constant pursuit of materials that are more improved and possess both high efficiency and durability. Some of the areas that have been affected are power generation together with aerospace, Boyer et al. (2015). In these areas Ni-based alloys have been considered as the traditional structural materials fit for the applications. Unfortunately, the materials have been faced with challenges such as physical limits, whereby their maximum operational condition are effective up to some range of high temperature ~ 1200°C Soboyejo (2006). According to Soboyejo (2006), high temperature coatings as well as sophisticated cooling systems can be used to raise the operational condition of materials to 1500 °C. For this to be achieved materials with high melting point, strength and resistance to oxidation are required. Thus, there is an active search for materials that can be used at high temperatures and for this reason, NbC and NbN being refractory materials are potential candidates. Moreover, in areas such as hard metal industry,the traditional structural materials such as diamond have some limitations which makes them inefficient in some

applications. For example, diamond has limited applications in machining ferrous alloys especially at high temperature. This is because at high temperatures C tend to dissolve into Fe and in return the tip is rendered ineffective, Shih (2000) and Ikawa & Tanaka (1971). Thus, in the recent years, researchers have focused on high-temperature niobium alloys whereby silicide and carbide are used for hardening the materials. This is done with the aim of replacing the nickel-aluminium superalloys applied in gas-turbine motor building, Karpov (2018), Karpov et al. (2012), Svetlov et al. (2017). The hardened niobium alloys have high melting points which allow design of materials that can operate at high temperatures such as 1500 °C. These operating temperatures are much higher compared to 300-350 °C which is the temperature range at which nickel-aluminium superalloys operate. Due to this limitation, there is a clearly need to develop other materials that can be used at high temperatures. This therefore requires that the materials chosen should not only have high melting temperatures but should also have high strength and stiffness together with high oxidation resistance when operating at high temperatures. Additionally, the material should have adequate mechanical behavior when being used at room temperature, Woodward et al. (2010), Kirchner et al. (2011). Several works by Nedfors et al. (2011), Wang et al. (2009), Yang et al. (2014), Benkahoul et al. (2004), that consider both NbC and NbN on mechanical properties have been performed which supports the high strength requirements of these materials. Obtaining properties such as elastic tensor through experimental methods is challenging owing to the difficulties experienced in synthesizing and working at high temperatures. In this regard, several *ab-initio* methods have been tested and confirmed to offer viable alternative approach that can be applied to obtain very critical properties related to the mechanical properties of a system. Various DFT-based *ab-initio* techniques have been put into practice by use of total energy, Bercegeay & Bernard (2005), stress-strain, Ganeshan et al. (2009) together with density functional perturbation theory approaches, Baroni et al. (1987).

1.5 STATEMENT OF THE PROBLEM

Presence of point defects such as vacancies is known to impact the stoichiometry of the crystal and to a large extent other pertinent properties. Thus, there is a need to understand the formation techniques, diffusion behaviours and other growth dynamics and mechanisms of defects in a material. Transition metal carbides and nitrides have a lot of uses in industry, but their mechanical properties are significantly affected by defects. Thus, knowledge gained will guide the optimization of the desired properties. This arises from the fact that nonmetal vacancies tend to be the source of the nonstoichiometry in materials. Apprehension of the impact of the vacancies on the mechanical characteristics is crucial when designing hard materials. For instance, the effect of anionic vacancies on the mechanical characteristics of TMCNs is still an open question. This is because the vacancies are expected to reduce the number of chemical bonds and hence the strength of the materials although the hardness of TMCNs violates this picture of coordination counting. From earlier studies, mechanical strength is enhanced when vacancies act as pinning centers which inhibit dislocation motion. Also, the hardness of systems behave extraordinarily when two unsaturated electronic bands appears near the Fermi level which respond oppositely to shear stress, Seung-Hoon & Jisoon (1997).

In ultra-hard and related industries, equipment operate at high temperatures and pressure which may affect the performance and durability of components. Moreover, the synthesis of the TMCNs require high temperature as well as high pressure, Ningthoujam & Gajbhiye (2015) under such conditions formation/occurence of defects is inevitable. However, the effect of defects and temperature on the mechanical performance and integrity of carbides and nitrides such as NbC/N is not well understood. In addition most studies overlook such aspects since it can be complex and expensive. Hence, there is a need for predictive studies that can guide future experimental work.

According to earlier studies by Seung-Hoon et al. (2001) and Yu et al. (2015), the mechanical properties of nitrides decrease with increase in vacancy concentration while for the carbides, as the vacancy concentration rises the values of mechanical properties

also increases. However, it is not clear why there is disparity in response to vacancy concentration for these two classes of materials. This is regardless of the two compounds possessing almost similar bonding structures. Thus, this work will investigate the impact of vacancy concentrations on the mechanical characteristics of Niobium Carbide together with Niobium Nitride in three different crystal structures, namely, rocksalt, zincblende and wurzite. The study will elucidate the origin of the anomalous behavior of the mechanical properties by using the electronic structure methods. Experimental synthesis of stoichiometric transition metal nitrides has been a challenge over years. The difficulty is attributed to the high kinetic barriers of the TMNs which limits the formation of stoichiometric nitride. These barriers include dissociation of N_2 as well as exhibition of loss of nitrogen at high temperatures, Zhang et al. (2016) which results into formation of point defects. Thus, experimentally synthesis of NbN is difficult without the presence of some defects. Hence studying the effects of defects on different properties of a solid is crucial.

Several studies have been performed on both NbN and NbC at zero temperature. However, high temperature studies on how the mechanical properties of these materials are affected by high temperature using molecular dynamics simulations are relatively scarce. Currently, there are very few studies touching on the determination of elastic constants and hardness characteristics of NbC and NbN at high temperatures, but their findings are still inconclusive.

1.6 JUSTIFICATION OF THE STUDY

NbC and NbN are considered to be among the most important materials in the hard metal industry due to their excellent mechanical, physical and electronic properties. The materials have been found to be mechanically robust due to their high bulk modulus and Vicker's hardness, Korir et al. (2011), Muchiri et al. (2019), Isaev et al. (2007), Lailei et al. (2013), Kim et al. (2009) and Andrievski et al. (1991). Hard materials are important especially in applications where hardness is a necessity. Thus, there is a necessity to develop new materials that are cost effective with superior performance compared to the

traditional hard materials such as diamond, boron nitride and silicon carbide to cater for the demand. However, such improvements and developments can only be realised when the viability of these materials is tested through rigorous research entailing experimental and/or theoretical methods. Owing to recent advancements of more robust computational methods and resources, properties of these materials can be determined accurately via computer modelling. In particular, properties of pristine as well as NbN and NbC with point defects and operating at elevated temperatures can easily be probed using first principle studies. In this study, first principles calculations were performed so as to obtain all the desired properties. For instance, the study applied *ab-initio* molecular dynamics (AIMD) to determine the effect of temperature on the mechanical properties of NbC and NbN. *ab-initio* molecular dynamics approach is used due to its accuracy and its ability to determine properties at high temperature, Kresse & Hafner (1993a), Woodward et al. (2010), Kirchner et al. (2011), Hafner (2008).

1.7 OBJECTIVE

1.7.1 General objective

To investigate the effect of vacancy defects and temperature on the mechanical as well as electronic properties of Niobium Carbide together with Niobium Nitride in rocksalt, zincblende together with wurzite crystal structures.

1.7.2 Specific objectives

The objectives of this work are:-

1. To determine the structural properties of NbC and NbN such as lattice parameters, bond lengths and bond angles.
2. Analyse the effects of vacancy concentration between 1.56 % and 12.5 % on the mechanical properties as well as the electronic properties of Niobium Carbide and Niobium Nitride.
3. Calculate the vacancy migration energy in both NbC and NbN systems.
4. To evaluate the effect of temperature between 300 K and 1500 K on the mechanical

properties of Niobium Carbide and Niobium Nitride from *ab initio* molecular dynamics simulations.

CHAPTER TWO

LITERATURE REVIEW

2.1 TRANSITION METAL CARBIDES AND NITRIDES

The need for hard materials has grown exponentially in the recent past, and this has been the driving force among the researchers for the past few decades. Most of the research work has been focused on the synthesis of materials whose hardness is allied to that of diamond along with cubic boron nitride. These discovered super-hard materials are anticipated to possess excellent mechanical properties such as high bulk modulus, hardness, high refractive index as well as high shear modulus. The super-hard materials have Vicker's hardness that exceeds 40 GPa, Haines et al. (2001). The compounds that have been considered as potential candidates consist of elements such as carbon and nitrogen and transition metal carbides, nitrides and oxides, McMillan (1999). These compounds have been selected due to their extreme hardness, chemical inertness, and the increased demand for hard materials in the cutting, drilling, polishing and related industrial applications. Both experimental and theoretical research studies have established the TMCNs to be potential candidates for super hard materials due to their high cohesive energies and bulk modulus.

Among the refractory compounds, TMCNs have been of interest due to their fascinating properties. Both theoretical and experimental studies have revealed that these materials are associated with unusual covalent, metallic and ionic bonding mechanisms which is thought to be the cause of unusual properties. The σ-bond of the states existing between p orbitals of N/C and the d orbitals of transition metal resists shearing strains resulting in an unusual enhancement of hardness in these materials, Jhi et al. (1999). Pang et al. (2023) observed that the covalent bonds in the carbides are responsible for the high strength of these materials. For instance, TMCs in rocksalt structure are used in cutting tools as the coating metal, optoelectronic devices, low temperature fuel cells as well as magnetic storage devices, Eck et al. (1999). This behavior has motivated several

researchers to study both the cohesive energies and bonding mechanism in TMCNs. For instance, Fernandez et al. (1992) and Korir et al. (2011) examined the cohesive energies of the 4d transition metal carbides. According to Korir et al's findings, NbC and NbN are among TMCNs with highest values of cohesive energies and bulk modulus and thus regarded as super-hard materials.

2.1.1 Niobium Carbide

NbC is one of the transition metal carbides that is of scientific interest due to its various industrial applications. NbC is considered a versatile compound due to a combination of its physical, chemical, electrical and mechanical properties including high hardness, good electrical conductivity and high-temperature strength, Rathod et al. (2011). These properties arise due to interaction of different types of bonding including metallic, ionic and covalent as mentioned earlier. They provide unusual combinations of bonding mechanism which manifest in some important macroscopic properties. In the case of mono carbides, the overall bonding nature associated with it is covalent i.e between the carbon and metal states. However, ionic character also exist whereby there is transfer of electrons from Nb to C atoms, Klein et al. (1980). Furthermore, the metallic bonding which form short bonds make the transition metal carbide to be super hard. As a result, the mono carbides have various applications such as in high-temperature structural materials and they are also used as hard constituents in metal matrix composites. Moreover, there are technological applications of NbC such as developing wear-resistant coatings used in ball bearings and cutting machine tools, Cuppari & Santos (2016) and Stampfl et al. (2001).

According to Weber (1973), extreme physical properties of ZrC, NbC as well as HfC studied from lattice dynamics are associated with the strong covalent bonds existing between the transition metal and carbon atoms. Mohammed et al. (2023) identified the matallic and covallent bonding in NbC as well as the mechanical stability. On the other hand, Isaev et al. (2007), studied the phonon related lattice dynamics on body centered cubic (BCC) V_b-VI_b TMs, monocarbides as well as group III_b-VI_b transition mononitrides

from first principle density functional perturbation theory and they established the systems to be dynamically stable.

Several researches have identified different physical properties of NbC. For example, strain-induced NbC precipitation result into softening retardation in the thermomechanical process involving a high-Mn twinning-induced plasticity of steel microalloyed together with Nb at 1000^oC, Llanos et al. (2015). According to Zhi et al. (2008), the addition of Nb to hypereutectic high chromium cast irons result into formation of NbC in the process of solidification as the liquid looses some carbon content. This results into carbides refinement as well as morphology of the M_7C_3 changing with carbide becoming more isotropic. This supports the fact that NbC is an important compound in ferrous alloys. One of the major reasons associated with limited applications of NbC is its poor sinterability and synthesis techniques that include spark-plasma sintering and hot pressing which have been proposed as a way forward with Co being incorporated, Woydt & Mohrbacher (2015). The study showed that pristine NbC with 8% Co has high wear resistance. This allows the compounds to compete with typical hard metals in various applications and ceramics. Different approaches have been used to prepare NbC that include direct high-temperature reaction, self-propagating reaction, Munir (1988), carburization of niobium oxides, Shimada et al. (1983) as well as atomic layer deposition, Klug et al. (2011). The carburization process is a heat treatment procedure whereby either iron or steel absorbs carbon as the metal is heated in the presence of a carbon-bearing material, for instance charcoal or carbon monoxide. The process affects the surface of the material as its intent is to make the metal harder and more wear resistant, Shimada et al. (1983). From these experiments, it was noted that crystals of niobium carbides exist in substoichiometry and carbon vacancy was also found to exist in these crystals.

NbC has various applications that include hard metal industries, technological applications among others, Nedfors et al. (2011). Noble metals with low electrical resistance are commonly used for coating the electrical contacts although they have high costs as well as poor wear resistance. This challlenge can be solved by use of NbC as the

coating since the compound is electrically conductive and has high wear resistance.

Several works have been reported about NbC on their compressibility as well as elastic properties. Chen et al. (1988) used the method of total energies to determine the mechanical properties of NbC. In this study, it was noted that the bulk modulus of NbC is 332 GPa while in other studies such as Isaev et al. (2007) using the first principles calculations, the system was reported to have a bulk modulus of 301 GPa. Moreover, Lailei et al. (2013) used the indirect calculation to obtain a value of 299 GPa as the bulk modulus of NbC. Apart from zero temperature calculations, some studies have also considered high pressure. For instance, Kim et al. (2009) studied the bulk NbC system and obtained Vickers hardness of 22 GPa together with a fracture toughness of $7MPam^{\frac{1}{2}}$. The high-energy ball milled NbC powder was sintered at high frequency using induction-heated sintering method. Moreover, according to Song et al. (2022), the bulk modulus of NbC is 305 GPa, the Young's modulus is 533 GPa while the shear modulus is 221 GPa and a value of 0.21 for the Poisson's ratio.

Recently, Lailei et al. (2013) applied density functional theory to explore the elastic properties of B1 of selected TMCNs and established that the systems have outstanding mechanical properties due to the complex chemical bonding comprised of metallic, ionic as well as covalent. Similarly, Chen et al. (1988) studied the elastic constants of NbC in the rocksalt structure and found the system to have high values. For instance, the bulk modulus was obtained as 332 GPa, which was comparable to experimental value of 340 GPa. C_{11}, C_{12}, and C_{44} were found to be 640 GPa, 180 GPa and 140 GPa, respectively against experimental values of 620 GPa, 200 GPa and 150 GPa, respectively. Other studies have investigated the effect of temperature and defect concentration on the mechanical properties of carbides. In particular Jun et al Jun & Shaffer (1970), explored the elastic moduli of carbides such as $NbC_{0.95}$ and $TaC_{0.99}$ and showed that it tend to decrease with increase in porosity. For example, the Young's modulus of $NbC_{0.95}$ and $NbC_{0.964}$ are $4.781x10^{12}$ $dynes/cm^2$ and 4.88410^{12} $dynes/cm^2$ at room temperature. At high temperature, both Young's modulus and shear modulus decreases. Further, Sangiovanni et al. (2021) investigated the effect of temperature on the mechanical

properties of refractory carbides and results obtained show that the elastic constants of the TMCs decrease with increasing temperature with exception of C_{12}. In addition, according to Valeeva & Gusev (2021), the elastic constants of disordered NbC_y decrease as the niobium carbide composition deviates from stoichiometry. The deviation from stoichiometry is also accompanied by decrease of the elastic anisotropy of the material. Zhao et al. (2019) observed that as the decrease in carbon carbon increased the hardness for $NbC_{1.0}$ and $NbC_{0.5}$ from 8 GPa to 12 GPa. Also, Balasubramanian et al. (2018b) from the First-principle calculations, ductility of carbides and nitrides increase with increase in the valence electron concentration. Another observation by Shi-Yu et al. (2022) shows that the brittleness of carbides decreases with increase in valence electron concentration.

2.1.2 Niobium Nitride

Similar to NbC, the electronic properties of NbN have also been reported widely by Amriou et al. (2003), Isaev et al. (2007) and Lailei et al. (2013). Much emphasis has been on the electron states of the elements involved in bonding. For example, the 4d state of Nb and 2p state of N leads to formation of covalent bonds which contribute to promoting the hardness of the material, Klein et al. (1980). NbN is a TMN which exhibits interesting properties such as high hardness and has been studied by several researchers. For instance, nanostructured films of NbN are used as wear-protection coating on cutting tools. This is due to high hardness and corrosion resistant. The hardness of the films has been found to be higher than that of the bulk material. For example, the hardness of the films deposited by arc deposition systems ranges between 34-49 GPa as reported by Andrievski et al. (1991) and Bendavid et al. (2003). These values ranges between 13.3 - 20.0 GPa for NbN in rocksalt structure, Friedrich et al. (2011). The mechanical properties have also been studied using Vickers indentation method and bulk modulus where it has been found to be close to those of cubic boron nitride, Zhigang et al. (2008). Moreover, mechanical properties of NbN have been studied in detail using DFT by Wang et al. (2009), which established that the mechanical properties of NbN are connected to their electronic structure. Bulk modulus of 313 GPa and 310 GPa were obtained for

the cubic and hexagonal NbN structures. Other works related to NbN focus on bulk, electronic as well as structural properties such as bonding Amriou et al. (2003), Lailei et al. (2013). Stampfl and co-workers Stampfl et al. (2001), have extensively discussed the bulk moduli, lattice constants, cohesive energies and densities of states of 3d, 4d and 5d TMN in the rocksalt structure.

Point defects such as cation and anion vacancies together with interstitials have an impact on the properties of TMNs. For instance, according to Kubel et al. (1988) and Mei et al. (2015) cation and anion vacancies in semi-metallic ScN induce metallic conduction as a result of the vacancies acting as dopants of n- and p-type. Similarly, vacancies cause an increase in elastic moduli of NbN, Kindlund et al. (2013). Also, experimentally the presence of point defects in TMNs such as NbN has been reported in various works such as Kindlund et al. (2013) and Sangiovanni et al. (2016) implying that point defects such as cation and anion vacancies as well as anion interstitials are present in these nitrides.

High hardness is one of the significant property of this compound that plays a key role in its applications. This has resulted into considerable efforts being devoted to determining the mechanical properties of NbN Fan et al. (2006). For instance, Wu et al. (2005) and Fan et al. (2006) determined the hardness of NbN by use of Vickers indentation method to study the mechanical properties of $\delta - NbN$ which showed that the compound has Vicker's hardness that is close in terms of magnitude to sapphire while the bulk modulus was found to be close to that of cubic boron nitride. Other studies have identified ideal strength which is the critical stress at which structures of ideal crystals become unstable seem to provide a greater understanding of the hardness of these materials as well as mechanical behaviours when under large strain Jhi et al. (2001) and Zhang et al. (2007).

Several studies on TMNs have been carried out to determine the effects of temperature on various properties. For example, Fu et al. (2015) performed MD simulations on TiN (001) so as to investigate the deform behaviour of this system for the temperatures between 0 K and 300 K and it was found that the hardness of the system tend to decrease with increase in temperature as a result of migration of slips taking place at high temperature. Other studies investigating the effects of temperature and defects have been reported.

Ruicheng et al. (2018) analyzed the elastic constants of γ-TiAl using molecular dynamics method at high temperatures and varying vacancy concentrations which showed that the elastic modulus of the single crystal decrease with increase in temperature and vacancy concentration. In addition, Steneteg et al. (2013) studied the elastic properties of TiN at room temperature and elevated temperature of 1800 K that corresponds to the operational conditions when these materials are used as cutting tool coatings. The elastic constants of TiN was found to decrease as the temperature increase in nearly a linear trend. This represents normal temperature dependence as a result of anharmonicity. In particular, the C_{11} elastic constant was found to strongly dependent on temperature as the values decrease by 28% as the temperature rises from room temperature to 1800 K. Similarly, there was 20% to 25% decrease of bulk modulus, shear modulus and Young's modulus within the same temperature range. Despite the significant amount of work on transition metal carbides and nitrides, open questions still exist which are yet to be handled. For instance, it is still not clear how anionic vacancies at low concentration below 25 % affect the mechanical properties of NbC/N. Also, depending on the applications of these materials the most appropriate mechanisms that can help in controlling the levels of these defects is still not clear although the information is relevant in tailoring the materials for mainstream applications. Moreover, materials are normally used at elevated temperatures which is generated in the process of their use and as such the information on the impact of temperature on the mechanical characteristics as well as defect diffusion energy are limited although they are necessary in understanding the behaviors of these materials. According to Xinyu et al. (2021), nitrides are mechanically stable and ductile. Alexander et al. (2016) studied the mechanical properties of NbN and established the high values of hardness of 28 GPa which agree well with other studies.

CHAPTER THREE

THEORY

3.1 INTRODUCTION

This chapter provides background information on the simulations performed as well as the general principles of the method used as implemented in the computational codes. Both Quantum ESPRESSO (Quantum opEn Source Package for Research in Electronic Structure Simulation and Optimization), Giannozzi et al. (2009) and Vienna Ab-initio Simulation Package (VASP), Kresse & Hafner (1993b) codes were used to study the different properties of the materials considered. In this study, structural, electronic and mechanical properties of both Niobium Carbide as well as Niobium Nitride in rocksalt, zincblende and wurzite crystal structures have been investigated via density functional theory approach.

3.2 MANY BODY PROBLEM

The discovery of electron by J.J. Thomson in 1896, Thomson (1897) offered an opportunity for scientists to develop models and theories that can define electrons and their interaction. According to the Thomson model, the electrons are randomly distributed in a sphere occupied by positive charges. Later, there was an improvement of this model by Rutherfold who came with a model that describes the components of an atom including electrons, protons and nucleus, Rutherford (1911). The electrons and the ions are the major components of an atom which collectively make up the crystals and they provide the fundamental understanding of any material based on the electronic structure. Between the two major components of an atom, the electrons play a key role in determining the characteristics of a material. Thus, salient information about different properties of matter can be derived from the study of electrons using different models. The electronic structures can either be determined at ground state or the excited state, Martin (2004). Figure 3.2.1 is a representation of the Thompson atomic model which

shows that an atom is made of electrons which are surrounded by positive charges.

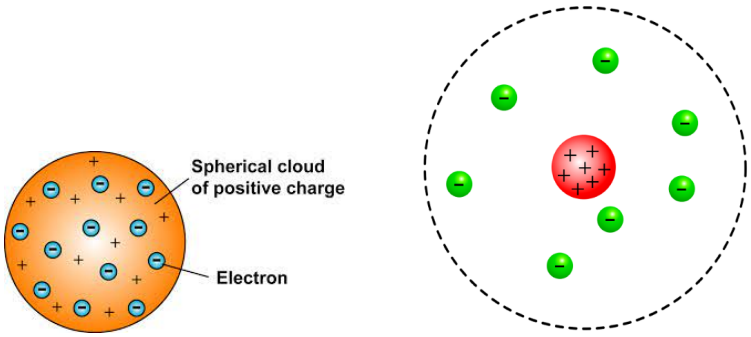

(a) Thompson atomic moodel (b) Rutherford model

Figure 3.2.1: Illustrations of Thompson atomic model and Rutheford model, Classes (2017)

Apart from simple atoms such as hydrogen, many others that are of fundamental importance consist of large number of electrons. Therefore, the need to describe these many-particle systems has existed as an important goal among theoretical physicists for many years. There have been numerous attempts to describe the many-particle systems fully just as if one is describing a one-electron system and obtain the exact solution based on the Schrödinger equation (SE). However, solving the Schrödinger equation of a many-particle system is challenging compared to that with few electrons due to the difficulty in solving the equation exactly numerically. This challenge has motivated the use of approximation techniques that have made the solving of SE possible although the accuracy is sacrificed in the process, Martin (2004).

Electronic structure methods emerged as a workforce for predicting the properties of solids, molecules amongst other forms of matter. The electronic structure methods used to determine these properties include Density Functional theory (DFT), Quantum Monte Carlo (QMC) and molecular dynamics which are the common techniques employed in these studies, Hohenberg & Kohn (1964) and Kohn & Sham (1965).

In quantum mechanics, the wave-like property of a system is described using the time-independent Schrödinger equation. The eigen values of all the energy states are specified using the Hamiltonian equation given by equation 3.2.1, we have;

$$H\psi_{\mathrm{i}}(\vec{r}) = E_{\mathrm{i}}\psi_{\mathrm{i}}(\vec{r}) \tag{3.2.1}$$

ψ, $\vec{r}$ and E represent the wavefunction, position and energy, respectively, in the i$^{\text{th}}$ position.

Here the Hamiltonian of the system is given as in equation 3.2.2;

$$H = -\frac{\hbar^2}{2m}\nabla^2 + V(\vec{r}) \tag{3.2.2}$$

where $\hbar = \frac{h}{2\pi}$

h = Plank's constant

m = mass of the particle

$V(\vec{r})$ = potential energy of the particle in the electrostatic field

When only one electron is involved such as in a hydrogen atom, the Schrödinger equation can be solved as in equation 3.2.3, where;

$$V(\vec{r}) = \frac{-e^2}{4\pi\epsilon_0 r} \tag{3.2.3}$$

$\vec{r}$ is defined as the distance of separation between the electron and proton.

The time independent form of the Schrödinger equation with M nuclei and N number of electrons can be used to represent a many body system as shown in equation 3.2.4, Cuevas & Scheer (2010):

$$H\psi_{\text{i}}(r_1, r_2, ..., r_{\text{N}}, R_1, R_2, ..., R_{\text{M}} = E_{\text{i}}\psi_{\text{i}}(r_1, r_2, ..., r_{\text{N}}, R_1, R_2, ..., R_{\text{M}}) \tag{3.2.4}$$

where r represent the electronic coordinates while R are the nuclear coordinates. The Schrödinger equation can also be written as a time dependent equation as in equation 3.2.5, Fiolhais et al. (2003).

$$H\psi(r_1, r_2...r_N, R_1, R_2, ...R_M) = i\hbar\frac{\partial}{\partial t}\psi(r_1, r_2...r_N, R_1, R_2, ...R_M) \tag{3.2.5}$$

the wavefunction $\psi(r_1, r_2...r_N, R_1, R_2, ...R_M)$ represent the eigen function of electrons and nucleus, respectively.

On the other hand, the Hamiltonian, H is given by equation 3.2.6:

$$H = -\frac{\hbar^2}{2m}\sum_i\left(\frac{\partial^2}{\partial {x_\mathrm{i}}^2}+\frac{\partial^2}{\partial {y_\mathrm{i}}^2}+\frac{\partial^2}{\partial {z_\mathrm{i}}^2}\right)-\frac{\hbar^2}{2M}\sum_n\left(\frac{\partial^2}{\partial {x_\mathrm{n}}^2}+\frac{\partial^2}{\partial {y_\mathrm{n}}^2}+\frac{\partial^2}{\partial {z_\mathrm{n}}^2}\right)+V_{\mathrm{ee}}+V_{\mathrm{nn}}+V_{\mathrm{en}} \quad (3.2.6)$$

The nuclei and electrons are represented by n and e while their masses are given by m and M, respectively. On the R.H.S of equation 3.2.6, the first and the second terms give the kinetic energies of electrons and nuclei, respectively. The other terms represent the Coulomb repulsion between the electrons, the Coulomb repulsion between nuclei and attraction between nuclei and electrons.

Solving the Schrödinger equation of a system with high number of electrons and nuclei, for example, greater than four is challenging. The Hamiltonian of such a system cannot be solved not even on the fastest super computers. This arise as the number of particles are given in the order of 10^{23} and the higher the number of particles the more it becomes challenging to solve the problem. Thus, approximations are made and errors estimated, Sholl & Steckel (2001) and Thijssen (2007).

3.3 THOMAS-FERMI THEORY

The ground state properties among other properties of a system determined by electrons in the presence of an external field can be studied based on the knowledge of the distribution of the electron density. Thomas-Fermi Theory is one of the oldest 'statistical theory' and simple method proposed by L.H.Thomas and E. Fermi to obtain fair approximation to the solution of Schrödinger equation, Thomas (1927). The method is based on Fermi-Dirac statistics as the electrons are assumed to form a gas and the electron-electron interaction energy is given by the classical Coulomb potential. Atoms in ordinary matter are always close to ground state and thus Thomas-Fermi theory Thomas (1927) is one of the oldest methods of determining the ground state properties. However, the results obtained from this approximation are less accurate compared to other methods that will be discussed latter such as the Hartree-Fock method and density functional theory. One of the importance of this method is that it can be used to obtain

effective potentials, which can be applied as initial trial potential when self-consistent field methods are used. In metallic systems the method is appropriate, although it does not put into consideration the exchange effects, Dirac (1930a).

The Thomas and Fermi method is used to determine the effective potential energy experienced by an infinitesimal test charge as well as finding the electron density around positive charges in an atom. Local density approximation is used to determine the kinetic energy whereby at a point r with a density of $n(r)$ the contribution is obtained using the kinetic energy of a homogeneous gas with corresponding density Guerra & Robotti (2008). The theory is defined by different terms; one of them being the TF energy functional, the TF Euler equation C.-S. Wang (1992). The TF Euler equation for the electron density is defined as shown in equation 3.3.1;

$$\frac{5}{3}C_k n(r)^{\frac{2}{3}} + e^2 \int dr' \frac{n(r')}{|r - r'|} + V_{ext}(r) + \lambda = 0 \tag{3.3.1}$$

Here, $C_k = \frac{3\hbar^2(3\pi^2)^{\frac{2}{3}}}{10m}$. The external potential is given by V_{ext} while λ is a Lagrange multiplier. If a system with N nuclei with charges greater than 0 i.e $(Z_i > 0)$ which are fixed at locations R_i in space, the TF energy functional is given as in equation 3.3.2;

$$E(\rho) = \frac{3}{5}\frac{\hbar^2}{2m}(3\pi^2)^{\frac{2}{3}}\gamma \int_{R^3} \rho(x)^{\frac{5}{3}} d^3x - \int_{R^3} V(x)\rho(x)d^3x + \frac{1}{2}\int_{R^3}\int_{R^3} \frac{\rho(x)\rho(y)}{|x-y|} d^3x d^3y + U \tag{3.3.2}$$

where,

$$V(x) = \sum_{j=1}^{K} Z_j |X - R_j|^{-1} \tag{3.3.3}$$

$$U = \sum_{1 \leq i < j ! l \leq K} Z_i Z_j |R_i - R_j|^{-1} \tag{3.3.4}$$

$$\gamma = (3\pi^2)^{\frac{2}{3}} \frac{\hbar^2}{2m} \tag{3.3.5}$$

The first term in equation 3.3.2 on the R.H.S represents the minimum quantum-mechanical kinetic energy which in this case is a semiclassical energy of a system with N

electrons which is needed to give the electron density $\rho(x)$. The electrons are fermions and the exact minimum energy can be obtained in the limit of fixed $\rho(x)$ and N approaching infinity.

The second term represent the Coulomb potential V which is an attractive potential when N electrons interact with K nuclei.

The electron-electron repulsive energy is given by the third term.

The last term U gives the nuclear-nuclear repulsion. This is an important term as it determines the possibility of bonding happening i.e causing some effect on energy (lower energy or not) when nuclei move far apart from each other.

The application of TF theory at high pressures and density is a great achievement. However, the theory fails to provide proper description of the outer parts of the atom. The charge density should decay exponentially, but for the TF theory the n(r) decays as r^{-6} far from the nucleus. Moreover, TF theory uses local density approximation to obtain kinetic energy implying that shell structure is absent in the TF atom. Thus, the periodic variation of different properties dependent of changing Z are not reproducible. Furthermore, TF approach fails to describe bonding, assuming ergodicity. The electron density fills all phase space to the Fermi energy regardless of whether the phase space parts are dynamically connected or not. As a result, dynamical processes in either atoms or molecules are constrained by this assumption, Nordholm (1987).

3.4 THOMAS-FERMI-DIRAC THEORY

The Thomas-Fermi theory was improved by Dirac who introduced the exchange term into the existing theory Dirac (1930a). Dirac recasted the Hartree-Fock theory through density function although there was no reference to the idea of many-electron wave function. In the Thomas-Fermi theory the function results in correction to the energy obtained from the exchange energy of the homogeneous electron gas Bloch (1929). The potential as defined by Dirac is as shown in equation 3.4.1;

$$V_x^{Dirac} = -(\frac{1}{\pi})[3\pi^2 n(r)]^{\frac{1}{3}} \tag{3.4.1}$$

The modified TF by Dirac is known as Thomas-Fermi-Dirac equation.

3.5 THE BORN-OPPENHEIMER (BO) APPROXIMATION

Most of the atoms apart from hydrogen are composed of more than one electron and obtaining the solution to the Schrödinger equation is not direct and exact. This means that the solution is unknown. This is encountered in different real life systems due to the presence of 3(M+N) degrees of freedom which give rise to a number of variables to be determined for different systems. Here, 3 represent the different ways in which the atoms posses kinetic energy while M + N stand for the sum of electrons and nuclei. Different approximations are employed in attempts to solve the equation, Cuevas & Scheer (2010). According to mechanics of fundamental particles in modern physics, the electric charge possessed by either the electron or the nuclei results in a force which has the same magnitude. These forces may alter the momenta of the particles in the same manner, implying that the change in momenta would be the same. Due to the variation in masses of electrons and the nuclei, this approximation treats the nuclei as stationary as compared to electrons which are 2000 times lighter than nuclei and are mobile through decoupling of the motion of these components. The characteristic frequencies of the electrons and nuclei differ significantly and this makes it easy for the decoupling the many-particle wave function into two parts, that is, one for electron and the other for nuclei. The velocity of the nuclei is smaller compared to the electrons, Born & Oppenheimer (1972). Thus, this approximation tends to lighten calculations by use of outstanding mass differences of the nuclei together with electrons which help to determine the energy as well as wave function of physical systems. This implies that when the time-scale of nuclear motion is considered, the light electrons will tend to relax to some instantaneous ground-state configuration. This means the kinetic energies of both the nuclei and electron can be treated separately. Through decoupling, the Hamiltonian for the electron is generated by use of static configuration of the nuclei present and the part dealing with nuclei treats the electronic energy $E_{(R)}$ as the potential, Thijssen (2007). Therefore, the system can

be described by a wave function which has both electronic and nuclear components. Classical Newtonian mechanics is then used to describe the ionic motion, Mayer (2003).

$$\psi(r,R) = \psi_{electronic}(r,R) \times \psi_{nuclear}(R) \tag{3.5.1}$$

The hamiltonian representing the electrons and nuclei when solving the time independent Schrödinger Equation can be written as shown in equation 3.5.2;

$$H = \left(-\sum_i \frac{\hbar}{2M_i}\nabla_i^2 - \frac{1}{2}\sum_\alpha \frac{\hbar^2}{2m_e}\nabla_\alpha^2 - \frac{1}{2}\sum_{i,j}\frac{Z_i Z_j e^2}{|\vec{R_i} - \vec{R_j}|} + \frac{1}{2}\sum_{\alpha,\beta}\frac{e^2}{|\vec{r_\alpha} - \vec{r_\beta}|} + \sum_{\alpha,\beta}\frac{Ze^2}{|\vec{r_\alpha} - \vec{R_\beta}|} \right) \tag{3.5.2}$$

From equation 3.5.2 the first two terms represent the kinetic energies of nuclei together with electron, respectively, the fifth together with the fourth term represent the interaction energies of the electron-nuclear as well as the electron-electron, respectively, while the third term is for the interaction between the nuclei. The massses of nuclei and electrons are given by M_i and m_e, respectively, while the positions of nucleus and electrons are given by R_i and r_i, respectively. Equation 3.5.2 has a potential energy similar to equation 3.2.3. The Coulomb law is not applicable here as strong nuclear force is responsible of holding the nucleus together and thus the Coulomb law constant in equation 3.2.3 has been dropped in equation 3.5.2. This equation can be written in terms of Hamiltonian for the N electrons in an environment with stationary nuclei as shown in equation 3.5.3;

$$H^{\text{elec}} = -\frac{\hbar^2}{2m}\sum_{i=1}^{N}\left(\frac{\partial^2}{\partial {x_{\text{i}}}^2} + \frac{\partial^2}{\partial {y_{\text{i}}}^2} + \frac{\partial^2}{\partial {z_{\text{i}}}^2}\right) + V_{\text{ee}} + V_{\text{en}} \tag{3.5.3}$$

Equation 3.5.3 has three terms representing the kinetic energy of the electrons, force of repulsion between electrons and attraction between electron and nuclei, respectively. Solving this equation give rise to wave functions together with structural energy $\text{E}_{(\text{R})}$ which are dependent of the nuclear configuration. The structural energy is incorporated into the Hamiltonian of the nuclei as a potential energy. The Hamiltonian representing

the nuclei becomes;

$$H^{\text{nuc}} = -\frac{\hbar^2}{2M}\sum_{i=1}^{N}\left(\frac{\partial^2}{\partial {x_{\text{n}}}^2} + \frac{\partial^2}{\partial {y_{\text{n}}}^2} + \frac{\partial^2}{\partial {z_{\text{n}}}^2}\right) + V_{\text{nn}} + E_{(\text{R})} \tag{3.5.4}$$

Since the nuclei are assumed to be heavy and at fixed positions, the solution to the equation is obtained by solving the electronic Schrödinger Equation using the electronic coordinates. The electrons are assumed to be at ground state and thus, the properties at the ground state can be obtained. The potential energy, $V_{\text{nn}} + E_{(\text{R})}$ is used to determine the geometry of the system through minimisation. The nuclear probability distribution is obtained by solving the nuclear part in the S.E. The total energy is given as the sum of energies due to electrons together with energy from the S.E representing the nuclei, Thijssen (2007). According to the Pauli exclusion principle, two electrons should occupy different quantum states. This implies that electrons will always repel each other if they are of the same spin and in the same quantum state. This effect is associated with some change in energy known as the exchange energy. This exchange energy is as a result of repulsion between electrons. Electrons have motion which is correlated and the wavefunctions are instead comprised of complicated functions of positions. This makes it difficult to determine the exchange energy analytically.

3.6 HATREE APPROXIMATION

Unlike in Born Oppenheimer approximation whereby the motion of the electrons is correlated, here the electrons are uncorrelated and independent. In this kind of approximation, the motion of the nuclei is assumed and ommitted. Instead, the electrostatic energy of the nuclei is considered and summed up with the energy due to electrons in the presence of static nuclei so as to give rise to the total ground state energy of the system. The wavefunction for the N-electron atom can be approximated to be the product of the individual wavefunctions of the N-electrons in the atom. Since the electrons are independent it is possible to approximate the wavefunction of the individual electrons. The wave function for the atom with N-electrons is a product *ansatz* and is

given in the form as shown in equation 3.6.1;

$$\psi_{\mathrm{i}}(\vec{r}_1, \vec{r}_2, ...\vec{r}_{\mathrm{N}},) = \psi_1(\vec{r}_1)\psi_2(\vec{r}_2).....\psi_{\mathrm{N}}(\vec{r}_{\mathrm{N}}) \tag{3.6.1}$$

This equation is known as the Hartree approximation, Hartree (1928). The main difference between Hartree approximation and BO approximation is that the former does not take into consideration the effects of exchange energy. The wave function of the selected system comprises of product of orthonormal molecular orbitals. Here, the interaction only occurs between the electrons and the mean field created by other electrons. The nuclei are considered to be at fixed positions and the electronic wave function determination is difficult due to existence of many degrees of freedom arising the electron-electron interactions, Sholl & Steckel (2001). The Hartree Approximation which gives a non-trivial wave function fails to satisfy the Pauli exclusion principle condition. Thus, further approximations necessary for the electron interactions.

3.7 HATREE-FOCK APPROXIMATION

On the other hand, the Hatree-Fock approximation which is treated as a one electron approximation considers exchange energy through the use of Slater determinant. This is in attempts to modify the Hartree Approximation which ignored the electron-electron interaction. The Hartree approximation does not show how the particular configuration of the (N-1) electrons affect the electrons. This is realized as the solution of the many body problem given by a set of wave functions which are treated as function of individual co-ordinates of the N electrons present. This implies that it is a function of 3N coordinates and its value need to be approximated, Ostlund & Szabo (1996). The approximations can be done using the Hatree product defined before as shown in equation 3.7.1 ;

$$\psi\left(r_1, r_2, r_3, ..., r_N\right) = \psi_1(r_1)\psi_2(r_2)\psi_3(r_3)....\psi_N(r_N) \tag{3.7.1}$$

ψ on the L.H.S of equation 3.7.1 represent the electronic wave function while the individual wave functions are given as $\psi_1(r_1)$, Sholl & Steckel (2001) & Mizutani (2001).

The total energy of the system is obtained when the wave function $\psi_i(r_i)$ representing the many electrons satisfies the form of Schrödinger equation given in equation 3.7.2;

$$-\frac{\hbar^2}{2m}\left(\frac{\partial^2\psi_i(r)}{\partial x_i^2}+\frac{\partial^2\psi_i(r)}{\partial y_i^2}+\frac{\partial^2\psi_i(r)}{\partial z_i^2}\right)+V_{H(r)}\psi_{i(\vec{r})}+V_r\psi_{i(\vec{r})}=E_i\psi_{i(\vec{r})} \tag{3.7.2}$$

The first term is the kinetic energy of the electrons while the third term provides the Coulomb force of attraction between the particles of opposite charges. The second term on the L.H.S is known as Hartree potential which represent the Coulombic force of repulsion between the electron and the entire electron density depending on the number of electrons in the system. Mathematically, it is represented as $V_H(r)=e^2\int\frac{n(r)'}{|r-r'|}d^3r'$. In this kind of scenario, individual electrons move in an average field associated with other electrons present in the system, Sholl & Steckel (2001) & Mizutani (2001).

In the Hartree-Fock approximation, the Slater determinant which uses the antisymmetrised product involving the one-electron wave function of all the N electrons in the atom is generated to represent the Hartree-Fock wave function using a N x N determinant. This implies that H-F approximation can be termed as a one electron system. This is used since the Hartree product fails to satisfy the principle of indistinguishability as well as antisymmetry. In H-F approximation, the antisymmetric wave function is determined using the single Slater determinant of a matrix of single electron wave function $\psi_i(r_i)$, Slater (1951). In Hartree-Fock approximation method, the electrons' wave functions can be represented as shown in eqn. 3.7.3;

$$\psi(\vec{r}_1,\vec{r}_2,.....\vec{r}_N)=\frac{1}{N}|\psi(\vec{r}_1,\vec{r}_2,.....\vec{r}_N)| \tag{3.7.3}$$

Due to the treatment of the wave function as a single Slater determinant of uncorrelated and independent electrons the anti symmetry rule is satisfied. Also, the exchange and correlation energy is treated in an exact manner. This is relevant in systems comprised of molecules and large number of electrons, Slater (1951). The Hartree equation is modified to give a SE whose effective Hamiltonian depending on the state is as illustrated in eqn.

3.7.4;

$$H^i_{eff}\psi(r) = \left(-\frac{\hbar^2}{2m_e}\nabla^2 + V^{i,\sigma}_{(eff)}r\right)\psi^\sigma_i r = E^\sigma_i \psi^\sigma_i r \tag{3.7.4}$$

$V^i_{eff}, \sigma r$ is defined as the effective potential which act on every electron with a given spin σ located at point r. It is expressed explicitly as given in equation 3.7.5;

$$V^i_{eff}, \sigma(r) = V_{(ext)}(r) + V_{Hartree}(r) + V^i_x, \sigma(r) \tag{3.7.5}$$

The first, second and third term on the R.H.S of the equation represent the external potential, Hartree potential and the exchange potential, respectively. The last term representing the exchange potential is obtained from the sum over orbitals with identical spin as σ

$$V^i_x, \sigma(r) = -\sum_j \int r'\psi^{\sigma *}_j(r')\psi^\sigma_i(dr')\frac{1}{|\vec{r} - \vec{r'}|}\frac{\psi^\sigma_j(r)}{\psi^\sigma_i(r)} \tag{3.7.6}$$

$\sum_i \psi^{\sigma *}_j(r')\psi^\sigma_i d(r')$ represent the Coulomb potential as a result of exchange density for each state i,σ.

The BO and HF approximations give a difference in energy known as correlation energy. This energy is due to redistribution of electrons caused by contrast between waves which are delocalised as well as point charge descriptions. In Hatree-Fock approximation, the Slater determinant is used to represent the wavefunctions and the correlation energy is omitted, Slater (1951). The omission of the correlation energy limits the Hartree-Fock approximation from being used in some cases such as where experimental results are used for comparison and other approaches that put into account the correlation energy have to be considered.

$$\psi\left(r_1, r_2, r_3, ..., r_N\right) = \frac{1}{\sqrt{N!}}\begin{vmatrix} \psi_1(r_1) & \psi_1(r_2) & \dots & \psi_1(r_N) \\ \psi_2(r_1) & \psi_2(r_2) & \dots & \psi_2(r_N) \\ \vdots & \vdots & \vdots & \vdots \\ \psi_N(r_1) & \psi_N(r_2) & \dots & \psi_N(r_N) \end{vmatrix} \tag{3.7.7}$$

Equation 3.7.7 represents the slater determinant (SD) which is used in Hatree fock approximation to determine the exchange energy. The SD satisfies both the principle of indistinguishability and antisymmetry. Electrons are characterised by either up or down spin and Pauli Exclusion Principle (PEP) has to be obeyed. PEP has to be employed to cater for the repulsive interaction between electrons with identical spin which should not occupy same quantum state. This form of interaction give rise to the exchange energy. Thus, in H-F approximation the electrons are distributed depending on the orientation of the spin so as to ensure that PEP is not violated. The distinguishable electrons overlap at different points and the expectation value of the distance at which the overlap occurs is affected by the exchange energy. Thus, the single determinant as defined by slater does not provide the exact wave function as Coulomb correlation is ignored. With the omission of the Coulomb correlation, total electronic energy obtained from this approximation is different from the exact value obtained using the Born-Oppenheimer approximation. In fact, the H-F energy is higher than the exact energy. An energy known as correlation energy emerges from the variation between exchange energy due to parallel spin and Coulomb correlation. The correlation energy measures the movement of a single electron as influenced by other electrons. However, metals are an exception as the presence of ionic potentials leads to inhomogeneous distribution of electrons unlike in the electron gas whereby the distribution is homogeneous and the Coulomb correlation is spin independent, Mizutani (2001).

3.8 DENSITY FUNCTIONAL THEORY

The approximations described in the earlier sections ignore the correlation energy, and therefore, there was a need to develop an approach that would take into account the correlation energy so as to estimate the energy of a system more accurately. An *ab initio* approach known as Density Functional Theory was established in 1964 by Hohenberg, Kohn and Sham to account for the correlation energy, Hohenberg & Kohn (1964), Kohn and Sham (1965). Unlike in the previous approximations whereby the individual electrons were considered and their wavefunctions determined, this approach is grounded on the

electron density distribution *n(r)* Kohn et al. (1996).

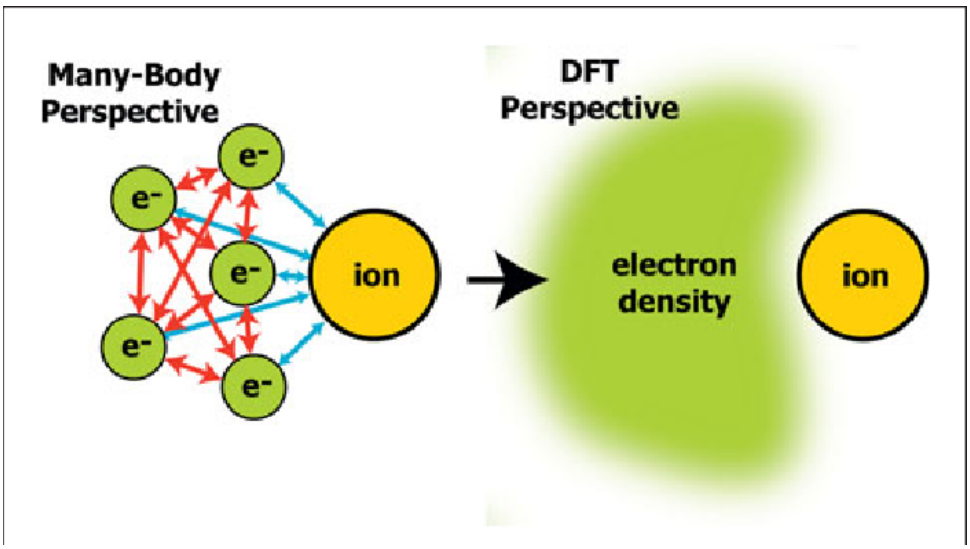

Figure 3.8.1: A description of density functional theory, Lusk & Mattsson (2011)

.

In many-electron systems the electrons involved are indistinguishable and thus it is convenient to use total electron density and abandon the idea of wavefunctions. Three spatial coordinates are used to describe the electron density irrespective of the size of the system used, thus the idea of 3N coordinates is invalid where N refers to the number of electrons present. According to the DFT approach, the electron density is important as it can be used to determine the Hamiltonian of the system and in return provides the ground state energy. Thus, this energy can be termed as the functional of the electron density. Also, according to this theory, the energy can be considered as the ground state when the input electron density corresponds to the actual ground state density. The energy of the overall functional is minimized by the electron density which is termed as the true electron density equivalent to the solution of the Schrodinger equation, Sholl & Steckel (2001). The ground state as obtained in DFT helps in determining the equilibrium volume, lattice constants as well as mechanical characteristics such as bulk modulus among other numerous properties. DFT is also known for determining the electronic properties of simple systems as well as other properties such as magnetic and electric susceptibilities of complex systems, Kohn et al. (1996). Although DFT is well known for determining the ground state properties, the excited state properties of different systems

can be described to some extent using DFT. However, the excited state properties are well expressed using time dependent density functional theory (TDDFT). The TDDFT method uses some functionals and adiabatic approximation. This connection between ground state and excited state calculations is enhanced by the fact that the external potential in which the particles move in, is determined from the density at the ground state of the electronic system considered. The external potential is associated with the Hamiltonian operator which describes both the ground state and excited states of the system, Görling (1996).

3.9 HOHENBERG AND KOHN FORMULATION

The idea of DFT was proposed by Hohenberg and Kohn, Hohenberg & Kohn (1964). They proposed that the many body total energy can be approximated by use of ground state electron density $n(r)$, which turned out to be sufficient. From their studies they also showed the existence of a universal functional $F_{HK}[n(r)]$. Provided the numeral value of the particles is $N = \int n(r)(r)dr$ is held constant, this functional can be minimized with respect to the variations in electron density given that an external potential V(r) is predetermined to obtain the actual value of the ground state energy E together with the electron density $n(r)$ of the system using the relation :

$$E[n(r)] = F_{HK}[n(r)] + \int V(r)n(r)d^3r$$

3.10 KOHN SHAM EQUATIONS

In the Kohn-Sham approximation, the approach is similar to the Hatree-Fock approximation as the Kohn-Sham equations are treated as one-particle equations describing the properties of solids from first principles. However, in Kohn-Sham approximation, Kohn & Sham (1965), the N electron system as defined in the Hatree-Fock approximation is reduced into N non-interacting one-electron systems also known as Kohn-Sham orbitals. However, the big challenge of coming up with accurate and time

efficient methods that can solve the Kohn-Sham equations sufficiently was encountered. Other methods such as those using pseudopotentials were proposed. In this case the static atomic cores are substituted with a pseudo potential as well as a set of pseudo-valence states orthogonalized to reproduce the elemental states are applied, Wimmer et al. (1981); Kerker (1980). The Physicists, Kohn and Sham came up with a integrated collection of differential equations which they used to calculate the density at ground-state $n_0(r)$ of a non-interacting system. The aim of Kohn-Sham approach was to replace the many-body interacting system which obeys the many-body general Hamiltonian equation given by equation 3.5.2, which is difficult to solve, with an auxiliary system. According to Kohn and Sham, the original interacting system is assumed to have ground state charge density matching that of the non-interacting system. Following this assumption, independent-particle equations describing the non-interacting system are created and are assumed to be solved exactly regardless of the presence of challenging many-body terms present in the exchange-correlation functional of the electronic density. Solving the generated Kohn-Sham equations leads to electronic ground state density as well as energy of the interacting system whose accuracy is limited to the approximations of the exchange-correlation functional employed. The definite calculations are carried out using the auxiliary independent-particle system described by Hamiltonian H^{σ}_{aux}. Hartree atomic units are used as $\hbar = m_e = 1$ and the Hamiltonian is simplified as in equation 3.10.1;

$$H^{\sigma}_{aux} = -\frac{1}{2}\nabla^2 + V^{\sigma}(r) \tag{3.10.1}$$

The potential $V^{\sigma}(r)$ takes a form that is not specified at this point. The squares of the orbitals of each spin contribute to the density of the auxiliary system as expressed by eqn 3.10.2:

$$n(r) = \sum_{\sigma}\sum_{i=1}^{N^{\sigma}} |(\psi^{\sigma}_i(r))|^2 \tag{3.10.2}$$

The particle has an independent energy defined as;

$$T_s = \frac{1}{2}\sum_{\sigma}\sum_{i=1}^{N^{\sigma}} |\nabla\psi^{\sigma}_i|^2 \tag{3.10.3}$$

Classically, the Coulomb self interaction energy of electron density can be defined as;

$$E_{Hartree}[n] = \frac{1}{2}\int d^3r d^3r' \frac{n(r)n(r')}{|\mathbf{r\text{-}r'}|} \tag{3.10.4}$$

The interacting many-body problem can be defined using the Kohn-Sham method at the ground state by involving the Hohenberg-Kohn expression in the form,

$$E_{KS} = T_s[n(r)] + \int dr V_{ext}(r)n(r) + E_{Hartree}[n(r)] + E_{11}[n(r)] + E_{XC}[n] \tag{3.10.5}$$

The nuclei and other external fields give rise to an external potential represented by $V_{ext}(r)$ and the interaction between nuclei is given by E_{11}. Thus, a system with electrons and nuclei has a Hamiltonian with potential interactions given by the sum of the terms V_{ext}, $E_{Hartree}$ together with E_{11}. It is difficult to determine the electron-electron energy functional of the Hohenberg-Kohn system. In a synthetic system, the energy is a sum of different energies which include the kinetic energy of the non-interacting electrons, energy due to interaction between the electrons and the nuclei, coulomb energy together with the exchange-correlation energy. The latter energy is unknown and need to be determined using iterative steps, which are used to obtain the self-consistent electron density of the Kohn-Sham Schrödinger equation. The many electron problem can be solved using DFT by following some simple steps iteratively;

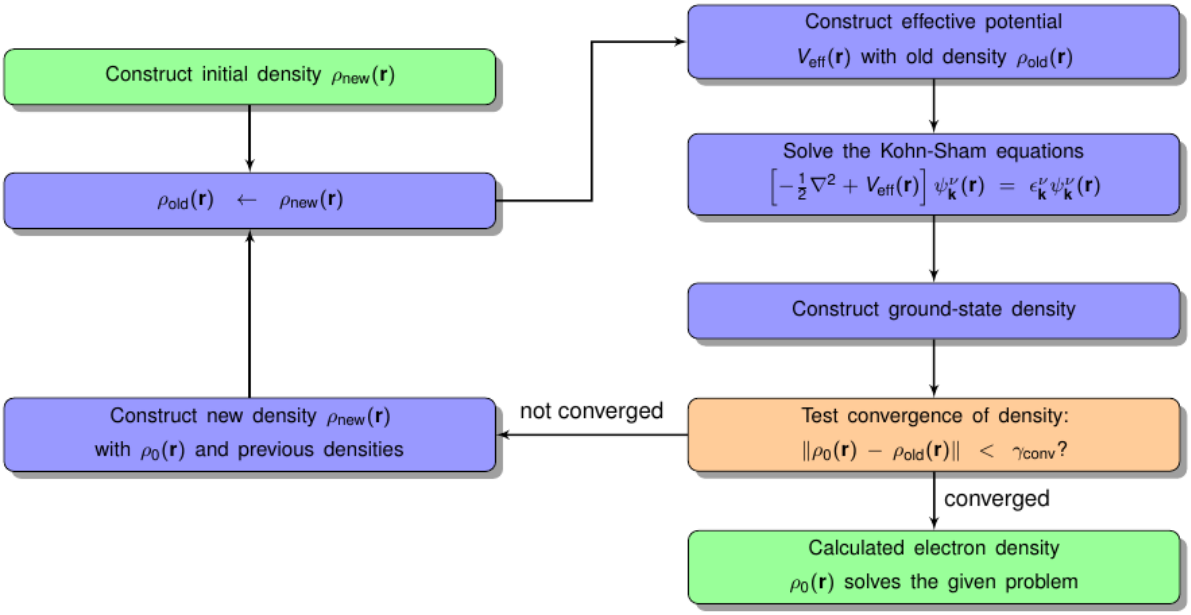

Figure 3.10.1: An illustration of the self consistent loop

The solution obtained following the process is self-consistent. The equations can only be solved if the exchange correlation functional is defined. However, as mentioned earlier the exact form of the functional is unknown and need to be approximated.

3.11 EXCHANGE-CORRELATION ENERGY

3.11.1 Local Density Approximation

According to Perdew & Zunger (1981), the exchange-correlation energy of an electron considered to be in a homogeneous electron gas whose density is $n(r)$ can be used to determine the value of the term $E_{EX}[n(r)]$ as given by equation 3.11.1;

$$E_{XC}^{LDA}[n(r)] = \int E_{EX}[n(r)]n(r)dr \tag{3.11.1}$$

Local Density Approximation functionals when used in different calculations tend to reproduce the ground state accurately when compared to the experimental data. For example, according to Korir et al. (2011), the LDA approximation reproduced the bulk properties and structural properties of 4d transition metal carbides and nitrides (TMCNs). However, LDA is unable to accurately determine the charge density, Leung et

al. (1991), and hence some properties such as magnetic structure are wrongly predicted. Another failure of this method was reported by Grüning et al. (2006) whereby it could not predict the band gap of semiconductors accurately. On the other hand, LDA works well in some material, especially in some simulations such as equations of state, elastic constants, among other properties of silicates as well as oxides in both crystalline and amorphous states, Da Silva et al. (1999).

3.11.2 Generalized Gradient Approximation

Generalized Gradient Approximation method was developed so as to correct the drawbacks associated with the LDA method. Unlike in LDA, GGA uses the gradient of the charge density in the E_{XC} functional. This functional is a great improvement to the previous approximation as it considers the inhomogeneity of the electron gas. Thus, the GGA approximation is a functional of charge density which is taken from a specific point together with the charge density's first-order gradient taken at the same point as the charge density, Perdew et al. (1998). For each particle in the electron gas, the exchange-correlation energy is written in the form;

$$E_{XC}^{GGA}[n] = \int d^3r f(n, \Delta n) \tag{3.11.2}$$

For small molecules, GGA gives better results in terms of energy, although, it is computationally expensive as it takes more time due to the added terms compared to LDA. GGA improves the prediction of the ground state properties of materials with light atoms and molecules and also predict the correct magnetic properties of transition metals compared to LDA, Singh & Nordström (2006). According to Proynov et al. (1995), in spite of these advantages, GGA fails to treat the hydrogen bond accurately which results into softening of bonds.

3.12 BASIS SET OF WAVEFUNCTIONS

The Kohn-Sham orbitals of both atoms and molecules can be described by use of a basis set of wavefunctions. For crystalline materials such as solids, the wavefunctions can be

reduced by considering a single unit-cell to represent the entire crystal. This case is considered since for periodic systems the single unit cells are a representation of the repeated units in all directions. Thus, the wavefunctions required for the simulation can be represented as the sum of plane waves, whereby the wave vectors are the reciprocal lattice vectors of the crystals and are referred to as basis set. The plane wave basis set has an associated error which can be solved by increasing the size of the single unit-cell or the k-point sampling of the energy which is the Brilloiun zone. The first Brillouin zone is termed as the primitive cell in the reciprocal space, Rappe et al. (1990).

3.13 BAND CALCULATIONS IN PERIODIC SYSTEMS

An electron within a solid possess a range of energies which are best described using the band structure. Allowed quantum mechanical wave functions for the electrons in periodic lattices of atoms are examined and thereafter, the information can be used to study the bands as well as the band gaps of the system. The band theory provides information on the physical properties as well as optical properties, which is used as basis for the development of devices. Some of the common methods for band calculations are pseudopotential and projected augmented waves (PAW), discussed in the proceeding subsections.

3.13.1 PSEUDOPOTENTIAL METHOD

The self-consistent equations as developed by Kohn and Sham are solved via approximations since it is difficult to obtain the exact solution. Following these numerical approximations, new developments have emerged in the field of materials modelling so as reduce computational cost. This is achieved for example by enhancing rapid convergence but ensuring the accuracy and outcome of the simulations are not compromised. As mentioned in the earlier sections, atoms are comprised of electrons and nuclei as the major components. The electrons are further classified into core and valence electrons. The core electrons which are close to the nuclei are highly oscillating and they possess high kinetic energy. With this characteristic they require more plane waves to expand

them as their wave functions and have numerous nodes. This implies that the method of including the core electrons is generally computationally expensive. When considering the electrons that influence the properties of a system, the core electrons have less effect and also their participation in bonding is less regardless of them requiring large number of plane waves. The solutions obtained by use of many plane waves would mean high kinetic energy compared to low energy of the valence electrons which are very important in bonding. The core and valence electrons are properly described in the pseudopotential so as to allow the adequate involvement of plane wave basis sets when performing electronic structure calculations of different systems, Rappe et al. (1990). It is worth noting that the properties of a material are dependent on the valence electrons present.

As such, first-principle pseudopotential methods were developed, which consider only the active valence electrons, Marvin & Volker (1970) and excludes the inner core electrons together with the strong potential binding the core to the nuclei. According to the plane wave pseudopotential theory, the wavefunctions of the inactive core electrons are replaced with weak and slowly varying pseudopotential. This results into less expensive computational cost compared to the all-electron methods which have to include a lot of plane waves to represent the inner states. This is as illustrated in Figure 3.13.1.

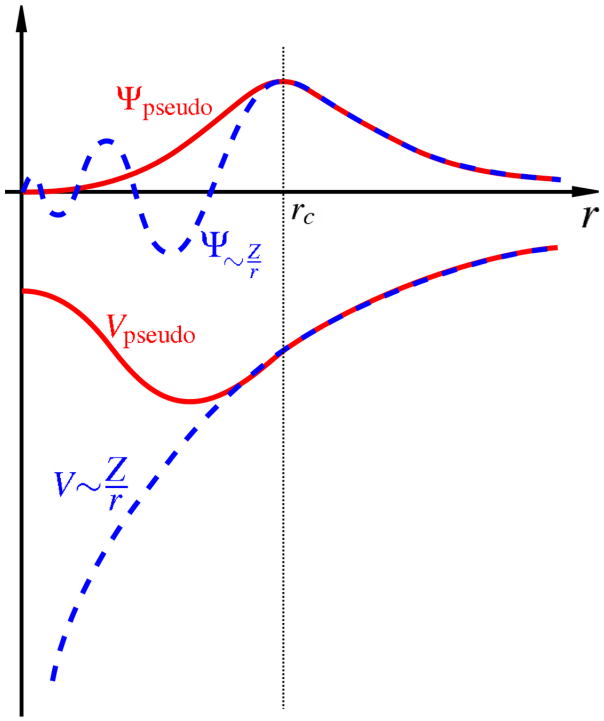

;

Figure 3.13.1: The true potential of the nucleus (solid lines) and the pseudopotential (dashed lines), Payne et al. (1992).

According to the pseudopotential approach, the system has both ionic cores together with valence electrons. Each ion experiences a force which is a sum of electrostatic forces imposed by ionic cores and the force due to the valence electrons. Depending on the system of interest, different pseudopotentials can be used such as ultra-soft, Vanderbilt (1990), norm-conserving, Hamann et al. (1979) as well as the projector augmneted wave (PAW), Kresse & Joubert (1999a). The upper core states are included in the PAW method when performing the self consistent iterations, thus, making the method unique over the others.

3.13.2 AUGMENTED PLANE WAVE METHOD

In this method, the core state are surrounded by the valence states. The valence wavefunctions tend to possess rapid oscillations especially near the ion cores. This is due to the orthogonality property between the valence and the core states. However, this imposes some problems since more fourier components such as very fine mesh are needed so as to accurately describe the wavefunctions. The method developed by Blöchl solves the problem by ensuring that the rapid oscillating wavefunctions are transformed into

smooth wavefunctions. The smooth wavefunctions become more computationally usable, Bloch (1929).

3.14 K-POINT GRID

In DFT calculations, the Brillouin zone is sampled using the Monkhorst-Pack grid and gamma point. In this sampling technique, special points in the Brillouin zone are generated as well as their integration weights. This information is very useful as it helps in integrating periodic functions when working in the k-space, Hendrik & James (1976). The choice of the integration plays a key role in the accuracy of integration. Thus, the Monkhorst-Pack technique helps in sampling the Brillouin zone as a whole and also integration of specific portions of the complete Brillouin zone. Depending on the symmetry of the cell used, the points on the Brillouin zone can be reduced, which in return reduces the computational cost.

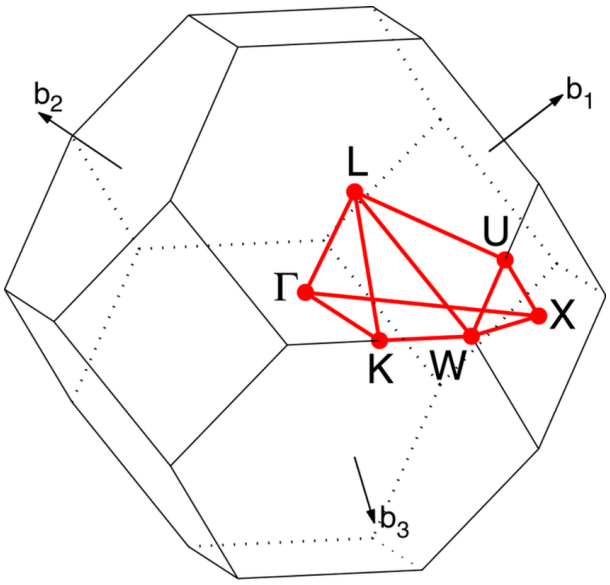

Figure 3.14.1: An example of brillouin zone for a FCC crystal structure system, Setyawan & Curtarolo (2010)

.

Figure 3.14.1 represents a BZ along various high symmetry points with b1, b_2, b_3 as the reciprocal base vectors.

3.15 ELASTIC CONSTANTS

3.15.1 Hooke's law

In a solid, the arbitrary displacement is given by equation 3.15.1;

$$(\vec{R})(\vec{r}) = u(\vec{r})\hat{x} + v(\vec{r})\hat{y} + w(\vec{r})\hat{z} \tag{3.15.1}$$

while the strain components are represented as follows

$$\begin{aligned} e_1 = e_{xx} &= \frac{\partial u}{\partial x} \\ e_2 = e_{yy} &= \frac{\partial v}{\partial y} \\ e_3 = e_{zz} &= \frac{\partial w}{\partial z} \\ e_4 = e_{yz} &= \frac{\partial v}{\partial z} + \frac{\partial w}{\partial y} \\ e_5 = e_{zx} &= \frac{\partial w}{\partial x} + \frac{\partial u}{\partial z} \\ e_6 = e_{xy} &= \frac{\partial u}{\partial y} + \frac{\partial v}{\partial x} \end{aligned} \tag{3.15.2}$$

The relationship between strain and stress can be summarised using the Hooke's law and is valid for small distortions whereby stress is directly proportional to the strain with a constant of proportionality. Materials have elastic domains which give the range of strain where the law applies. Higher order effects are noted beyond the elastic domain and materials become deformed and may even be damaged as illustrated in Figure 3.15.1, William D. Callister (2013). Thus, it is important to ensure that the material is within the elastic domain when the material is under strain.

The Hooke's law is given by the equation 3.15.3;

$$F = -k.x \tag{3.15.3}$$

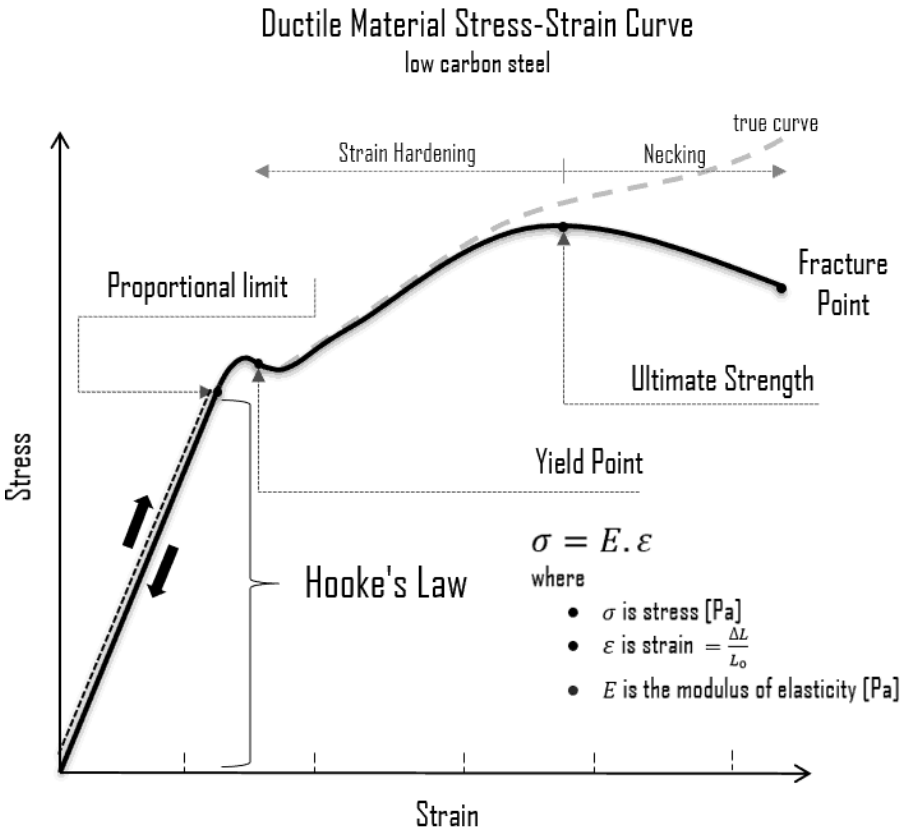

Figure 3.15.1: Strain vs stress curve, Ashby et al. (2007).

According to this equation, the strain is directly proportional to stress and the law usually describes continuous elastic materials. This implies that the material can be stretched along one direction, compressed in another direction as well as sheared and the processes take place at the same time. The stress (σ) and strain (ϵ) are described as 2nd rank tensors;

$$\sigma_{ij} = \sum_k \sum_l \gamma_{ijkl} \epsilon_{kl} \tag{3.15.4}$$

Hooke's law can be expressed using index notation as follows;

$$\epsilon_{ij} = S_{ijkl} \sigma_{kl} \tag{3.15.5}$$

Strain tensor is given by ϵ_{ij} and the fourth order compliance tensor by S_{ijkl} while σ_{kl} represents the stress tensor. The elasticity tensor S_{ijkl} is a tensor of rank 4 with 81

components. Due to symmetric nature of the strain, stress and elasticity tensors, 21 components from the total of 81 are independent. Additional symmetries reduces the independent components further. According to Cauchy, every component of the stress tensor couples linearly with strain tensor and can be expressed in matrix form as shown in equation 3.15.6 Glass & Winicour (1973);

$$\begin{bmatrix} \epsilon_{11} \\ \epsilon_{22} \\ \epsilon_{33} \\ \epsilon_{23} \\ \epsilon_{13} \\ \epsilon_{12} \\ \epsilon_{32} \\ \epsilon_{31} \\ \epsilon_{21} \end{bmatrix} = \begin{bmatrix} S_{1111} & S_{1122} & S_{1133} & S_{1123} & S_{1113} & S_{1112} & S_{1132} & S_{1131} & S_{1121} \\ S_{2211} & S_{2222} & S_{2233} & S_{2223} & S_{2213} & S_{2212} & S_{2232} & S_{2231} & S_{2221} \\ S_{3311} & S_{3322} & S_{3333} & S_{3323} & S_{3313} & S_{3312} & S_{3332} & S_{3331} & S_{3321} \\ S_{2311} & S_{2322} & S_{2333} & S_{2323} & S_{2313} & S_{2312} & S_{2332} & S_{2331} & S_{2321} \\ S_{1311} & S_{1322} & S_{1333} & S_{1323} & S_{1313} & S_{1312} & S_{1332} & S_{1331} & S_{1321} \\ S_{1211} & S_{1222} & S_{1233} & S_{1223} & S_{1213} & S_{1212} & S_{1232} & S_{1231} & S_{1221} \\ S_{3211} & S_{3222} & S_{3233} & S_{3223} & S_{3213} & S_{3212} & S_{3232} & S_{3231} & S_{3221} \\ S_{3111} & S_{3122} & S_{3133} & S_{3123} & S_{3113} & S_{3112} & S_{3132} & S_{3131} & S_{3121} \\ S_{2111} & S_{2122} & S_{2133} & S_{2123} & S_{2113} & S_{2112} & S_{2132} & S_{2131} & S_{2121} \end{bmatrix} \begin{bmatrix} \sigma_{11} \\ \sigma_{22} \\ \sigma_{33} \\ \sigma_{23} \\ \sigma_{13} \\ \sigma_{12} \\ \sigma_{32} \\ \sigma_{31} \\ \sigma_{21} \end{bmatrix} \tag{3.15.6}$$

For homogeneous systems, 81 independent compliance coefficients are required and defined as shown in equation 3.15.7;

$$\begin{bmatrix} \sigma_{11} \\ \sigma_{22} \\ \sigma_{33} \\ \sigma_{23} \\ \sigma_{13} \\ \sigma_{12} \\ \sigma_{32} \\ \sigma_{31} \\ \sigma_{21} \end{bmatrix} = \begin{bmatrix} C_{1111} & C_{1122} & C_{1133} & C_{1123} & C_{1113} & C_{1112} & C_{1132} & C_{1131} & C_{1121} \\ C_{2211} & C_{2222} & C_{2233} & C_{2223} & C_{2213} & C_{2212} & C_{2232} & C_{2231} & C_{2221} \\ C_{3311} & C_{3322} & C_{3333} & C_{3323} & C_{3313} & C_{3312} & C_{3332} & C_{3331} & C_{3321} \\ C_{2311} & C_{2322} & C_{2333} & C_{2323} & C_{2313} & C_{2312} & C_{2332} & C_{2331} & C_{2321} \\ C_{1311} & C_{1322} & C_{1333} & C_{1323} & C_{1313} & C_{1312} & C_{1332} & C_{1331} & C_{1321} \\ C_{1211} & C_{1222} & C_{1233} & C_{1223} & C_{1213} & C_{1212} & C_{1232} & C_{1231} & C_{1221} \\ C_{3211} & C_{3222} & C_{3233} & C_{3223} & C_{3213} & C_{3212} & C_{3232} & C_{3231} & C_{3221} \\ C_{3111} & C_{3122} & C_{3133} & C_{3123} & C_{3113} & C_{3112} & C_{3132} & C_{3131} & C_{3121} \\ C_{2111} & C_{2122} & C_{2133} & C_{2123} & C_{2113} & C_{2112} & C_{2132} & C_{2131} & C_{2121} \end{bmatrix} \begin{bmatrix} \epsilon_{11} \\ \epsilon_{22} \\ \epsilon_{33} \\ \epsilon_{23} \\ \epsilon_{13} \\ \epsilon_{12} \\ \epsilon_{32} \\ \epsilon_{31} \\ \epsilon_{21} \end{bmatrix} \tag{3.15.7}$$

In equation 3.15.7, C_{ijkl} represent the elasticity tensor.

The anisotropic materials experience symmetry of the Cauchy stress tensor and this also applies to the Hooke's law where $C_{ijkl} = C_{jikl}$

Due to symmetry, the 81 elastic constants are reduced to 36 as follows;

$$\begin{bmatrix} \sigma_{11} \\ \sigma_{22} \\ \sigma_{33} \\ \sigma_{23} \\ \sigma_{13} \\ \sigma_{12} \end{bmatrix} = \begin{bmatrix} C_{1111} & C_{1122} & C_{1133} & C_{1123} & C_{1113} & C_{1112} \\ C_{2211} & C_{2222} & C_{2233} & C_{2223} & C_{2213} & C_{2212} \\ C_{3311} & C_{3322} & C_{3333} & C_{3323} & C_{3313} & C_{3312} \\ C_{2311} & C_{2322} & C_{2333} & C_{2323} & C_{2313} & C_{2312} \\ C_{1311} & C_{1322} & C_{1333} & C_{1323} & C_{1313} & C_{1312} \\ C_{1211} & C_{1222} & C_{1233} & C_{1223} & C_{1213} & C_{1212} \end{bmatrix} \begin{bmatrix} \epsilon_{11} \\ \epsilon_{22} \\ \epsilon_{33} \\ \epsilon_{23} \\ \epsilon_{13} \\ \epsilon_{12} \end{bmatrix} \tag{3.15.8}$$

Apart from the symmetry of the cauchy stress tensor, the elastic constants are further reduced by the shear components relationship given by $ij = ji$. Also, the diagonal components of the 6 x 6 matrix have a common characteristic in which they have a relationship to the normal stress as well as strain. With these features the Voight notation can be introduced to reduce the indices 11, 22, 33, 23, 13, 12 to 1, 2, 3, 4, 5, 6, respectively. Further, the other 30 elastic constants due to shear relationship are divided by two. After the reductions are performed a total of 21 components remain resulting into 21 elastic constants, Menéndez-Proupin et al. (2011), Jiang et al. (2008).

$$C_{ij} = \begin{pmatrix} C_{11} & C_{12} & C_{13} & C_{14} & C_{15} & C_{16} \\ & C_{22} & C_{23} & C_{24} & C_{25} & C_{26} \\ & & C_{33} & C_{34} & C_{35} & C_{36} \\ & & & C_{44} & C_{45} & C_{46} \\ & & & & C_{55} & C_{56} \\ & & & & & C_{66} \end{pmatrix} \tag{3.15.9}$$

When elastic deformation take place, there is a corresponding change in energy. For example, when a spring is used to illustrate the Hooke's law, compressing the spring

describes how energy is stored in a spring while expanding the string to the original state releases the energy. This can be described as follows;

$$F = -k.x \tag{3.15.10}$$

Upon integration of the Hooke's law with respect to the x, one obtains the energy of the system as

$$E = \frac{1}{2}k.x^2 \tag{3.15.11}$$

From equation 3.15.11, the elastic energy is proportional to both elastic constant and the square of the strain.

3.15.2 Voight, Reuss and Hill Averaging Schemes

The mechanical properties of a material such as bulk modulus, shear modulus and elastic constants can be determined using Voight-Reuss-Hill averaging schemes. Using the Voight method means that the strain is assumed to be uniform and as a result it gives values on the upper limit of the numerical data obtained. Contrary to the upper limit data from the Voight method, the Reuss method gives the lower limit of the data obtained assuming that stress is uniform. The average of the two methods is obtained by use of Hill method, Ching. et al. (2009), Shein & Ivanovskii (2008).

Using Voight method, bulk and shear moduli are given respectively as ;

$$B_{\mathrm{v}} = \frac{2}{9}[C_{11} + C_{12} + 2C_{13} + \frac{1}{2}C_{33}] \tag{3.15.12}$$

$$G_{\mathrm{v}} = \frac{1}{30}[C_{11} + C_{12} + 2C_{33} - 4C_{13} + 12C55 + 12C_{66}] \tag{3.15.13}$$

Reuss method calculates the bulk and shear moduli as shown in equation 3.15.14 and 3.15.15

$$B_R = \frac{[5C_{55}C_{66}(C_{11} + C_{12})C_{33} - 2C_{12}^2]}{C_{11} + C_{12} + 2C_{33} - 4C_{12}} \tag{3.15.14}$$

$$G_R = \frac{[5C_{55}C_{66}(C_{11} + C_{12})C_{33} - 2C_{12}^2]}{2\{3B_V C_{55}C_{66} + [(C_{11} + C_{12})C_{33} - 2C_{12}^2](C_{55} + C_{66})\}} \tag{3.15.15}$$

The average bulk and shear moduli from the voight and reuss methods as given by Hill's method are;

$$B_H = \frac{1}{2}(B_V + B_R) \tag{3.15.16}$$

$$G_H = \frac{1}{2}(G_V + G_R) \tag{3.15.17}$$

3.15.3 Vicker's Hardness

The resistance of a material to scratching defines its hardness, Q. Yang et al. (2000). Hardness is dependent on several properties such as inter-atomic distances, co-ordination and nature of chemical bonds among others. Up to date, there are several methods that can be used to determine this physical property successfully. Among them is Mohs, Vickers, Shore test, Brinell and Knoop test, Tabor (1954), R. Smith & Sandly (1922), Hill et al. (1989). The Vickers test method is as illustrated in figure 3.15.2.

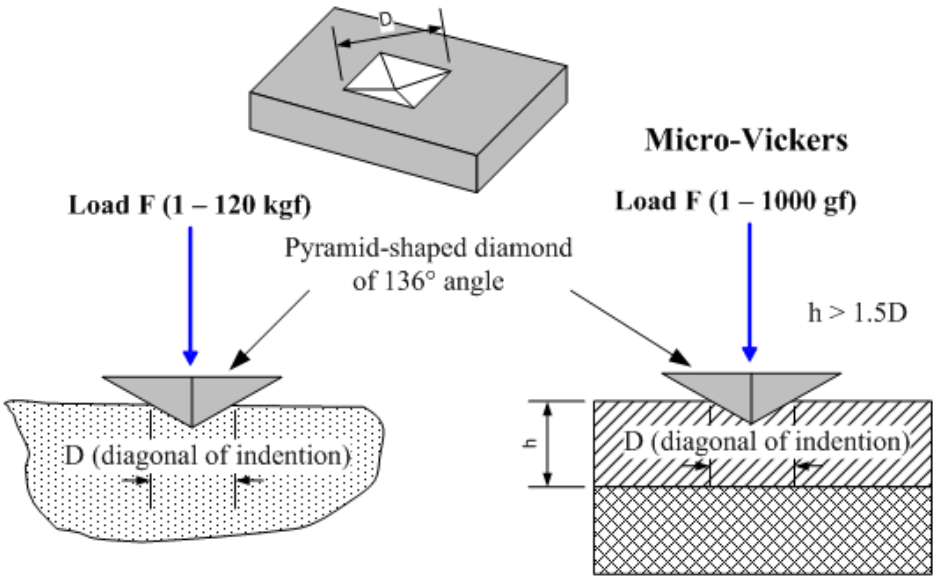

Figure 3.15.2: An illustration of Vickers hardness test, Ghose et al. (2014).

In this study, the hardness of NbC and NbN was determined theoretically using Vickers method given by equation 3.15.18, Xing Qiu et al. (2011);

$$H_v = 2(k^2 G^{0.585}) - 3 \tag{3.15.18}$$

In this equation, k is the Pugh's ratio given by the ratio B/G. G is the shear moduli while

B is the bulk modulus. It is important to note that the hardness depends on the elastic constants of the material and thus there is a need to determine the elastic properties of the material. Elastic constants of a materials describes how the system behaves when force is applied on it and the elastic properties describe the relation between strain and stress as explained earlier.

3.16 MOLECULAR DYNAMICS

3.16.1 Theory of Molecular Dynamics

This section will lay the background theory of molecular dynamics as well as the factors that should be considered when extracting the elastic constants from MD simulations. However, before the MD simulations are set, it is always critical to decide on the most appropriate ensemble that suites the calculation. The ensembles are large collections of systems possessing common macroscopic properties which describe the microscopic particle interactions. There are several ensembles that can be applied in the MD calculations which include the microcanonical (NVE), canonical ensemble (NVT) and NPT ensembles. For the NVE calculation both the total energy, volume and number of particles are conserved as it occurs in an isolated system. In NVT, the number of particles, volume and temperature are conserved. The temperature remains constant in NVT to resemble that of a system in a heat bath. For NPT, the system is assumed to be exposed to conditions such as pressure. The macroscopic properties including temperature, energy or pressure are obtained from the averages performed over the ensemble members following time evolution whereby members of the ensemble under initial microscopic conditions evolve. In statistical mechanics, the microscopic state which is a system with N particles can be determined using generalised positions and momenta given as

$$\mathbf{q} = (q_1, q_2, ..., q_{3N})$$

and

$$\mathbf{p} = (p_1, p_2, ..., p_{3N})$$

respectively of each particle. The space containing these points is known as phase space. When determining the averages of these ensembles, the distribution function of the phase space $f(\mathbf{x}, t)$ which is defined as $f(\mathbf{x}, t) = f(\mathbf{x}, t)d\mathbf{q}d\mathbf{p}$ is introduced as the fraction of all accessible states in the volume $d\mathbf{x}$ of the entire phase space. Thus, the average can be determined as;

$$\langle A \rangle = \int f(\mathbf{x}, t)A(\mathbf{x})d\mathbf{x} \tag{3.16.1}$$

For the two commonly used ensembles, that is, micro canonical (NVE) and canonical ensemble (NVT), their distribution factors are perfomed to a constant normalisation factor as;

$$f_{NVE}(x) = \sigma(H(x) - E) \tag{3.16.2}$$

$$f_{NVT}(x) = exp(-\frac{H(x)}{k_B T}) \tag{3.16.3}$$

k_B is the Boltzmann constant, T is the temperature, E is energy and H is the hamiltonian.

3.16.2 Molecular Dynamics Approach Basics

DFT is a technique used for static simulations whereby calculations are performed at 0 K. For static simulations, kinetic energy from thermal motion is absent as well as negligence of zero-point energy being evident. If zero-point energy is included in the calculation it would imply that the unit-cell parameters would expand by approximately 0.2%, Wu & Cohen (2006). The effect of atomic vibration is very important when studying materials at elevated temperatures. Some of the commonly used techniques in these simulations include lattice and molecular dynamics. These methods include the thermal vibrations which are present when temperatures are raised.

According to Vocadlo & Dobson (1999), lattice dynamics deal with systems in a simulation box containing harmonic oscillators. The frequencies of the oscillators change with cell volume. This method determines the motion of atoms assuming that they take the form of wave-like lattice vibrations. Also quasiharmonic approximation of phonons is used to determine the motion. The individual particles are assumed to vibrate collectively

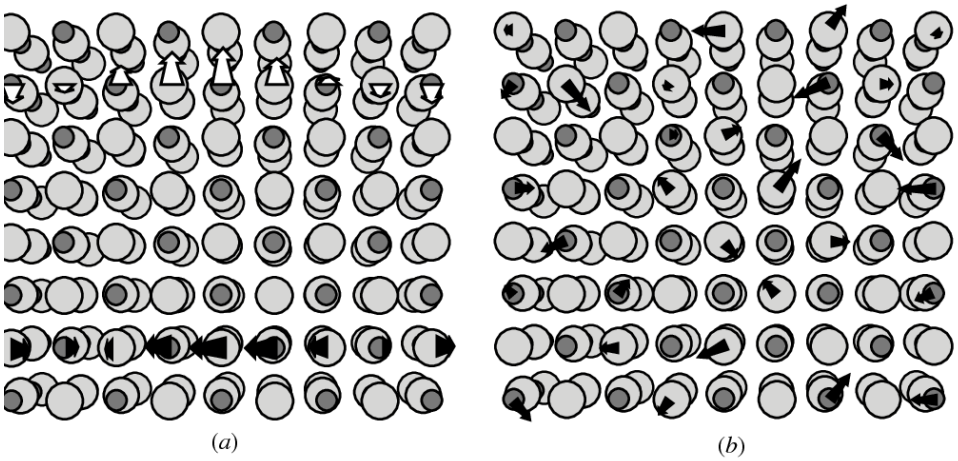

Figure 3.16.1: An illustration of (a) lattice dynamics and (b) molecular dynamics, Vocadlo & Dobson (1999).

as a phonon. As illustrated in figure 3.16.1 (a), the vibration of the atoms is assumed to be in the form of quantized harmonic oscillator. However, one of the shortcoming of this technique is that it ignores the anharmonic effects experienced as a result of phonon-phonon interactions which is crucial at high temperatures.

On the other hand, MD simulations treat the motion of individual particles explicitly and describe the time-dependent behaviour of the system atomic levels. This technique simulates the motion of atoms under predefined conditions, which may include temperature, pressure and external forces among other conditions. After setting the predefined conditions several properties can be studied such as elastic properties and dynamical processes. Properties such as diffusion coefficients and phase diagrams as well as response functions can be studied. Radial distribution functions (RDF) are some response functions that can also be studied using molecular dynamics. In MD, external corrections are unneccessary unlike in the case of DFT calculations. Here, atoms are allowed to move in discrete time steps denoted as t which is usually within the range of 1-3 fs. During these time steps one can visualize how the system is equilibrating by use of relevant visualization software. By use of classical molecular dynamics, hundred of atoms can be studied as it allows long range interactions. However, this method has its own drawbacks which limits its usage in the field of material science. Classical MD neglects electronic effects and also raises the need for adequately parametrized force field

for the simulation to be performed. These drawbacks led to the developments of *ab initio* molecular dynamics (AIMD) approach which uses DFT as the substitute for the interatomic force fields found in a dynamic setting, Martin (2004).

Quantum mechanical MD allows atoms to move according to Newtonian classical mechanics for a set of atoms provided that the initial configuration is provided. This is achieved through numerical integration where time is discretized into small time intervals referrred to as time step. There are noticeable changes on both the position and momenta of the nuclei as the simulations are performed from one time step to the next while solving the Newton's equations. At each step, the interactions between atoms which give rise to the interatomic forces can be determined using DFT or classical potentials. Initially, a particle which is located at position $\vec{r_0}$ and with velocity $\vec{v_0}$ is subjected to force F within the set duration of time t. As a result, the particle moves to new position $\vec{r_t}$ which according to classical mechanics can be expressed as;

$$r(\vec{t}) = \vec{r_0} + (\vec{v_0}t + 0.5\vec{a}t^2)$$

$$\vec{a} = \frac{\vec{F}}{m} \tag{3.16.4}$$

$$\vec{F} = \frac{dU}{\vec{dr}} \tag{3.16.5}$$

An assumption is made that the acceleration is constant in the given time interval, t, although this acceleration is not constant. However, this approximation is improved by choosing a small time step during the simulation. The electron energies are determined by assuming that the sub-system of the electron is at its ground state and the nuclei's positions are static when each time step comes to a completion. This is the Born-oppenheimer approximation described earlier. Another important assumption is the conservation of both the kinetic energy of the nuclei as well as electron energy at ground state and the volume is fixed. When a simulation is performed without controlling the temperature, the MD is treated as a microcanonical ensemble. Here, the number of

particles, N, the volume, V and energy, E are constant (i.e constant N, V, E). Through this ensemble, it is difficult to predict the resulting temperature and can be high especially when incorrect geometry is used at the beginning, giving rise to high potential energy. For such cases, a thermostat algorithm is applied so as to control the temperature where temperature and velocities of the particle are related to each other via the equipartition principle of energy as follows:

$$E = \frac{3}{2} N K_{\mathrm{B}} T_{inst} = \sum_{i=1}^{N} \frac{m_i v_i^2}{2} \tag{3.16.6}$$

where E is the total kinetic energy, N is the number of particles and K_{B} is the Boltzmann constant and T_{inst} is the instantaneous temperature.

According to Woodcock (1971), several thermostat algorithms can be applied at every timestep, the simplest being the velocity Verlet algorithm given as;

$$\vec{r_i}(t + \Delta t) = \vec{r_i}(t) + \Delta t \vec{v_i}(t) + \frac{\Delta t^2}{2m_i} \vec{F_i}(t + \Delta t) \tag{3.16.7}$$

$$\vec{v_i}(t + \Delta t) = \vec{v_i}(t) + \frac{\Delta t^2}{2m_i} (\vec{F_i}(t + \vec{F_i}(t + \Delta t)) \tag{3.16.8}$$

Δt is the integration time step.

However, this kind of algorithm is not efficient as it is considered to be more realistic when a system under constant temperature is studied. Such systems tend to mimic the experimental situations closely. Nose-Hoover thermostat is considered to be more efficient system's thermostat for controlling the temperature as it applies friction coefficient and a heat bath Q, Nosé (1984) and Andersen (1980).

3.17 NUDGED ELASTIC BAND METHOD

Transition state theory can be used to study slow transition events. The theory is designed on some basics assumptions which include;

(a) A Boltzmann distribution can be established as well as being maintained since the reactant state rate is slow.

(b) A dividing surface whose dimension is D-1 can be identified to represent the point along the reacting trajectory from initial to final state which is crossed once. D represents the degrees of freedom present in the system. Graphically the dividing surface is the bottleneck for the transition, Jaffe et al. (1973).

Atoms in crystals are typically packed and different properties of these systems are determined at temperatures below the melting temperature. This allows the application of harmonic approximation into Transition State Theory (TST) in studies involving diffusion, Voter & Doll (1985).

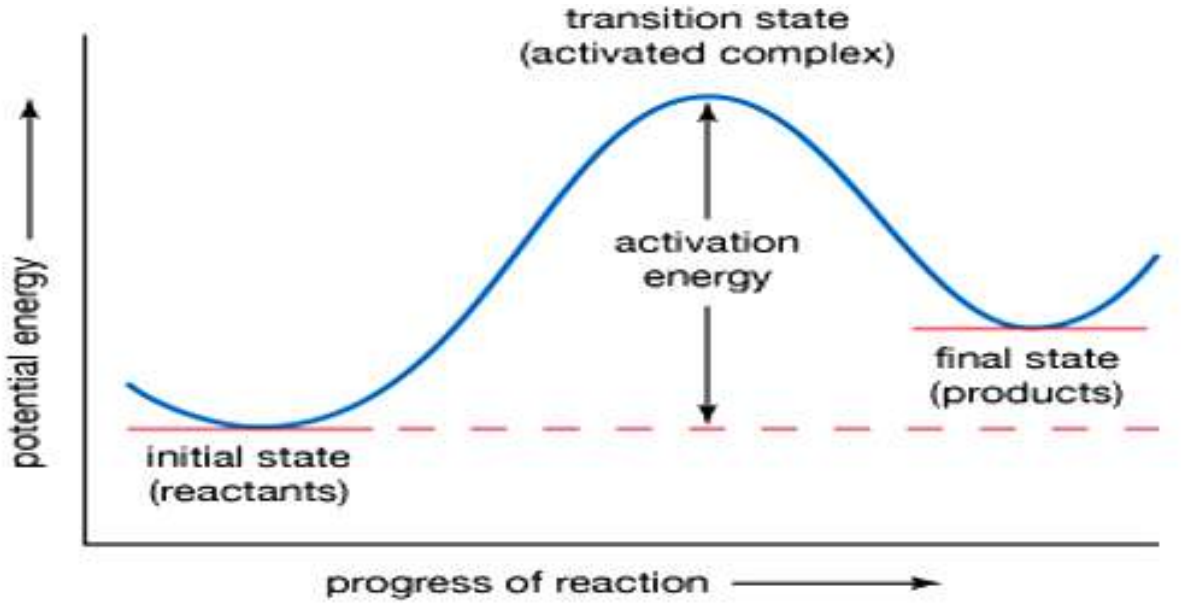

Figure 3.17.1: Illustration of transition states, Laidler (2022).

This makes the process of estimating the transition rates simple. The process of determining the optimal transition state only involve the search for lowest saddle points appearing at the edge of the basin of the potential energy representing the initial state. Thus, using both the energy and frequency of normal modes obtained at the saddle point as well as the initial state, the rate constant for the transition taking place around each saddle point can be obtained, Wert & Zener (1949),

$$k^{hTST} = \frac{\pi_i^{3N} \vec{v}_i^{init}}{\pi_i^{3N-1} \vec{v}_i^{SP}} e^{-\frac{(E^{SP}-E^{init})}{k_B T}} \tag{3.17.1}$$

Saddle point energy is E^{SP}, potential energy of the initial state is given by E^{init} while $\vec{v_i}$

are the normal mode frequencies. Here the quantities are evaluated at zero temperature using potential energy surface although the entropic effects are catered for through harmonic approximation. However, determining the saddle point is the main challenge. Atoms evolve around the two configurations and the minimum energy path (MEP) is used to describe the process. MEP represent the path connecting both the initial and final states. This quantity describes the chemical reactions as well as diffusion processes occurring in solids. The activation energy barrier is determined from the maximum in the potential energy obtained along the MEP. Along the MEP the force on each atom points along the path while the energy is stationary for perpendicular degree of freedom. As illustrated in Figure 3.17.1, the saddle point is the maximum point on the MEP on the potential energy surface.

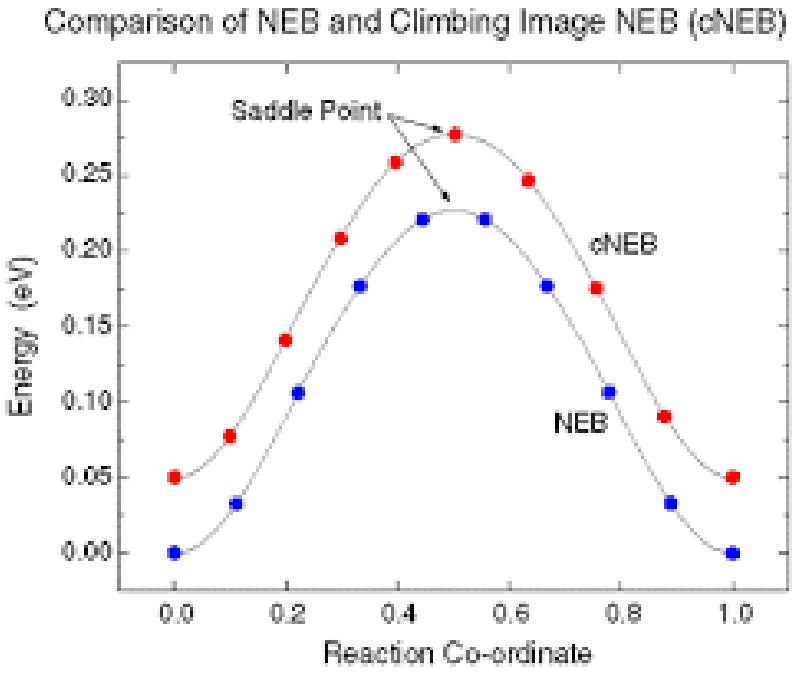

Figure 3.17.2: An illustration of Nudged Elastic Band theory and climbing image nudged elastic band. Retrieved from https://docs.mat3ra.com/models/auxiliary-concepts/nudged-elastic-band/#links

NEB is one of the method employed to determine the local maximum and is based on two point boundary condition, Jonsson et al. (1998). Between the two configurations, chains of images are generated and optimized simultaneously. This makes parallel computing suitable. The acting on the images is parallel to the chosen path ensuring better convergence to the MEP.

3.17.1 Plain Elastic Band, PEB

The NEB method can be classified as *chain of images* method which uses a series of images generated between the initial and final configurations. This is different from other methods that tend to start from a local minima and the path is found using a sequential manner. In the PEB method, several images are chosen and connected using springs of zero natural length which trace the path. This defines the object function to be minimized.

$$S^{PEB}\left(\vec{R}_1, ...\vec{R_{P-1}}\right) = \sum_{i=0}^{P} V(\vec{R}_i) + \sum_{i=1}^{P} \frac{Pk}{2}\left(\vec{R}_i - \vec{R}_{i-1}\right)^2 \quad (3.17.2)$$

On the R.H.S of equation 3.17.2, the first term represent the sum over the 'true' potential while the second term is the elastic force. The intermediate images are given by P, the strength of the springs joining two adjacent images is represented by k, i is the index while $\vec{R}_i$ is the vector position of individual images. When the above object function is minimized, the MEP can be obtained with respect to the intermediate images. For this condition to be achieved, the initial states and final states, $\vec{R}_i$ and $\vec{R}_p$, respectively, are fixed. However, MEP suffers from convergence issues and there is a need to modify equation 3.17.2 in order to achieve more accurate results.

3.17.2 Climbing image NEB method

The NEB method can undergo a small modification to give rise to the climbing image NEB method. From the earlier method, the shape of the MEP as shown on Figure 3.17.1 is retained while a rigorous convergence is obtained to the saddle point. The regular NEB is performed and after a few iterations, the image associated with high energy is obtained.

$$\begin{aligned} F_{imax} &= -\nabla E(\vec{R_{imax}}) + 2\nabla E(\vec{R_{imax}})|_{||} \\ &= -\nabla E(\vec{R_{imax}}) + 2\nabla E(\vec{R_{imax}}) \cdot \vec{\tau_{imax}}\vec{\tau_{imax}} \end{aligned} \quad (3.17.3)$$

τ_i represent the normalized local tangent at image i, E is the energy of the system which is a function of all the atomic coordinates. From equation 3.17.3 F_{imax} is the full force as a result of potential with the component along inverted elastic band. It should be noted that the spring forces do not affect the maximum energy image.

The potential energy surface is moved up by the climbing image along the elastic band. Also, the potential surface is moved downwards perpendicular to the band. Convergence of the images in the band occurs at the MEP which helps in providing the reaction coordinate around the saddle point.

CHAPTER FOUR

METHODOLOGY

4.1 OUTLINE OF CALCULATION

The calculations in this work were carried out using Quantum ESPRESSO computer code, Giannozzi et al. (2009) together with Vienna *Ab initio* Simulation Package, Kresse & Furthmüller (2007). The two codes which are based on DFT were used to solve Kohn-Sham equations. In VASP, projector augmented wave (PAW) method is used. Some of the properties that can be described using DFT include equilibrium volume, lattice constants, electronic properties and mechanical properties among others. The DFT formalism is based on electronic density distribution *n(r)* instead of the many electron wave function, Kohn & Sham (1965). Before Kohn and Sham introduced the idea of electronic density distribution, many body systems were represented using the Hamiltonian equation given as;

$$\hat{H} = \sum_{i=1}^{N} \left(-\frac{\hbar^2}{2m_i}\nabla_i^2 + \frac{1}{2}\sum_{i=1}^{N}\sum_{j\neq i}^{N} \frac{Z_i Z_j}{4\pi\epsilon_0 |\mathbf{r}_i - \mathbf{r}_j|} \right) \tag{4.1.1}$$

r denotes spatial positions and Z the charges of the individual nucleus.

Density Functional Theory uses plane wave basis sets together with pseudopotentials. The electron-ion potential is described by a chosen type of pseudopotential. Here ultra-soft pseudopotentials and PAW were used to give all the required properties. The ultra-soft pseudopotential allows energies to converge with small number of plane waves which in return reduces the computational cost, Rappe et al. (1990). In this study, the plane wave self-consistent calculations were employing DFT methodology with generalized gradient approximation (GGA) for the exchange correlation functional using Perdew-Burke-Ernzerhof (PBE) scheme, Perdew et al. (1998). The kinetic energy cut-off was used to provide plane waves that best describes the system and it is worth noting that more plane waves give more accurate results although it's computationally expensive. Conjugate gradient minimization method, Štich et al. (1989) was used in ionic

relaxation process in order to minimize the Hellman-Feynman forces which exist among the constituent atoms. For periodic structures, the systems can be described in k-space. In such cases, the part covered by the k-points for any given system which is referred to as Brillouin zone was sampled using the Monkhorst-Pack grid where the grids are in x, y and z directions, Monkhorst & Pack (1976). The atomic positions were relaxed until the difference between forces is smaller than 10^{-3} a.u. After the relaxation, the total energies of the relaxed systems were extracted, from which different properties of the materials were obtained, Giannozzi et al. (2009).

4.2 EFFECTS OF DEFECTS

The compounds were simulated at their substoichiometric structures by use of supercell methods, Hull & Bacon (1984). The unit cells were enlarged to create the supercells by increasing them in different dimensions as follows; 2x2x2, 2x2x1, 2x3x2, 3x2x1 and 3x1x1, Hull & Bacon (1984). For any given vacancy concentration and supercell, plane-wave total energy calculations were always performed. Structural parameters as well as atomic positions were fully relaxed until when the Hellmann-Feynman forces were considered to be less than 0.02 eV/Å. The relaxation process gave a structure at equilibrium on which small strains (-0.002 to 0.002) were applied and stresses calculated. Elastic constants were then determined using Hooke's law. Particular attention was paid to the tensile, bulk and shear stiffness which give rise to the Young's modulus, Bulk modulus and shear modulus, respectively. Shear stiffness at different vacancy concentrations were considered since, shear modulus is known to provide a measure of rigidity of a material against deformation of the shape as involved in the microhardness identation experiment Teter (1998), Gilman (1996). Different vacancy concentrations were used ranging from 1.04 % to 25 %. The vacancies locations were selected at random since for normal preparing conditions, vacancies have no specific locations. With this in mind, the bulk modulus, shear modulus and Young's modulus were averaged using all the possible vacancies configurations in this study. The average moduli were determined using Voigt-Reuss-Hill method, Simmons & Wang (1971). The dynamical stability of the systems was also

tested. The phonon dispersion curves were obtained using the linear response method. Others were obtained using finite displacement method in the PHONOPY code, Togo et al. (2008).

4.3 WORK FLOW

Most of the work in this study was conducted using the VASP code, Kresse & Hafner (1993b), Kresse & Furthmüller (1996) and Kresse & Joubert (1999b). The code uses 4 basic input files. These files are INCAR (this file determines what the code will calculate and how it should be done; POSCAR (provides the ionic positions of the involved ions); KPOINTS (provides the Monkhorst-Pack used); POTCAR (gives the details of the pseudopotential of every element). The INCAR, KPOINTS and POSCAR are obtained from the materials project database, Jain et al. (2013). However, the files have to be edited so as to satisfy the criteria of both energy cut-off as well as the density of the k-point grid. After preparing the files, volume optimization was initially executed. In this process, the initial structure was subjected to uniform scaling. Different volumes were obtained, with partial relaxation being done at each volume. Here, both the atomic positions as well as cell shapes were allowed to relax, while the volume was maintained at a consistent value, Kresse & Furthmüller (1996). The obtained lattice constants and energy were fitted into the Murnaghan equation of state, Cohen et al. (2000), where the values of lattice constants of the ground state structure were obtained for each system. From the fully relaxed systems, cohesive and formation energies, lattice constants and the volume of the cell were determined. Thereafter, the ground state structure was used to determine the mechanical properties of both NbC and NbN. In the process of computing the elastic constants the elastic tensor analysis tool was employed to extract all the necessary mechanical properties of the two compounds, Ortiz et al. (2013). Apart from elastic constants, the mechanical properties that were determined in this study using Voight, Reuss and Hill averaging scheme include Young's modulus, bulk modulus, shear modulus and Poisson's ratio. In order to evaluate mechanical stability of the system, Born stability was used, Born & Huang (1954), while phonon studies were used to predict

the dynamical stability of the system. Further, molecular dynamics calculations were performed using VASP code to determine the effect of temperature on the mechanical properties of NbC and NbN. Also, NEB calculations using VASP were performed to determine the vacancy diffusion energy.

4.4 CONVERGENCE TEST

Convergence tests were done to establish the most favorable value of parameters that describe the compounds. Various parameters were optimized among them cut-off energy, k-point grid and the cell dimensions. Each of these parameters was optimized independently by increasing its value and ensuring that there was constant change in energies between two consecutive steps. The test is applicable to plane wave basis set compared to localised basis set. In the former, the accuracy of the properties of interest is controlled by one parameter as compared to the latter. The convergence of all the energy related parameters depend on both the cut-off energy and the k-points, Martin (2004). This is supported by the information provided in section 6.3.

4.4.1 K-Points Convergence

Before performing any calculation it is neccessary to ensure k-point convergence is done so as to find a mesh that is sufficient for the integration of the first Brilloiun zone. Brillouin zone refers to a set of points in the k-space which can be accessed through the origin and no Bragg plane is crossed, Pack & Monkhorst (1977). The k-points which are in reciprocal lattice give details about the lattice of a system. In characterization of materials, diffraction is applied which happens in the reciprocal space. Since only periodic structures were involved in this study, the first Brillouin zone was enough to predict the Bloch states of the systems involved. Monkhorst Pack method was employed to sample the zone, Hendrik & James (1976), and appropriate grid size was utilized.

4.4.2 Cut-off Energy Optimization

The cut off energy provides information on the number of plane waves being used as the basis functions to describe the whole function. The optimization of the cut-off energy is

important as it provides a minimal value of the energy. An optimized value of the cut-off energy, was considered to have been achieved when a rise in the value of the cut-off energy leads to no noticeable change on the value of the total energies of the system between two values of cut-off energy, Martin (2004).

4.5 COHESIVE AND FORMATION ENERGY

4.5.1 Cohesive energy

For a solid to be separated into its constituent neutral free atoms at infinite separation, energy has to be applied into the system. This energy is referred to as cohesive energy. For this parameter to be determined the values of energy of the solid and that of the free atoms comprising the solid have to be known. For instance, in this study the solids of interest are NbN and NbC. Thus, the total energy of the product (compound) NbN or NbC and that of reactants, that, Nb, N and C which are the constituent atoms have to be calculated using the formula shown in equation 4.5.1, Ahmed et al. (2007).

$$Ecoh = E_{MX}^{solid} - \left[E_{Nb}^{solid} + E_{C/N}^{solid}\right] \tag{4.5.1}$$

MX denotes either NbN or NbC. M Nb and X is C/N

4.5.2 Formation energy

Cohesive energy is very important when determining the formation energy. The difference between cohesive energies of the products and the reactants gives the formation energy given as;

$$Nb + C/N \rightarrow NbC/N \tag{4.5.2}$$

The formation energy can be determined from:

$$E_F = \sum E_{coh}(products) - \sum E_{coh}(reactants) \tag{4.5.3}$$

4.6 PHONONS

Rigid crystal lattice have quantized modes of vibration known as phonons. Several physical properties such as thermal and electrical conductivity are dependent on the phonons. If the potential energy increases with respect to the atomic displacements then the solid is said to be dynamically stable at equilibrium. Specific heat and sound velocity are properties that can be determined from the vibrational properties of a system, Ackland et al. (1997). Phonon frequencies are provided by considering the forces that are as a result of different sets of displacements. This aspect is equivalent to the presence of phonons with positive frequencies in harmonic approximation. If negative frequencies are present, then the crystal is dynamically unstable, Togo & Tanaka (2015) and Togo et al. (2008). The phonons only gives the dynamical stability regardless of the total energy of any system being minimized. By use of *ab initio* approaches, the vibrational frequencies of a rigid crystal can be determined using any of the two methods, namely, linear response method and finite displacement method.

4.6.1 Linear response method

Linear response method is similar to DFT approach but uses derivative of change density and wavefunctions with respect to atomic displacements and is computationally viable. The periodic perturbation helps in determining the force constant at each wave vector, which is then transformed as a fourier to provide projections for the remaining wave vectors involved.

4.6.2 Finite displacement method

In this approach the displacements which constructs the dynamical matrix can be reduced easily by considering the symmetry of the system. Hessian matrix are filled by considering the symmetry displacements, Chaput et al. (2011). If the displacements are too small the results obtained are similar to those of linear response method, however, the displacements can always be increased when investigating the phonon anharmonicity.

4.7 ELASTIC CONSTANTS

Elastic constants provides information on how a crystal responds to external strain. Also the relationship between bonding and crystal structure can be obtained from elastic constants. When stress is applied on a body, it is expected to undergo strain and eventually deform and if the elastic limit is not exceeded it regains the original shape when stress is withdrawn. Thus, if the elastic behavior of a system can be determined it is easy to determine the structural stability, Li et al. (2008). Using first principles approach, the elastic constants were determined by applying small distortions. The system was then allowed to relax and thereafter the total energy of the system determined, Mehl et al. (1994).

4.7.1 Energy-strain method

This method uses the total energies from strain states. The strained crystal provide stiffness values that can be used to determine the optimal symmetry. Strains with varying values of magnitudes are applied from which total energies are obtained. From the relationship of energy and strain, stiffness can be obtained. The independent elastic constants are determined from lattice symmetry together with point type.

4.7.2 Stress-strain method

This approach is used to determine the elastic constants in VASP. Using a relaxed cell six finite distortions were performed so as to provide the elastic tensor required and thereafter, elastic constants were determined from the stress-strain relationship. After extracting the stiffness matrix, an elastic tensor analysis tool ELATE, Ortiz et al. (2013) was used to determine other mechanical properties. The Voight, Reuss and Hill averaging approaches were used to determine Young's, bulk and shear modulus. In addition, eigen values of the stiffness matrix are determined. Born stability criteria was used to determine the mechanical stability of NbC and NbN, Mouhat & Coudert (2014).

4.8 MOLECULAR DYNAMICS

4.8.1 Introduction

The MD evaluates the instantaneous electronic ground state at the given finite temperature. When performing the calculations, the free energy is used as a variational quantity. The evaluation occurs at each MD-step since the calculation are performed at a given range of steps using efficient matrix diagonalization schemes and Pulay mixing. *Ab initio* MD uses time step to determine the ionic positions as well as the electronic energy functional. Once one time step is completed, the change in position as well as momenta of the nuclei is calculated by applying the Newton's equation of motion, which are subjected to electrostatic forces. Large number of time steps are applied to determine the time averaged structural properties of materials through iterative method. The electron energies are determined assuming that the electron sub-system exists at the ground state and the nuclei are static at their positions as every time step elapses (BO approximation). During the simulations, the total energy, that is, kinetic energy of the nuclei + ground state energy is conserved while the volume of the unit cell is constant. For MD at low temperatures, the results are less accurate since the calculation involving the motion of the nuclei which ignores the quantum effects. From the average kinetic energy of the nuclei, the temperature is determined. However, for constant-temperature MD calculations Nosé thermostat statistical sampling is used together with a thermostat, Andersen (1980); Nosé (1984).

4.8.2 Molecular Dynamics using NVT ensemble

Molecular Dynamics calculations presented in this piece of work were performed using VASP code, Hafner (2008) within the context of canonical ensemble (NVT). The parameters considered in these calculations include size of the time step, duration of simulation, the working temperature and the integration algorithm among others. PAW-PBE potentials, Blöchl (1994) within GGA were used in the approximation of exchange and correlation functional. A timestep of 2 fs together with energy cutoff energy of 520

eV was used. On the other hand, electronic convergence set at 10^{-8} eV was used. For the kpoints, Gamma point sampling was the applied.

When using the AIMD approach, equilibrium structure as well as the lattice parameters were obtained at finite temperature first, Woodward et al. (2010). Since the systems involved in this study are periodic, one of the major assumption is that the parameters of the structures as obtained from AIMD embody the required physical properties of the two materials at the set finite temperatures. After successful optimization of lattice parameters and atomic positions at different temperatures stress-strain method from first-principles was applied to determine the mechanical properties of the systems, Yao et al. (2007). In MD simulation of NbC and NbN, the simulated temperature was set to equilibriate at 10000 time steps as shown in figure 4.8.1. The atomic thermal velocities were stored in CONTCAR file and used in other calculations. During each successive time step, the temperature was expected to vary since the momentum together with kinetic energy of the atoms change. The temperature equilibration was checked using a time step temperature vs time plot. Equilibrated systems were expected to display regular temperature oscillations. The relaxation of the unit cell parameters was performed for each temperature iteratively using a optimized chosen timestep ensuring a compromise between the reproduceability of results and computing time. After relaxation, equilibration was performed and CONTCAR output files were used as POSCAR input file for other simulations.

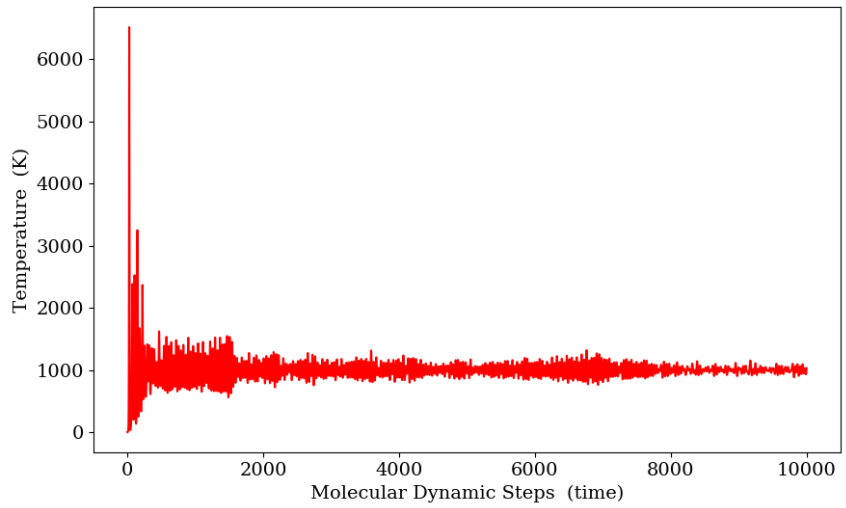

Figure 4.8.1: An illustration of equilibrated temperature at 1000 K

The elastic constants were determined as follows;

1. A desired MD cell was created and a relaxation calculation performed to ensure that the ions get into their equilibrium positions.

2. The systems are thermalized independently by bringing each of them to the target temperature usually below the melting point of each of the crystals.

3. The temperature is equilibrated.

4. The elastic constants were then obtained from the strain/stress relationship as presented in Figure 4.8.2.

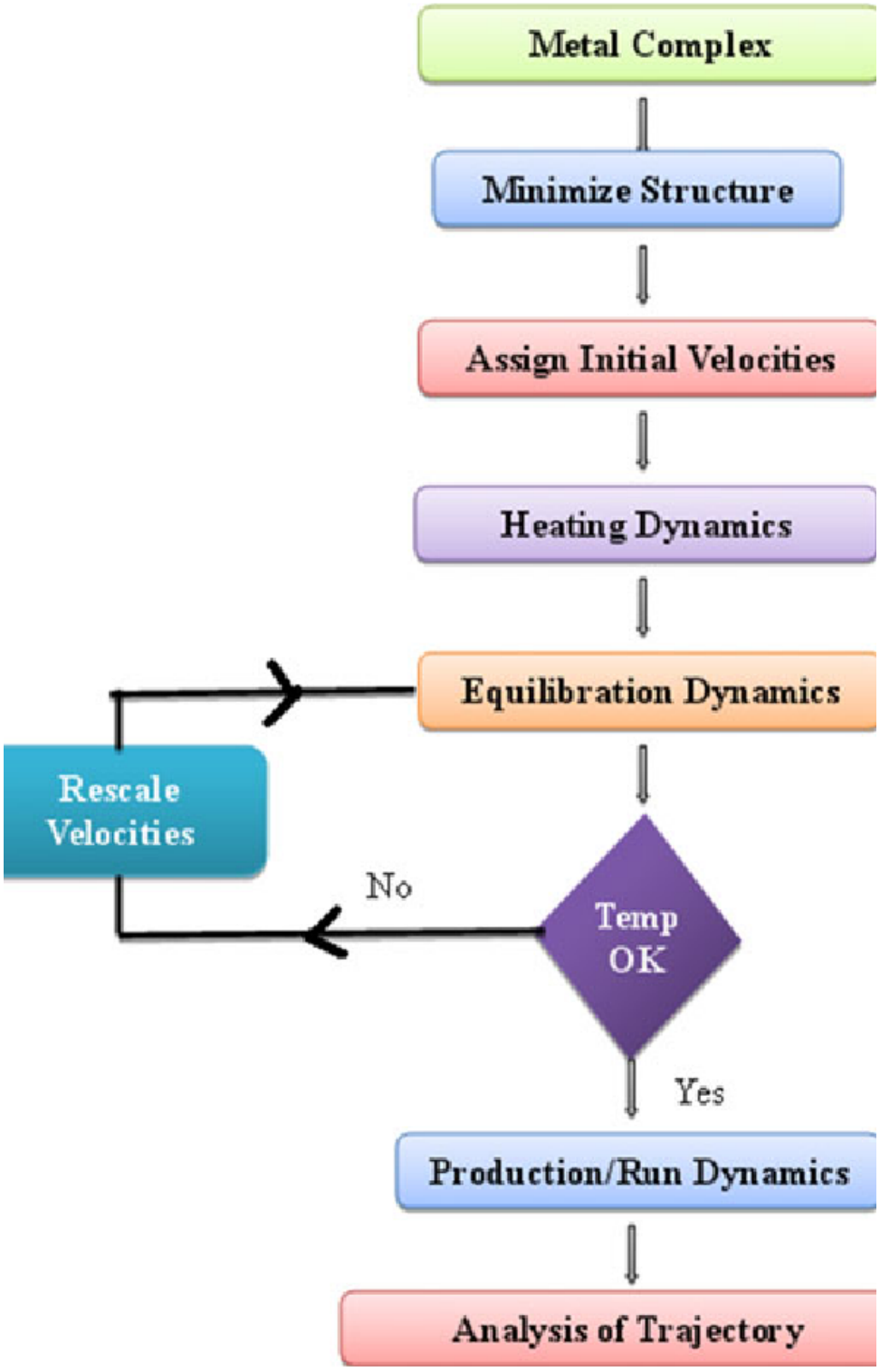

Figure 4.8.2: The MD flowchart, Nambigari et al. (2013).

CHAPTER FIVE

RESULTS AND DISCUSSION

This chapter contains detailed explanations of the results obtained from the study. The results are compared to the available experimental and theoretical data.

5.1 STRUCTURAL PROPERTIES

5.1.1 Bond lengths

Transition metal carbides and nitrides have attracted a lot of attention lately and many researchers have developed some interest in studying their properties. One of these properties is the intrinsic hardness which is governed by several factors. They include strength of interatomic forces as well as the crystal structure. According to Korir et al. (2011), high intrinsic hardness is specified by high values of cohesive energy, short bond-length together with high degree of covalent bonding. This implies that the strength of interatomic forces as well as the size of the bond lengths have a key role when determining the elastic properties of a material and its hardness. NbN and NbC exhibit three types of bonding, namely; metallic, ionic and covalent type of bonding. Generally, bonding in every compound usually affects both the size as well as the shape of the structure. This arises due to the effect of the repulsion of the nuclei of the bonded atoms and the attraction of the outer electrons by the nuclei. However, in order to fully understand the bonding mechanisms of the compound under investigation, it is essential to determine their bond-lengths. In this study, the Xcrysden program was used to extract the bond lengths together with the bond angles, Kolkaji (2003). Each of the optimized structure was obtained after rigorous energy optimization to accuracies of 10^{-4} Ry. Figure 5.1.1 shows the DFT-GGA optimized crystals structures of Niobium Carbide and Niobium Nitride in different structures using PBE functionals and ultrasoft pseudopotentials considered in this work.

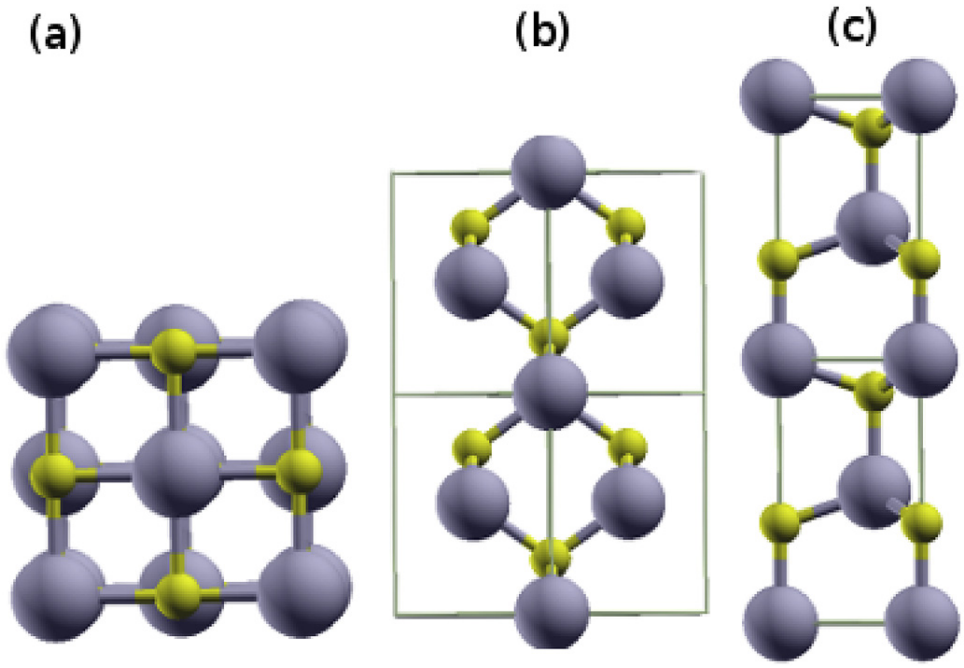

Figure 5.1.1: Representation of different crystal structures of Niobium Nitride and Niobium Carbide using ball and stick studied in this work: (a) rocksalt, (b) zinc-blende and (c) wurtzite. The bigger balls represent Niobium atoms while the small balls represent either Carbon or Nitrogen atoms.

Using the optimized structures, values of optimized bond lengths of each structure and the bond angles were extracted as indicated in Table 5.1.

Table 5.1: Calculated bond lengths together with bond angles for NbC and NbN in different crystal structures

Structure	Calculated		Theoretical	
	Bond Length (Å)	Bond angle	Bond Length (Å)	Bond angle
NbC (RS)	2.25	90	2.24 [a]	
NbC (ZB)	2.09	109.471	2.09 [a]	
NbC (WZ)	1.76	113.457	2.22 [a]	
NbN (RS)	2.20	90	2.01 [a]	
NbN (ZB)	2.06	109.471		
NbN (WZ)	1.71	113.457		

[a]Korir et al. (2011)

Bond lengths can be used to indicate the hardness of a material, i.e short bond lengths tend to suggest the existence of a robust bond connecting atoms and vice versa. From Table 5.1, it was observed that the bond length of Niobium-Carbon/Nitrogen for both

compounds in the identical structures recorded almost similar values of the bond lengths. The variation in the values ranges between 1.4 % and 2.8 % which can be associated with minor variation in atomic radii of the two non-metals in the structures. Both carbon and nitrogen are almost of the same size. For both compounds, the longest bond length was obtained in RS, followed by ZB and WZ structure with the shortest bond length.

5.1.2 Lattice Parameters

By use of the Murnaghan equation of state, the energy-volume data was fitted and used to determine the lattice parameters, Murnaghan (1944). The results for Murnaghan equation fitting were obtained from the calculations done using PBE-ultrasoft pseudopotentials. The results are as presented in Table 5.2.

Table 5.2: Calculated DFT-GGA Lattice parameters for NbC as well as NbN in different crystal structures

Crystal	height	Calc.	Theo.		Expt		Dev. %
	a_0 Å	c/a	a_0 Å	c/a	a_0 Å	c/a	
NbC (RS)	4.49		4.48 [a]		4.47 [b]		+2.2232
NbC (ZB)	4.82						
NbC (WZ)	3.70	1.10	3.71 [a]	1.20 [a]			
NbN (RS)	4.38		4.44 [a], 3.11 [d]		4.39 [e], 4.21 [f]		-0.2278, +4.038, respectively
NbN (ZB)	4.76		4.76 [c], 3.35 [d]				
NbN (WZ)	3.01	1.84	2.96 [c], 2.94 [d]	1.84[g]			

[a]Patricia et al. (2013), [b]Isaev et al. (2007), [c] Korir et al. (2011), [d]Yang et al. (2014), [e]Toth (1971), [f]Fernandez et al. (1992), [g]Fontbonne & Gilles (1969)

The values of lattice parameters determined in this study were comparable with both experimental and theoretical values where available. From the results obtained it was clear that Niobium Carbide reported the highest values of lattice parameters for all structures compared to Niobium Nitride. For instance, using GGA approach, NbC in ZB has the highest lattice constant of 4.82 Å while NbN in WZ recorded the least value of 3.01 Å. An agreement between the obtained and the experimental values was noted for both **a** and the **c/a** ratios. The deviation is between +4.038 % and -0.2278 %, Patricia

et al. (2013), Korir et al. (2011), Isaev et al. (2007), Yang et al. (2014), Toth (1971), Fernandez et al. (1992) and Fontbonne & Gilles (1969).

5.2 ANIONIC VACANCIES FORMATION

Transition metal carbides and nitrides are usually synthesized under conditions of high temperature and pressure, Ningthoujam & Gajbhiye (2015), where under these conditions anion vacancies are the most energetically favourable type of defects compared to other forms such as cationic defects among others, Tsetseris et al. (2007). In this study, the vacancy formation energies have been obtained using large supercells so as to minimize the errors associated with vacancy self-interaction. For the cubic structures of the two systems, supercells of size 3x1x1, 2x2x1, 3x2x1, 2x2x2 and 2x3x2 representing 24, 32, 48, 64 and 96 atoms, respectively, were used. On the other hand, 12, 16, 24, 32 and 48 atoms generated from supercells of size 3x1x1, 2x2x1, 3x2x1, 2x2x2 and 2x3x2 were used in the hexagonal structures.

After generating the supercells of different sizes, the suitable defect site was established. This was achieved by calculating the formation energies of defects at different sites and selecting the one with lowest value of formation energy as the most preferred site to be used even in subsequent calculations. Figure 5.2.1 shows the anionic vacancy sites in 3 crystal structures.

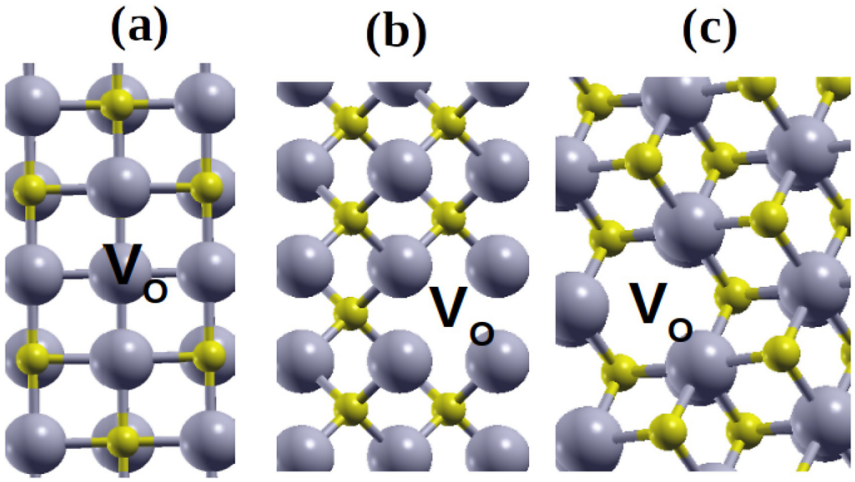

Figure 5.2.1: An illustration of anionic vacancy site at V_0 in rocksalt, zincblende and wurzite crystal structures of Niobium Nitride and Niobium Carbide.

The optimized bulk lattice parameters were used to optimize the defective structure before proceeding with other calculations. The vacancy formation energy for both NbN and NbC in the three crystal structures was determined using the equation 5.2.1;

$$\Delta E_v = E_v - E_s + \mu_{\frac{C}{N}} \tag{5.2.1}$$

E_v and E_s represent the total energies of the supercells with defects and the stoichiometric, respectively while $\mu_{\frac{C}{N}}$ is the chemical potential for the non metals as computed by Yu et al. (2015) and Balasubramanian et al. (2018a). The calculated formation energies of different vacancy concentrations in NbC and NbN are as shown in Figure 5.2.2.

In general, the formation energies can either be positive or negative. The positive values indicate that the defects can only occur under non-equilibrium conditions whereas for negative values of formation energies the defects tend to occur under equilibrium conditions. As presented in Figure 5.2.2, for the carbide within rocksalt, zincblende and wurzite crystal structures, the formation energies were negative. This indicates that the formation of anionic vacancies is favourable under equilibrium conditions these vacancies are likely to occur. Comparing the 3 structures, the rocksalt structure was established to favour most the formation of the carbon vacancies in comparison to zincblende as well

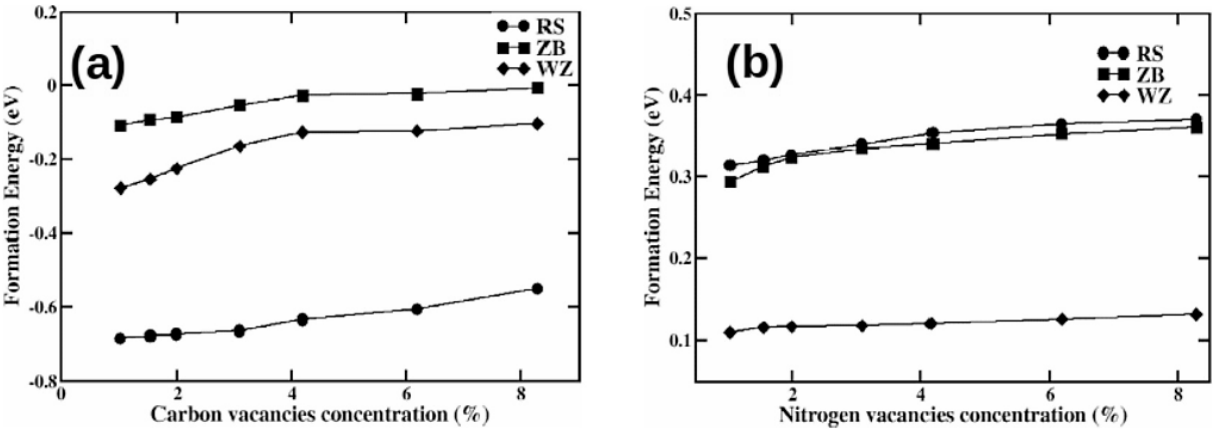

Figure 5.2.2: Formation energies of (a) C in three crystal structures of Niobium Carbide together with (b) N in Niobium Nitride.

as wurzite structures. However, the values of formation energies tend to move towards the positive with increase in defect concentration, well illustrated in Figure 5.2.2. For instance, the formation energy in RS structure increases upto 8% which is the maximum percentage used while in ZB and WZ beyond 4% there is negligible rise in values of formation energy.

Similarly, the defect formation energies of nitrogen in rocksalt, zincblende and wurzite structures of NbN were also determined. The anionic defects tend to be more likely to occur in WZ structure as compared to ZB as well as WZ. For the nitride, the formation energies increases sub-linearly up to 8 % implying that defect formation at high concentration is likely not possible. The RS and ZB structures have high values of defect formation energies which is an indication that N vacancies are not favoured in nitrides. In ZB the increase in formation energy tends to be marginal especially after 4 % while in RS similar trend occurs beyond defect concentration of 6 %. Thus, the anionic defects are anticipated to be stable and likely to occur in NbC as supported by negative formation energies compared to positive formation energies in NbN. These observations are in agreement with other studies, Seung-Hoon et al. (2001), Yu et al. (2015), Balasubramanian et al. (2018a) and Tsetseris & Pantelides (2008)

5.3 CHEMICAL BONDING

5.3.1 Electronic Structure of Pristine Systems

The mechanical properties of both NbC and NbN are well understood by calculating the electronic band structure together with the partial density of states (PDOS). TMCs are characterised by complex chemical bonding whereby they have covalent, metallic together with ionic bonding character. This is supported by the existence of the physical properties of these materials which include high hardness as well as high melting points. These properties are typically present in solids which have either ionic or covalent type of bonding. It has been noted earlier on that NbC has high thermal and electrical conductivity properties which are as a result of metallic bonding. All these findings have been supported by extensive studies reporting on the electronic structure of TMCs systems such as, Gubanov et al. (2005), Benco (1997), Hugosson et al. (2001), Vojvodic & Ruberto (2010), Korir et al. (2011). From the literature, the covalent bonding give rise to the main characteristics of these materials due to the hybridization of the $4d$ orbitals of the metallic atom such as Nb and $2p$ orbitals of the nonmetallic atom such as carbon, Gubanov et al. (2005). Similar results were obtained from our study. Figures 5.3.1 to 5.3.3 show the band structure together with projected density of states of Niobium Carbide as well as Niobium Nitride in the rocksalt, zincblende along with wurzite structures.
According to Figures 5.3.1-5.3.3, at the symmetry points the levels are connected by smooth curve. The bands cross each other as a result of relative magnitude of the effective mass. From each of these figures, the conduction band is formed by 4d states of Nb and 2p states of either C or N. However, the hybridization of the 2p and 4d states is less strong in the valence band and the bands tend to be curved. The electronic PDOS suggest that the formation of the chemical bonds is due to the carbon/nitrogen and niobium atoms. The regions near the Fermi level are dominated by the unoccupied 4d-Nb states. The peak of the PDOS corresponding to the 4d states are at 5 eV, -2 eV and -5 eV in RS, ZB and WZ structures. Figures 5.3.1- 5.3.3 only shows the states responsible for bonding in NbC and NbN. However, other core states such as 2s of C/N and 5s of Nb are ommited

as they do not take part in bonding.

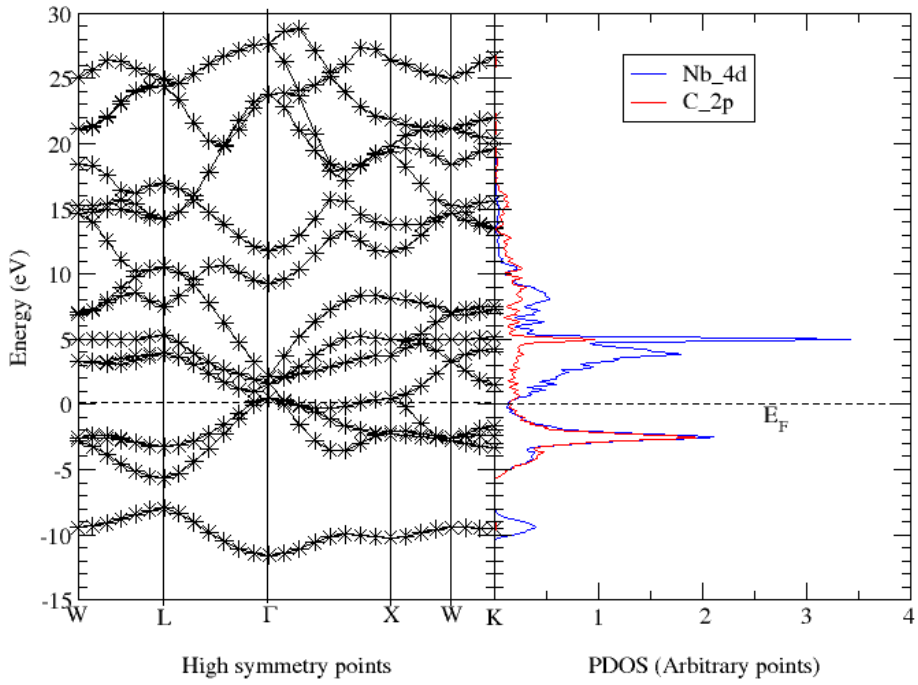

(a) NbC

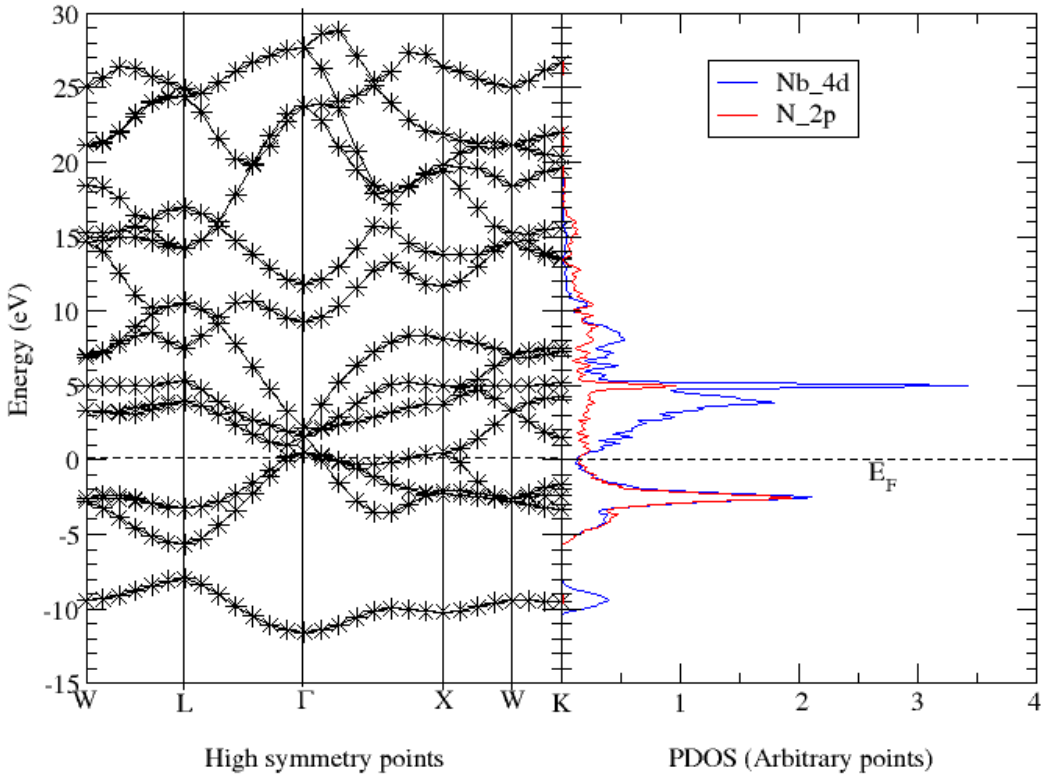

(b) NbN

Figure 5.3.1: Combined band structure together with PDOS of defect free Niobium Carbide as wel as Niobium Nitride in rocksalt crystal structure, respectively.

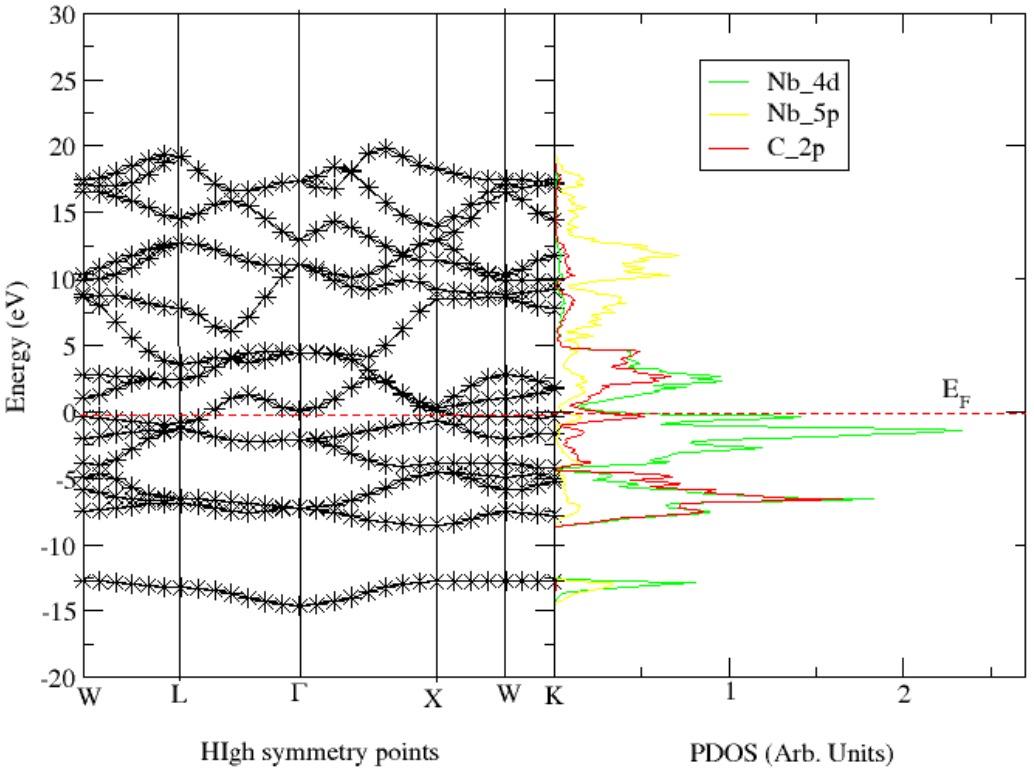

(a) NbC

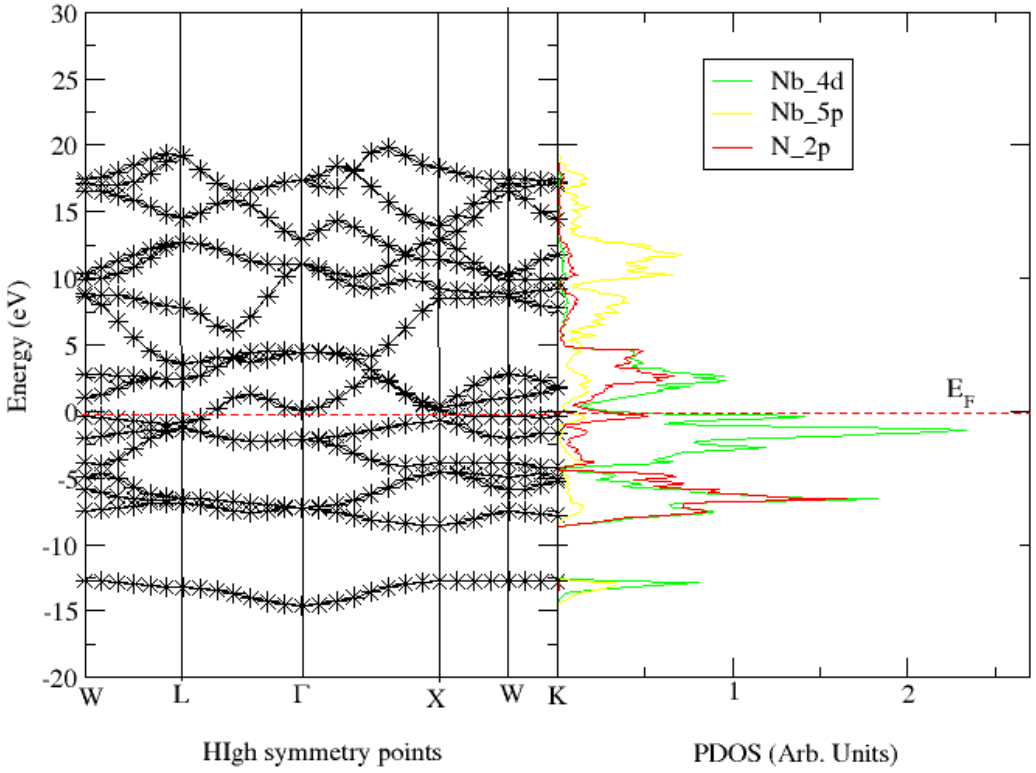

(b) NbN

Figure 5.3.2: Combined band structure together with PDOS of defect free Niobium Carbide as well as Niobium Nitride in zincblende crystal structure, respectively.

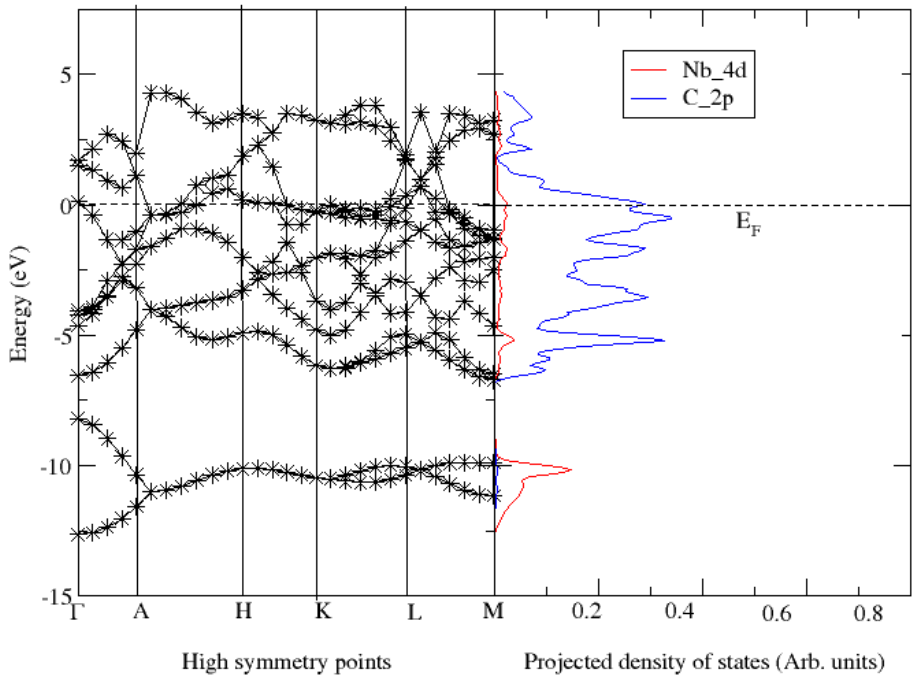

(a) NbC

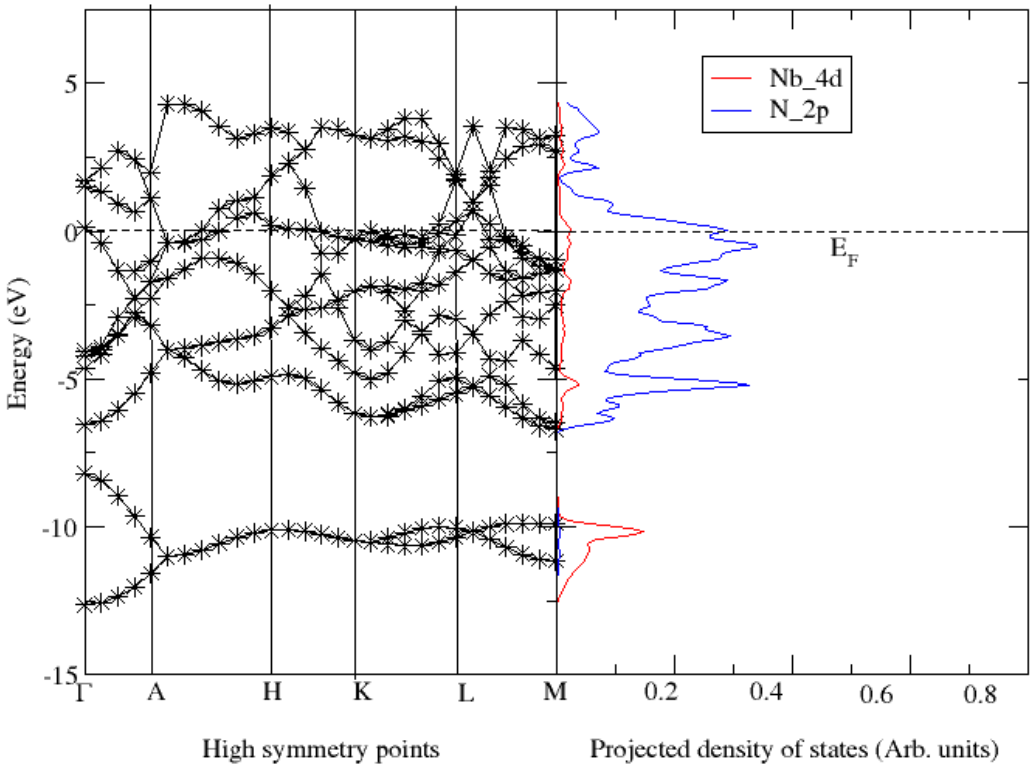

(b) NbN

Figure 5.3.3: Combined band structure together with PDOS of defect free Niobium Carbide as well as Niobium Nitride in wurzite crystal structure, respectively.

According to Toth (1971), Yefei et al. (2011), Gou et al. (2008) NbC exhibits metallic behaviour with Fermi level being characterised by non-zero PDOS values. The NbC system has strong covalent bonding as a result of the role of hybridization of the Nb and C states which overlap. From Mulliken charge population test Nb atoms have 0.29e positive charge while on the other hand, C atom has 0.29e which is a negative charge. The strong covalent bond contributes to the incompressibility of the carbide. Similarly, the d-p hybridization in NbN accounts for the incompressibility of the compound as shown in Figure 5.3.4.

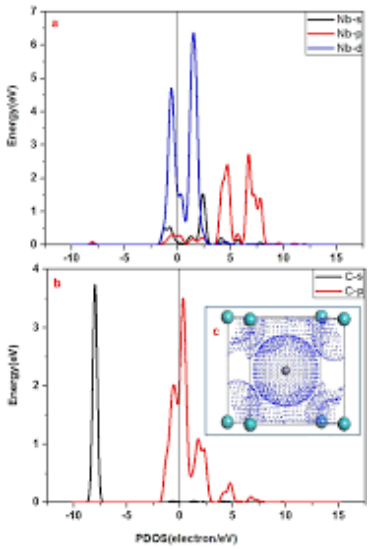

Figure 5.3.4: PDOS of NbC and electron density Liu et al. (2017).

In both NbC and NbN, there is octahedral coordination formed by the metallic and the non-metallic atoms. During chemical bonding, the valence shell of the metallic atom has an electronic configuration of $4d^4 5s^1$. The d orbitals of this shell are partially occupied and they are the orbitals responsible for the formation of a chemical bond with the p orbitals of the carbon or nitrogen atom. There exists degenerate d orbitals meaning they have the identical energy of the isolated Nb atom.

5.3.2 Effects of defects on the electronic Structure

Most of the studies which have reported on the electronic structure of TMC/Ns are performed on systems with stoichiometric composition and effects of vacancies are neglected. There are very scarce studies reporting either from experimental or theoretical

perspective the effects of the vacancies on both the bonding and the electronic structure of NbC and NbN. Vacancies are known to distort the crystal structures and in turn change the chemical bonding especially in the vicinity of the defects. In general, higher defect concentration (vacancy) increases the metal-metal bonds while the covalent bonding character tend to diminish, Klein et al. (1980), Pickett et al. (1986), Krajewski et al. (1998), Seung-Hoon et al. (2001).

In this study, changes in bonding were investigated due to the presence of anionic vacancies introduced at different concentrations. The vacancies affect the bond-lengths of the materials as well as the electronic structure. This study analysed the projected density of states (PDOS) of both the pristine systems as well as those with different defect concentrations so as to understand how the vacancies affect the electronic structure of both NbC and NbN as shown on Figure (5.3.5 -5.3.7) as well as their mechanical properties.

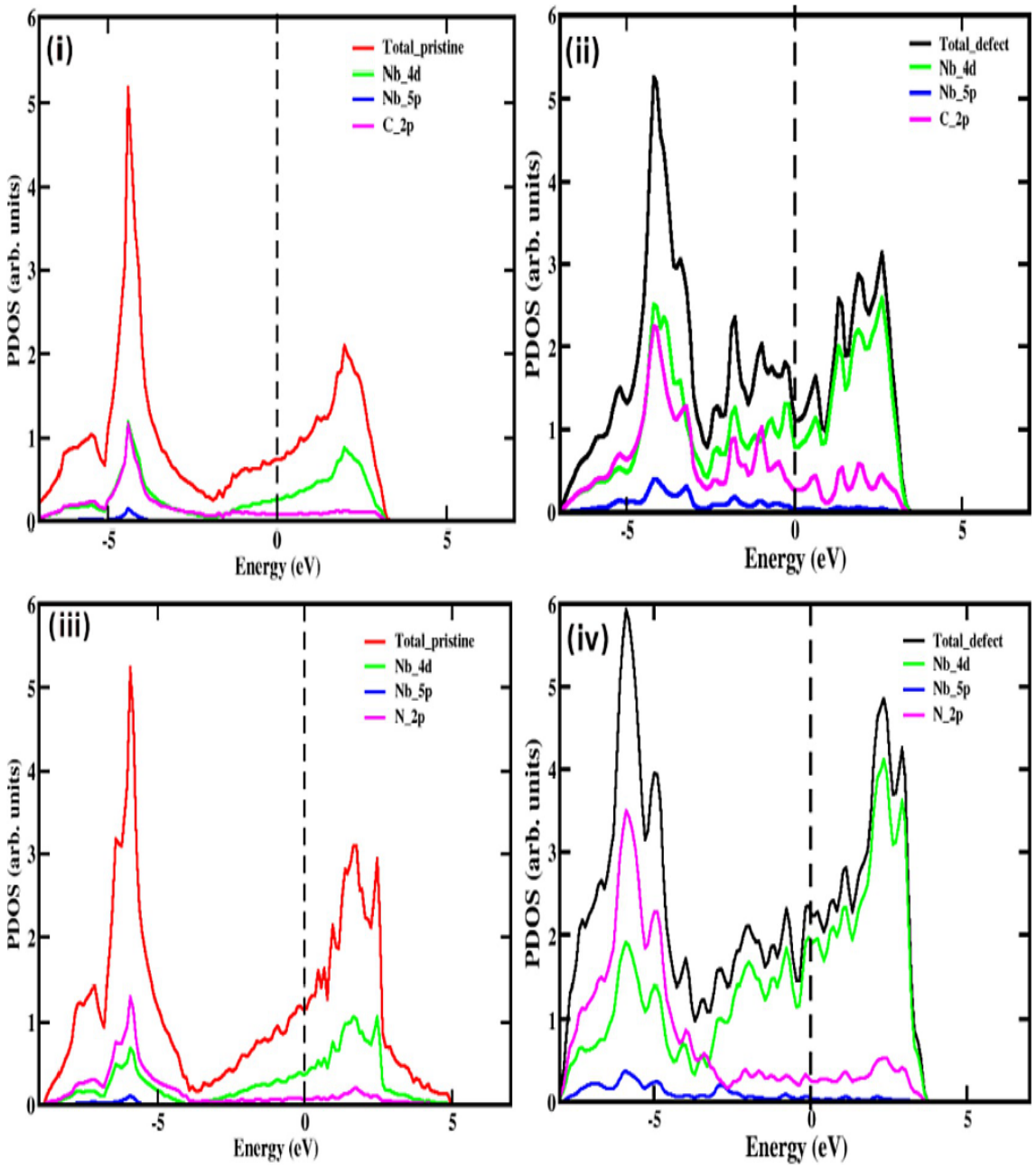

Figure 5.3.5: PDOS for Niobium Carbide as well as Niobium Nitride in rocksalt crystal structure, (i) Pristine Niobium Carbide, (ii) Niobium Carbide with 8% Carbon vacancies, (iii) pristine Niobium Nitride, and (iv) Niobium Nitride with 8% Nitrogen vacancies. Dotted line at 0 eV is the Fermi level.

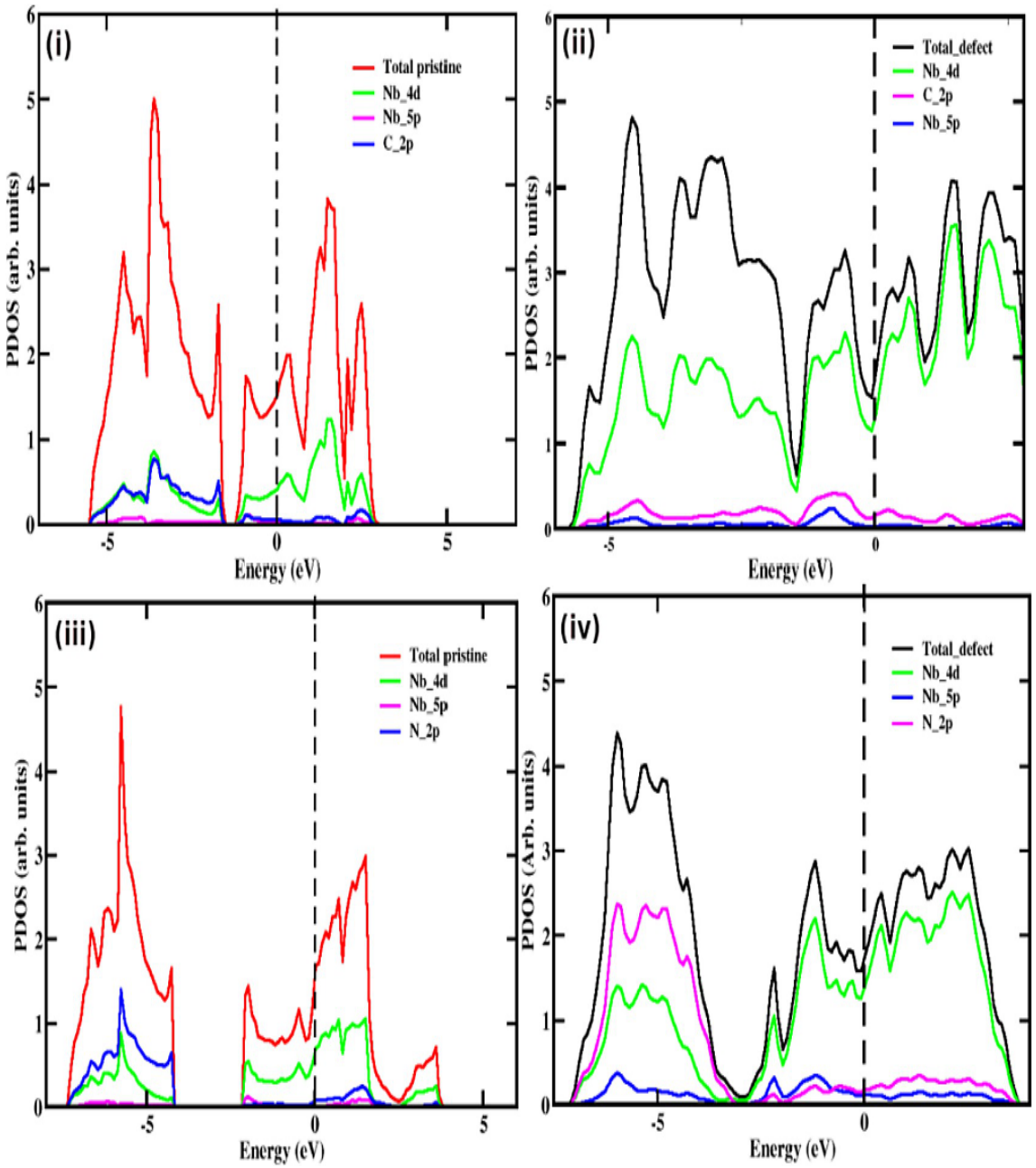

Figure 5.3.6: PDOS for Niobium Carbide as well as Niobium Nitride in zincblende crystal structure, (i) Pristine Niobium Carbide, (ii) Niobium Carbide with 8% Carbon vacancies, (iii) pristine Niobium Nitride, and (iv) Niobium Nitride with 8% Nitrogen vacancies. Dotted line at 0 eV is the Fermi level.

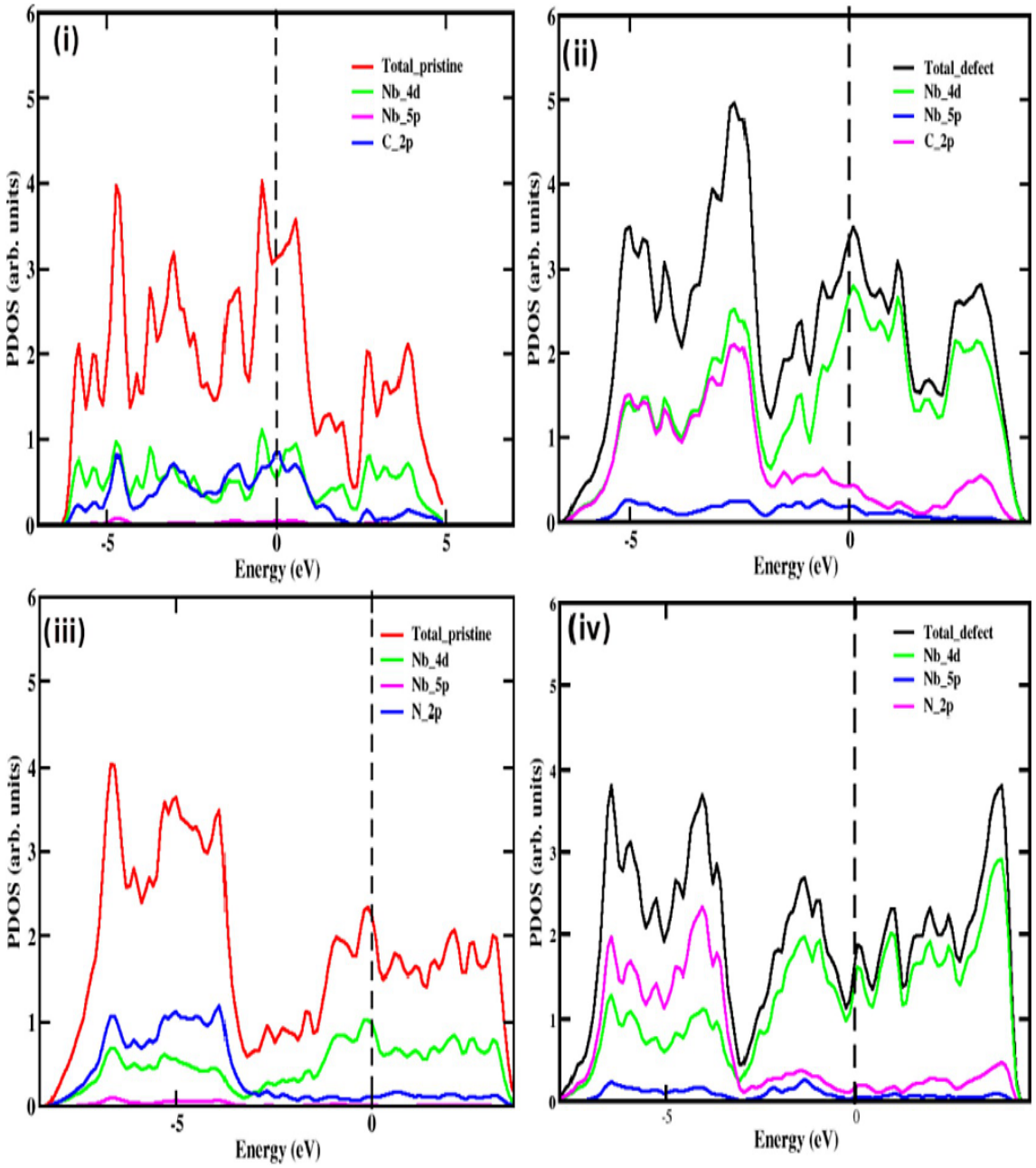

Figure 5.3.7: PDOS for Niobium Carbide and Niobium Nitride in wurzite crystal structure, (i) Pristine Niobium Carbide, (ii) Niobium Crbide with 8% Carbon vacancies, (iii) pristine Niobium Nitride, and (iv) Niobium Nitride with 8% Nitrogen vacancies. Dotted line at 0 eV is the Fermi level.

From Figures 5.3.5 (ii, iv), there are dominant peaks near -5 eV and 4 eV for the Niobium Carbide and Niobium Nitride in rocksalt with defect concentration of 8 %. These values were obtained with reference to the shifted Fermi level as shown on this figure. The peaks are associated with p and d orbitals bonding between the metal and the C/N atoms which results into covalent nature. This trend is noted in other structures too.

However, the sizes of the peaks differ depending on the system. For example, for NbC in ZB the intensity of the Nb 4d peak appears at 2 eV while for the nitride the height of the dominant peaks are at 1 eV showing a reduction. Thus, pd bonding is anticipated to reduce in nitrides compared to carbides as shown on Figure 5.3.6 (ii, iv). As shown on Figure 5.3.7 (ii, iv), the presence of carbon vacancies in WZ crystal structure slightly increases the intensity level of the peak at 0 eV although an increase on the height of peaks was noted for the ones located at 4 eV in both carbides and nitrides. Also, as the C/N vacancies increased the intensity of states near the Fermi level also increased for all structures considered in this study. This is as a result of dd bonding between the transition metal atoms due to the decrease in C/N atoms in the system which induces a transition of the NbC and NbN from covalent to metallic nature in terms of bonding. This reduces the strength of the bonds and as a result the mechanical properties also reduces.

5.4 MECHANICAL PROPERTIES OF PRISTINE NIOBIUM CARBIDE TOGETHER WITH NIOBIUM NITRIDE

The study of mechanical properties of NbN and NbC is crucial in understanding the response of these materials to applied forces. Elasticity is one of the important properties of a material that describe its response to an external strain that may be applied on it. Moreover, it also gives key information about the bonding strength that exists between nearest neighboring atoms. These features are only realized when the elasticity is calculated accurately and in turn help in understanding microscopic mechanical properties of compounds as well as in the design of hard materials. Nowadays mechanical properties can be calculated using first-principles calculations which have proven to be not only accurate or in good agreement with measurements but also can be useful under extreme conditions of high temperature and pressure which may not be accessible to experiments, Zhigang et al. (2008). DFT calculations often provide reliable results which compare very well with the experimental data thereby providing complementary information, Zou et al. (2015). Elasticity of materials is characterized by several parameters among them the

elastic constants. The elastic constants can be determined by the knowledge of curvature of the energy curve plotted as a function of strain as a result of specific deformations of the cell or using the stress-strain relationship.

In this study, the elasticity of the materials considered is characterized by the elastic constants of the respective materials. For the cubic crystal structures, three independent elastic constants namely, C_{11}, C_{12} and C_{44} are obtained while for the hexagonal structure five independent elastic constants are determined, namely, C_{11}, C_{12}, C_{13}, C_{33} and C_{44}. The calculated elastic constants for the two systems in the different crystal structures are as presented in Table 5.3. Elastic constants are also used to measure the mechanical stability of materials by satisfying the Born criteria, Qi-Jun et al. (2014). The criteria is satisfied when for the cubic system $C_{11} - C_{12}>0$, $C_{11}>0$, $C_{44}>0$, $C_{11} + 2C_{12}>0$ while the following has to be observed in hexagonal structure; $C_{33}>0$, $C_{44}>0$, $C_{12}>0$, $C_{11}>C_{12}$, $(C_{11} + 2C_{12})C_{33}>2C_{13}^2$. These criteria were satisfied by the systems under consideration.

Table 5.3: Calculated DFT-GGA elastic constants of Niobium Carbide together with Niobium Nitride in different crystal structures

Structure	$C_{11}(GPa)$	$C_{12}(GPa)$	$C_{13}(GPa)$	$C_{33}(GPa)$	$C_{44}(GPa)$
NbC (RS)	666.90 ,	115.90,			180.50,
	667.00 [a] ,	121.00 [c],			164.30 [b],
	627.10	134.60 [b]			151.00 [c]
Expt. NbC	620.00 [d]	200 [d]			150.00 [d]
(RS)					
NbC (ZB)	282.00	168.00			71.00
NbC (WZ)	589.77	192.28	92.33	815.02	216.34
NbN (RS)	603.50,	152.00,			66.30, 101.80
	718.00 [e]	134.00 [e]			[e]
Expt.	739.00 [f],	161.00 [f],			76.00 [f],
works NbN	608.00 [d]	122.90 [f]			117.00 [b]
(RS)					
NbN (ZB)	277.70,	189.80,			35.30, 23.90
	287.80 [e]	217.20 [e]			[e]
NbN (WZ)	520.52,	222.17,	144.58,	808.21,	206.83,
	560.00 [g],	220.00 [g],	132.00 [g],	770.00 [g],	216.30 [g],
	544.90 [h]	217.40 [h]	140.40 [h]	739.10 [h]	241.40 [e]

[a]Zhigang et al. (2008), [b]Rathod et al. (2011) , [c]Zaoui et al. (2005), [d]Weber (1973), [e]Li & Liu (2012), [f]Xiao Jia et al. (2005), [g]Zhen-Hua et al. (2011), [h]Zou et al. (2015)

Table 5.3 shows the elastic constants of NbC as well as NbN in the three structures studied in this work which are compared with the available experimental and theoretical values. In RS, both C_{11} and C_{12} are overestimated when compared with the experimental data while C_{12} is underestimated by 42.075 % in RS structure of NbC. Specifically, the C_{11} for the NbC RS crystal structure was overestimated by 7.57 % implying that DFT simulations tend to predict relatively harder materials than experimental work. From Table 5.3 it can

be noted that there is an agreement between the calculated values from this study and the available experimental data although there is some slight variance. For computational studies such as the first-principles calculations, the simulations are performed under ideal conditions and the systems are assumed to be perfect crystals although for experimental work such structures are unrealistic. The experimental conditions are almost unattainable in theory leading to the variance between experimental work and the theoretical work. Figure 5.4.1 shows the trend of elastic constants of Niobium Carbide aas well as Niobium Nitride as compared to Silicon Carbide and cubic Boron Nitride which are traditional hard materials. For all the structures considered in this study, C_{11} was found to be the highest among all the elastic constants computed in all structures except for ZB structure. Also it was noted that Born criterion was obeyed by all the independent elastic constants, Born & Huang (1954). This confirms that these systems are indeed mechanically stable.

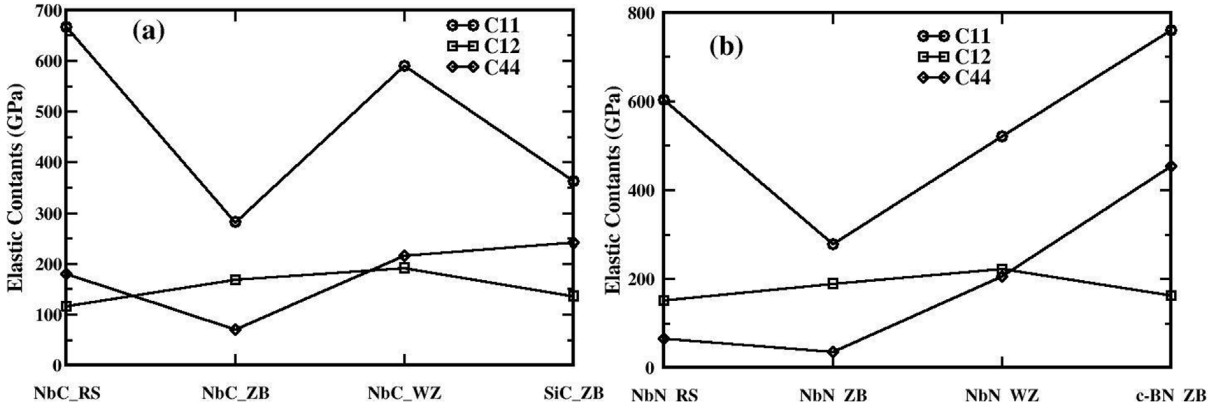

Figure 5.4.1: Calculated elastic constants of NbC along with NbN in rocksalt, zincblende as well as wurzite crystal structures.

As presented in Table 5.3, Niobium Carbide was established to have higher values of some of the elastic constants which include C_{11} , C_{33}, and C_{44} in all its structures compared to Niobium Nitride. Similarly, Niobium Nitride recorded the highest values of only C_{12} in all its structures compared to Niobium Carbide. Finally, it was also noted that the calculated C_{33} values were the largest amongst all the other elastic constants as observed in the wurzite structure of Niobium Carbide as well as Niobium Nitride. Thus, these

compounds are predicted to offer high resistance to compressive stress as shown in Table 5.3. The results of the carbide were compared to other carbides, with SiC being the chosen carbide used for comparative purpose. SiC reported higher value of C_{44} while the values of the other two elastic constants i.e C_{11} together with C_{12} for the cubic structure were basically lower in comparison to those of other compounds studied in this work. Based on the high elastic constants observed in rocksalt and wurzite structures, materials in such structures are anticipated to exceed those in zincblende in relevance to hardness related application.

5.4.1 Calculated DFT-GGA Bulk modulus (B), shear modulus (G), Young's modulus (E), Poisson ratio (v), Voigt-Reuss-Hill moduli as well as Vickers hardness (Hv) of both Niobium Carbide as well as Niobium Nitride in three different crystal structures

Apart from elastic constants, there are other crucial microscopic properties of materials that need to be analyzed. One of them is the bulk modulus which provide a reflection of how materials resist compressive deformation. It gives a measure of how a material resists volume change upon application of pressure. This property is dependent on the chemical bonds, strength as well as compressibility of the bonds contributing to the ability of the material to resist deformation. In general, bulk modulus is inversely proportional to bond length, for example, the small atomic size of carbon together with nitrogen give rise to short bond-lengths which result into large values of bulk modulus and elastic constants. Bulk modulus can be determined using equation 5.4.1;

$$B_0 = \frac{2}{9}C_{11} + C_{12} + 2C_{13} + \frac{C_{33}}{2} \tag{5.4.1}$$

In addition, shear modulus can also be used to determine the hardness of a material. This parameter measures how a material responds to force under volume conserving shear strain. In materials, it involves the stretching of metal-nonmetal bonds and bending of

the metal-metal bonds, Goble & Scott (1985).

Table 5.4: Calculated DFT-GGA Bulk modulus B_o, shear modulus (G), Young's modulus (E), Poisson ratio (v), shear Voigt-Reuss-Hill moduli G_{VRH} as well as Vickers hardness H_v of both Niobium Carbide along with Niobium Nitride in three different crystal structures

Structure	$B_0(GPa)$	G (GPa)	E (GPa)	v	$G_{VRH}(GPa)$	H_v
NbC (RS)	300.0, 293.0 [a] , 300.2 [b]	275.5	518.0	0.21	214.0	28.0
Expt work	302.0 [c]					
NbC (ZB)	206.1, 204.9 [b]	56.9	117.0	0.35	65.0	5.0
NbC (WZ)	305.4	196.6	511.0	0.22	209.0	26.0
NbN (RS)	302.5, 349.5 [d], 304.8 [b]	225.7	297.0	0.33	111.0	8.0
NbN (ZB)	219.1, 224.9 [b]	44.0	109.0	0.41	38.0	2.0
NbN (WZ)	332.0, 308.0 [e], 312.1 [f]	173.5, 211.0 [e], 199.0 [g]	461.0	0.26	182.0	18.0

Zhigang etal. (2008)[a], *Korir etal.* (2011)[b], *Weber* (1973)[c], *Li &Liu* (2012)[d],

Zhen − Hua etal. (2011)[e], *Zou etal.* (2015)[f],

Broser etal. (1982)[g]

According to Table 5.4, the bulk moduli of NbC and NbN in identical structures is comparable meaning that their resistance to change in volume is very close to each other. On the other hand, the shear modulus of NbC in all structures is higher compared to the values obtained in NbN structures. This suggests that the carbide suites the hardness applications which involve twisting and shearing. However, the shear modulus of NbC and NbN in the ZB was the lowest compared to other structures (57 and 44 GPa, respectively) suggesting that this structure may not be appropriate in applications that involve shearing.

Apart from ZB, RS and WZ were also considered in this study. For both NbC and NbN systems, the WZ structure recorded the lowest shear modulus compared to RS structure. This would imply that the cubic structure would give rise to higher resistance to mobility of dislocations and thus suitable for shear related applications, Pauleau (1995).

The stiffness of the crystals was also determined using Young's modulus (E) as shown in Table 5.4. as given by equation 5.4.2;

$$E = \frac{9G}{3+k} \tag{5.4.2}$$

with G being the shear modulus of the material and k the Pugh's ratio.

The rigidity of materials is indicated by high values of Young modulus as it gives the ratio of linear stress to linear strain. According to the results attained from this study as shown in Table 5.4, all structures of Niobium Carbide have high values of Young's modulus in comparison to identical structures of Niobium Nitride. For instance, it was noted that Niobium Carbide in rocksalt structure has the highest value of Young's modulus amidist all the structures of Niobium Carbide as well as Niobium Nitride regarded in this study. In general, Young's modulus of a material used for hardness related applications is expected to be extremely high, as supported by data shown in Table 5.4. It is thus anticipated that Niobium Carbide in rocksalt structure would work comparatively well as materials with high Young's modulus in such application as a result of its high Young's modulus as comparable with other structures of Niobium Carbide as well as Niobium Nitride studied in this study.

The Voight-Reuss-Hill approximation on the shear modulus was used to provide the magnitude of elastic anisotropy of the crystal, Pauleau (2012). The results presented on Table 5.4 represents the elastic properties of the two systems whereby the carbide was found to possess high values in all structures compared to the nitride.

High shear and high bulk modulus are some of the main characteristics of materials used for hardness and related applications. However, the applicability of these materials is not only limited to these mechanical parameters as there are other important parameters that are necessary when determine the applications of these materials. One of these important parameter is the toughness of a material which is used as a measure of the degree of plastic deformation (ductility) of the solids under mechanical loading. In this study, ductility of the systems of interest were explored using Pettifor criterion, Chung

& Buessem (1967). According to this criterion, the values of Cauchy pressure $C_{12} - C_{22}$ should be positive for metallic non-directional bonding compounds. For the region where these values are positive the material is considered to be ductile. The Pugh's modulus ratio criterion B/G, Pugh (1954), was also considered whereby the systems with $B/G > 0.57$ are termed as brittle. Both Pettifor's and Pugh's criteria were used to map the ductile together with brittle behaviour of NbC and NbN as shown in Figure 5.4.2.

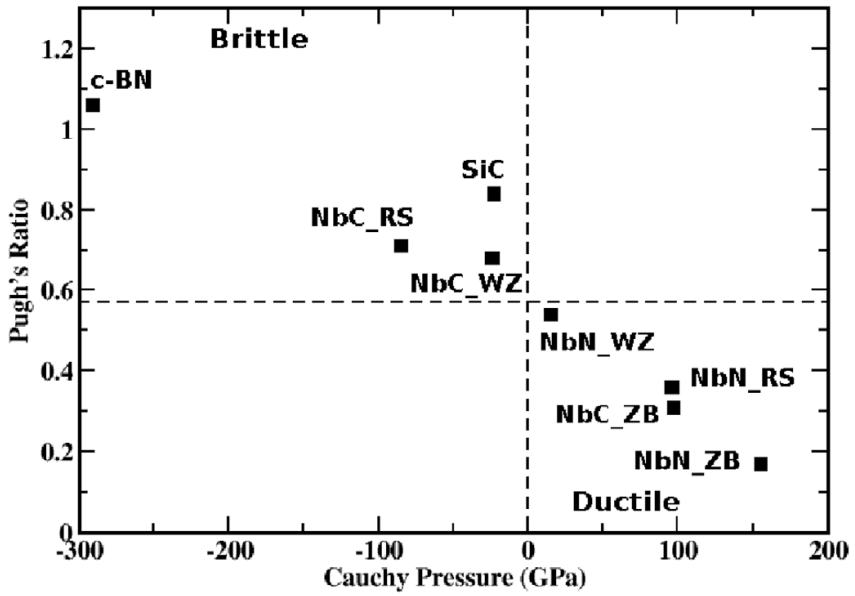

Figure 5.4.2: Ductility and brittleness mapping of Niobium Carbide and Niobium Nitride in different crystal structures compared to Silicon Carbide and c-BN.

It is shown that Niobium Carbide in rocksalt and wurzite structures are brittle similar to c-BN, while the zincblende structure of Niobium Carbide and all structures of Niobium Nitride are ductile. Similarly, the Poisson ratio is another parameter that can be applied to predict either the ductility or brittleness of a system. In such scenario, ductility together with brittleness of a material, are set apart by a value of about 0.26. In the case of where the value of Poisson ratio is greater than (less than) 0.26 the material coincides to ductility (brittleness) behaviour, Haines et al. (2001). According to the data provided in Table 5.4 these values range from 0.11 to 0.41. It is clear that Niobium Nitride in all structures together with Niobium Carbide in zincblende have Poisson ratio above 0.26 and therefore can be termed as ductile materials while Niobium Carbide in rocksalt together

with wurzite structures have values below 0.26 implying that they are brittle. These findings are consistent with the Pettifor's criterion presented earlier as shown in Figure 5.4.2. Pugh's ratio has been found to give a similar trend to that of Poisson's ratio and B/G ratio for the materials of interest in this work. For instance, the findings of NbC in zincblende and all structures of NbN show that these structures are ductile which is consistent with earlier studies. Thus, the ductile materials can be used in applications such as cutting and drilling while the brittle ones can be applied in aerospace related applications and electronics.

Both the shear modulus and bulk modulus have significant influence on the Vicker's hardness of a material. By examining the data presented in Table 5.4, the brittle systems are associated with high values of Vicker's hardness compared to the ductile structures. Further, the study analyzed the hardness of different structures of NbC and NbN through the empirical scheme presented by Xing Qiu et al. (2011). This method provides a correlation between the Vickers hardness as well as Pugh's modulus ratio of the material considered as supported by equation 5.4.3;

$$H_v = 2(k^2 G^{0.585}) - 3 \tag{5.4.3}$$

where k , G and B are pugh's ratio,shear modulus plus bulk modulus.

Table 5.4 provides the Vicker's hardness of different structures of NbC together with NbN. NbC in RS had the highest value of Vicker's hardness of about 28 GPa. This value is in comparison to that of SiC in zincblende structure which is 30 GPa, Wade-Zhu et al. (2015). In addition, NbC in wurzite structure had a value of 26 GPa, which is comparable to that of Niobium Carbide in rocksalt and SiC. From these findings the materials have comparable performance in terms of hardness related applications as anticipated amidst these systems. Other compounds, such as zincblende structure of Niobium Nitride as well as Niobium Carbide, and Niobium Nitride in rocksalt had lower Vicker's hardnesses of < 10, while Niobium Nitride in wurzite reported a higher value of 18 GPa. Using the calculated values of Vicker's hardness, the materials have been classified as hard, superhard or ultrahard based on the magnitude of their Vicker's hardness as shown in

Figure 5.4.3.

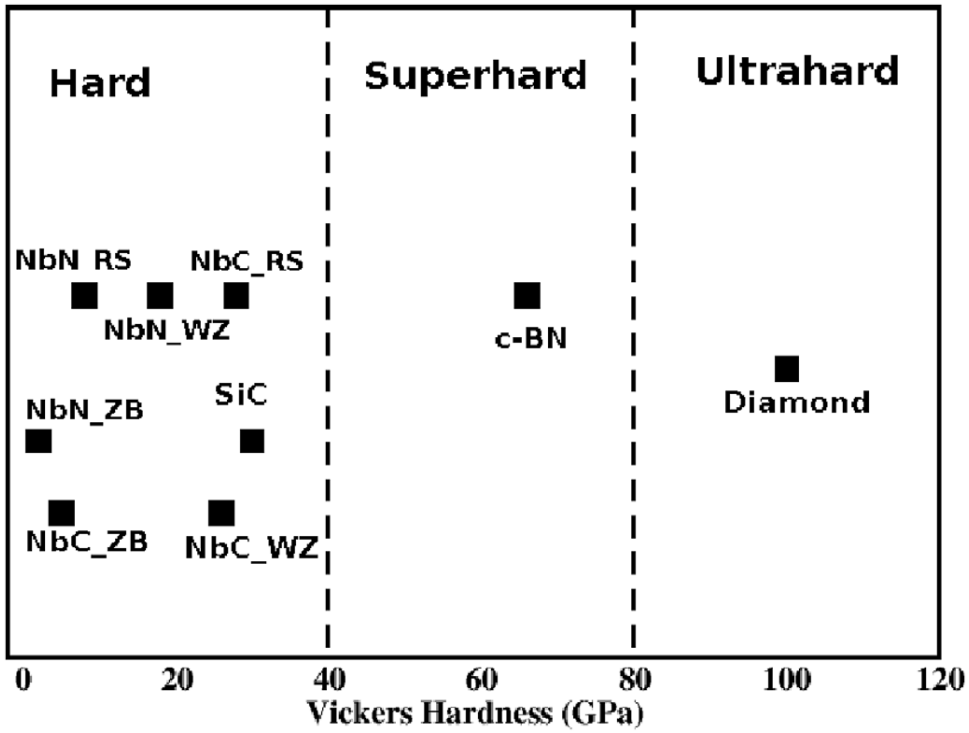

Figure 5.4.3: Classification of Niobium Carbide together with Niobium Nitride in terms of Vicker's hardness.

According to Figure 5.4.3, the various structures of NbC as well as NbN together with SiC were found to be hard structures, while on the other hand, c-BN was classified as a super-hard material as its Vicker's hardness lies between 40 GPa and 80 GPa.

5.5 EFFECT OF DEFECTS ON MECHANICAL PROPERTIES

5.5.1 Elastic constants

The effects of anionic defects on mechanical properties of TMCNs is overlooked yet the substantial concentrations of these vacancies have an impact on the mechanical properties. Generalized Hooke's law, Cocco & Masin (2010), is used to investigate how materials respond to forces via stress-strain relationship. There are several mechanical properties of materials such as elastic constants, bulk and shear moduli, Young's modulus among others that may be affected by the presence of defects in them. Elastic constants which

are some of the main properties investigated in this work provide insights on how crystal structure, bonding as well as stability of materials relate with each other by introducing small distortions to the system, Mehl et al. (1994) and Ortiz et al. (2013).

The effects of defects on the elastic constants of NbC and NbN were investigated in this study. These elastic constants are sensitive to different defect concentrations. A trend of decrease in elastic constants with rise in defect concentration is observed. The elastic constants of both pristine and systems with defects were calculated. For the pristine structures, the lattice as well as elastic constants were established to be accordant with other studies, Muchiri et al. (2019), Korir et al. (2011). The observed decrease in elastic constants with increase in defect concentration can be attributed to reduction in bonding coordination number as a result of missing anionic atoms. Figure 5.5.1-5.5.3 represent the elastic constants of the systems considered in this study.

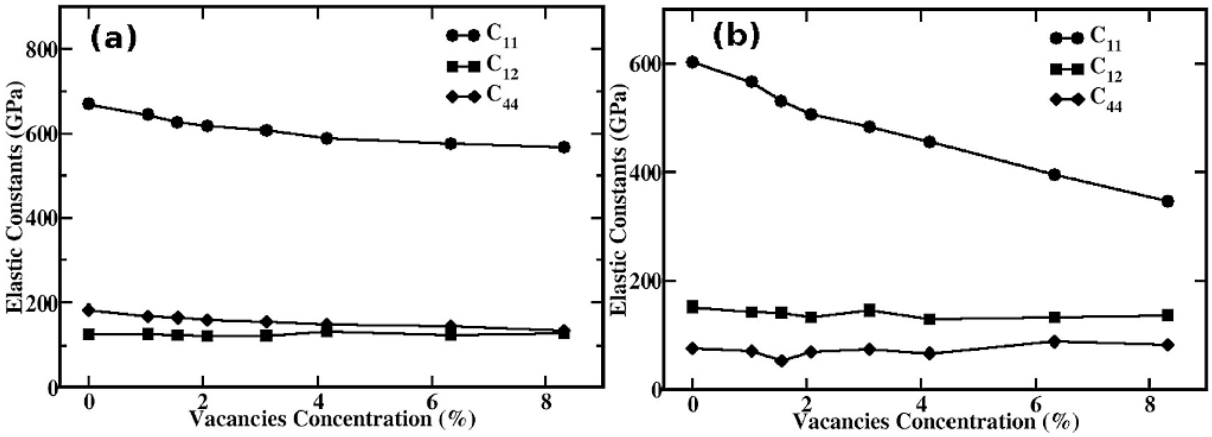

Figure 5.5.1: Elastic constants of (a) Niobium Carbide together with (b) Niobium Nitride in RS structure, respectively, as a function of C/N vacancies concentration.

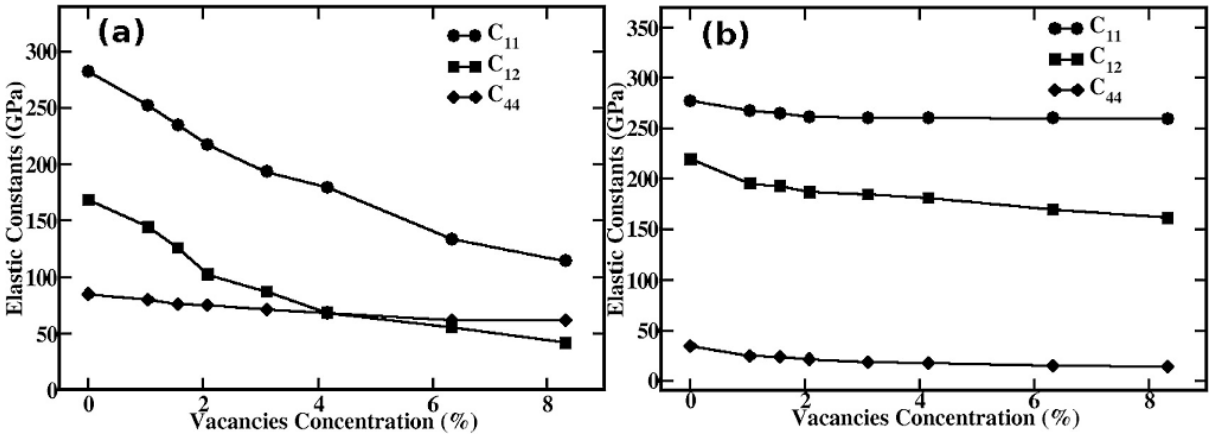

Figure 5.5.2: Elastic constants of (a) Niobium Carbide together with (b) Niobium Nitride in ZB structure, respectively, as a function of C/N vacancies concentration.

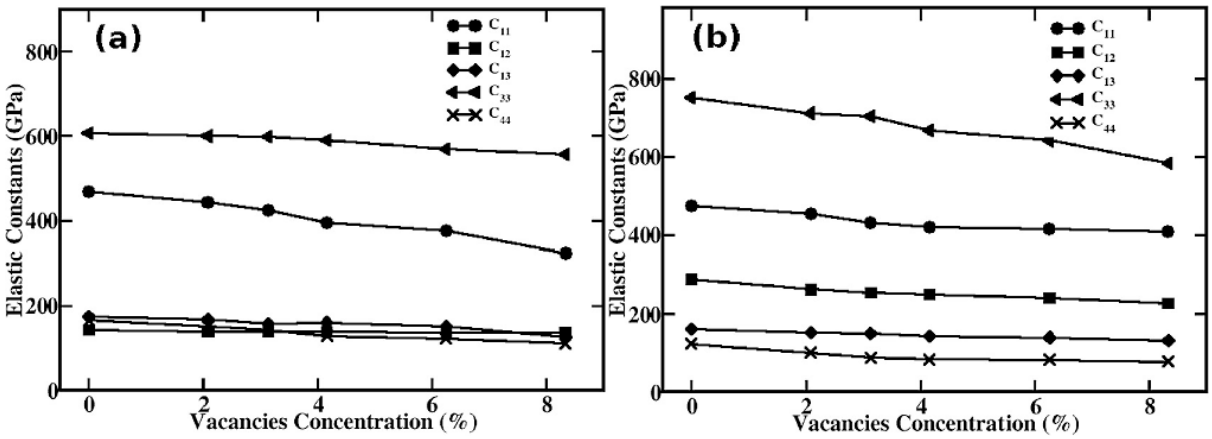

Figure 5.5.3: Elastic constants of (a) Niobium Carbide together with (b) Niobium Nitride in WZ structure, respectively, as a function of C/N vacancies concentration.

Different elastic constants have varying response to the presence of defects concentrations introduced into the systems. For instance, a marginal decrease in C_{12} together with C_{13} was noted in rocksalt as well as wurzite structures of NbC and NbN. This behaviour can be attributed to the non-axial nature of the stress applied to the system. When compared to other elastic constants such as C_{11}, these former elastic constants were found to have low values implying that small stress is required to be applied to a system for any given strain. Therefore, the values of elastic constants are slightly affected by the non-directional stress. Following further analysis of the data obtained, a significant reduction in C_{11} and C_{33} in WZ structure of NbN together with C_{12} for NbC in zincblende was noted.

C_{11} for Niobium Carbide along with Niobium Nitride in rocksalt was found to decrease

with increase in defect concentration while there was largely insensitive behaviour to changes in anionic defect concentrations by C_{12} and C_{44}. Following the different defect concentrations considered, there was decrease in values of C_{12} and C_{11} by 54 % and 57%, respectively, in the ZB structure as the defect concentration rose to 8 % for NbC. However, the C_{44} elastic constant was moderately affected by the presence of defects up to 12 % for the NbC. On the other hand, C_{11}, C_{12} as well as C_{44} of NbN were found to decrease with increase in defect concentrations up to 4 % as shown in Figures 5.5.1 - 5.5.3, while beyond this concentration only marginal effect was noted.

Similarly, for WZ structure the C_{11} is strongly affected by the increase in vacancy concentration especially in NbC where the decrease is quite significant with a 40 % change. Other elastic constants are slightly affected by anionic vacancies implying the decrease is of low percentage. In NbN, there was a decrease in C_{33} with increase in anionic vacancies concentrations although values of other elastic constants are moderately affected. For the cubic and hexagonal structures, the Born criterion was used to determine the mechanical stability of these structures, Born & Huang (1954), in the presence of defects. The stability was tested up to a defect concentration of 8 %. The tests were done since anionic vacancies are known to perturb the symmetry of systems and this may reduce the stability of the materials involved. The retention of the mechanical stability of NbN and NbC in the presence of defects suggests that the vacancies can occur in these systems without their properties being significantly compromised.

5.5.2 Calculated DFT-GGA Bulk modulus (B), shear modulus (G), Young's modulus (E), Poisson ratio (v), Voigt-Reuss-Hill moduli as well as Vickers hardness (Hv) of Niobium Carbide together with Niobium Nitride in different crystal structures

Apart from elastic constants, other mechanical properties such as Young's, shear and bulk moduli are important when predicting the response of materials to forces and their applications. These properties are determined using the expressions 5.4.2 and 5.4.1 as given by the Voight-Reuss-Hill approximation, Hill et al. (1989), while Vicker's hardness is determined using equation 5.4.3. These properties are as shown on Table 5.4 for the

pristine form of NbC and NbN.

The mechanical properties are also affected by the presence of defects in a system. For instance, the bulk modulus tend to decrease with increment in defect concentration although the parameter remains unchanged up to a defect concentration of 1.5 %. Overall, the bulk modulus decreases with increase anionic vacancies concentrations. Similarly, Young's modulus is also affected by the defects with a notable decrease observed. There was no change in Young's modulus beyond 4 %. The most affected structure is the RS while the least is ZB which was insensitive to increase in anionic vacancies concentrations resulting into negligible change on the values of Young's modulus. WZ structure gives a steady linear trend on the changes of Young's modulus as the defect concentration increase even at 8 % as shown in Figure 5.5.4.

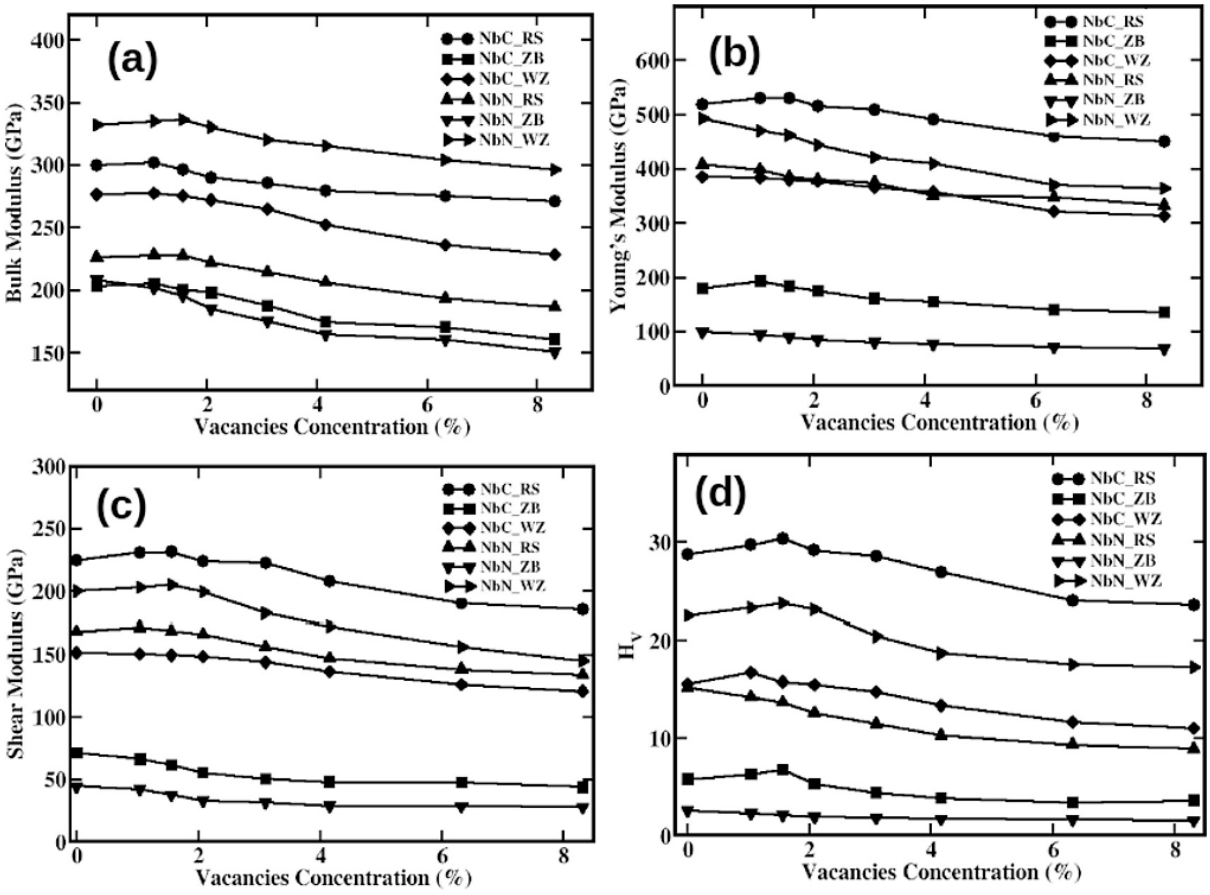

Figure 5.5.4: Mechanical attributes of NbC together with NbN in rocksalt, zincblende as well as wurzite crystal structures, respectively as a function of anionic vacancies concentration. (a) bulk modulus (b) Young's modulus (c) Shear modulus (d) Vicker's hardness.

Similarly, shear modulus as well as Vicker's hardness are affected by the rise in defect

concentration. Beyond 1.5 % these properties decrease with different rates as defect concentration rises which is consistent with the trend formed by other properties as shown in Figure 5.5.4 (c-d). The disparity in how the decrease happens may be attributed to the varying bonding dynamics. The shear modulus decreased significantly in WZ structure and negligible changes happened in the ZB structure. For the Vicker's hardness, RS had the largest decrease while the least took place in ZB structure. Overall, there was a decrease in all the mechanical properties with increase in defect concentration. Experimental work on RS structure of NbC and NbN was performed whereby there was marginal decrease in shear modulus as the vacancy concentration increases up to 12.5 %, Holleck (1986). However, our study considered lower concentrations but speculate that at higher defect concentrations beyond 12.5 % dramatic drop in values of shear modulus and other mechanical properties may emerge. This is because the current results achieved in this study are in concurrence with other studies, Rathod et al. (2011), Gou et al. (2008), Holleck (1986), which worked at lower concentrations. The Vicker's hardness of Niobium Carbide as well as Niobium Nitride deteriorated in the three structures and maybe an indication that these materials may not perform efficiently in hardness related application although they are classified as hard materials. For instance, there was a decrease by 36 % of the Vicker's hardness at 8 % for NbC in RS. Thus, there should be of control of defect concentrations in transition metal carbides and nitrides for their use in hardness related applications.

The robustness of materials is determined by determining the toughness of materials which measure the plastic deformation (ductility) of crystals when subjected to mechanical loading. Pettifor criterion as applied to the pristine systems was used to analyze the ductility of NbC and NbN using the Cauchy pressure (C_{12} - C_{44}) where by positive or negative represent ductile or brittle systems, respectively, Chung & Buessem (1967). Moreover, the Pugh's modulus was used to determine the toughness of both NbC and NbN. For $\frac{G}{B} > 0.57$ the system is brittle while for $\frac{G}{B} < 0.57$ the material is ductile, Pugh (1954). Thus, this study considered the two criteria in analysing the effect of defects on the toughness of Niobium Carbide along with Niobium Nitride in rocksalt,

zincblende as well as wurzite structures as shown on Figure 5.5.5.

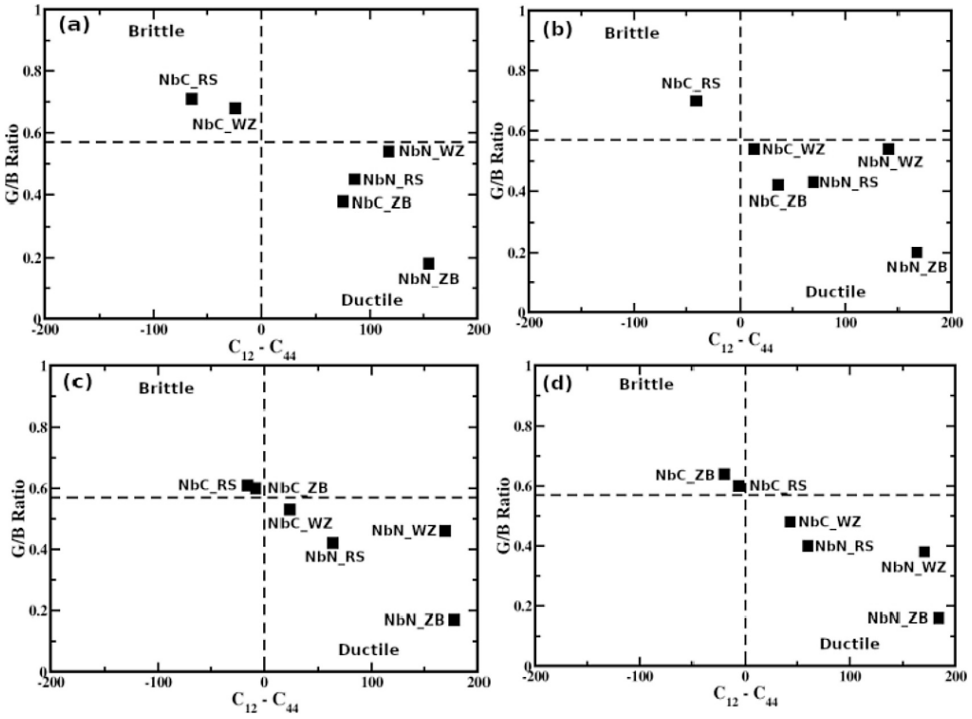

Figure 5.5.5: Brittleness and ductility maps of Niobium Carbide as well as Niobium Nitride in rocksalt, zincblende together with wurzite as a function of anion vacancy concentration (a) pristine (b) 2 % (c) 4 % (d) 8 %.

According to Figure 5.5.5, the rocksalt and wurzite structures of NbC were found to be brittle for the systems in pristine nature and all structures of Niobium Nitride and ZB of NbC were ductile. These results are consistent with those obtained by Muchiri et al. (2019). Upon introduction of anionic vacancies the toughness was also found to change. For example, for increased defect concentration up to 2 %, the brittleness of Niobium Carbide in rocksalt as well as wurzite structures tend to reduce while Niobium Carbide in WZ raises its ductility. It can thus be observed that ductility increases with rise in defect concentration. Niobium Carbide in rocksalt becomes brittle at 4 % defect concentration as the ductility of this system decreases with increase in defect concentration which is attributed to the rigidity of the bonds induced by the anionic vacancies as shown on Figure 5.5.5 (c). For the case of NbN in all structures the ductility behaviour is maintained with negligible change as the defect concentration rises up to 8 %. Thus, the vacancies concentration of up to 8 % tend to midly affect the ductility of NbN while dramatic effects are noted in the case of Niobium Carbide as shown in Figure 5.5.5 (b -

d).

Moreover, the Poisson's ration can also be used to determine the ductility and brittleness of materials. Ductility as well as brittleness are set apart by a value of 0.26 whereby ductile materials have a Poisson ratio more than 0.26 while for brittle ones the Poisson's ratio is below 0.26, Haines et al. (2001).

The Poisson's ratio of NbC and NbN in different crystal structures and defect concentrations ranges between 0.21 and 041 for this study as shown in Figure 5.5.6. The RS structure of NbC retains its brittleness nature even in the presence of carbon vacancies up to 8 % although the values tend to decrease. In WZ, NbC gains ductility nature beyond a defect concentration of 6 % while in ZB the NbC becomes brittle when vacancy concentration rises up to 6 %. For Niobium Nitride in all structures, the system remain ductile and is insensitive to the different anionic defect concentrations. These results are consistent with the findings observed earlier using Pettifor's and Pugh's criterion.

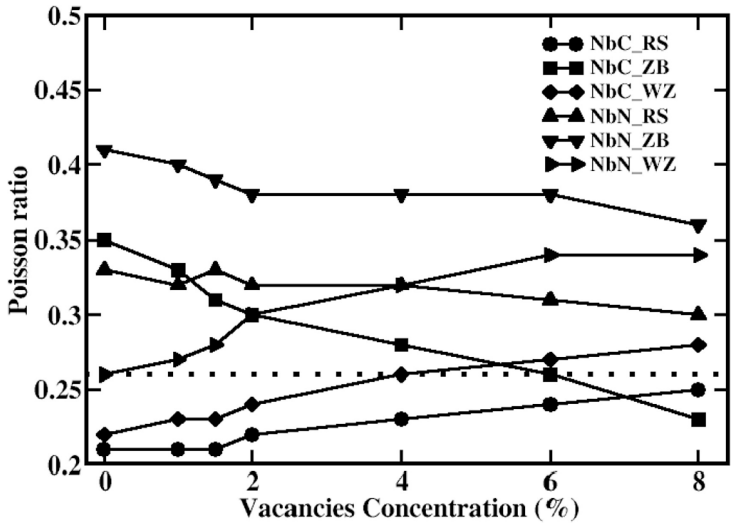

Figure 5.5.6: Poisson ratio for Niobium Carbide together with Niobium Nitride in rocksalt, zincblende as well as wurzite for pristine structure and defective structures with defects concentration between 1 % and 8 %. Britlle and ductile are separated by the dotted line.

5.6 EFFECTS OF TEMPERATURE ON THE MECHANICAL PROPERTIES OF NIOBIUM CARBIDE TOGETHER WITH NIOBIUM NITRIDE

This section focuses on how the elastic and mechanical properties of Niobium Carbide together with Niobium Nitride in rocksalt, zincblende as well as wurzite structures are affected by temperature within the range of 0 to 1500 K. Due to the high melting points of the refractory materials, TMCNs including NbC and NbN can be used as high-temperature materials with potential and application prospects at industries operating at high temperature conditions such as aerospace industry. In practice materials contain defects among them vacancies which tend to affect their mechanical properties. The TMCs are known to maintain their crystal structure with a carbon loss of up to 25 % at elevated temperatures. Studies on defects is critical in optimizing their use, for instance, Muchiri et al. (2022) noted a substantial deterioration in mechanical properties including the elastic constants of NbC and NbN with increase in vacancies concentrations. Elastic moduli as well as elastic stiffness constants of materials have primary importance when designing and optimizing materials. For instance, Born criterion conditions, Born & Huang (1954), have to be verified when in search of novel materials that are mechanically stable. For cubic structures $C_{44} > 0$, $C_{12} > C_{12}$ and $C_{11} + C_{12} > 0$, and for hexagonal structure $C_{33} > 0$, $C_{44} > 0$, $C_{12} > 0$, $C_{11} > C_{12}$, $(C_{11} + 2\ C_{12}\ )\ C_{33} > 2C_{13}^2$ as mentioned before. From this study all the structures studied at different values of temperature and defect concentrations have been found to be mechanically stable as these Born criterion conditions are satisfied. The stress-strain relationship as shown in Figure 3.15.1 at different temperature in the presence of various vacancy concentrations have been determined in this study. As reported by Muchiri et al (2019) the different vacancy concentrations in a material do not affect the stress-strain relation. The curves of this relation show the elastic deformation stage followed by the plastic deformation stage. On the other hand, temperature only slightly affects the elastic deformation stage. This is characterised by the thermal motion of atoms which become intense due to the

increase in the temperature and this results into the movement of atoms from their initial stable position. This movement is likely to result into plastic deformation. For instance, according to the elastic constants of NbC and NbN this yield phenomena does not occur especially at low temperatures but is quite prominent at high temperature such as 1500 K as shown in Figures 5.6.1 - 5.6.3. Brittleness prevails in most of the structures of NbC and NbN at low temperature below 1000 K. In some of the structures such as NbC in the zinc blende crystal structure, the yield phenomena is more pronounced as the temperature increases, suggesting that as the temperature rises the materials becomes ductile.

5.6.1 Elastic constants of Niobium Carbide along with Niobium Nitride with defects at elevated temperature

From the obtained results, the elastic constants from the MD at room temperature agree well with the corresponding results of static systems. Though there are limited studies reporting on the experimental measurements of temperature dependence on elastic properties of NbC and NbN, the reliability of the simulations in this study can be shown by comparing with the available data. An earlier study has determined some mechanical properties of NbC such as Young's modulus at room temperature, Shaffer (1964). This study provides some experimental data that helps in comparing with the current theoretical values from this work. From Shaffer's study, the Young's modulus of NbC with different defect concentrations were as follows; 478 GPa, 488 GPa and 451 GPa for $NbC_{0.95}$, $NbC_{0.964}$ and $NbC_{0.969}$, respectively. Furthermore, the values of shear modulus were 197.0 GPa, 198.7 GPa, 188.5 GPa for $NbC_{0.95}$, $NbC_{0.964}$ and $NbC_{0.969}$, respectively. This study reports on the mechanical properties of Niobium Carbide in rocksalt, zincblende as well as wurzite from zero temperature to moderate and high temperature ranging from room temperature to 1500 K which are typically the working temperatures in the machining industry. The defect and temperature dependency on mechanical properties of Niobium Carbide as well as Niobium Nitride in the RS, ZB together with WZ crystal structures have been investigated and compared with the available experimental and theoretical values. Figures 5.6.1 to 5.6.3 show the dependency of elastic moduli of NbC and NbN on the temperature for different vacancy

concentrations.

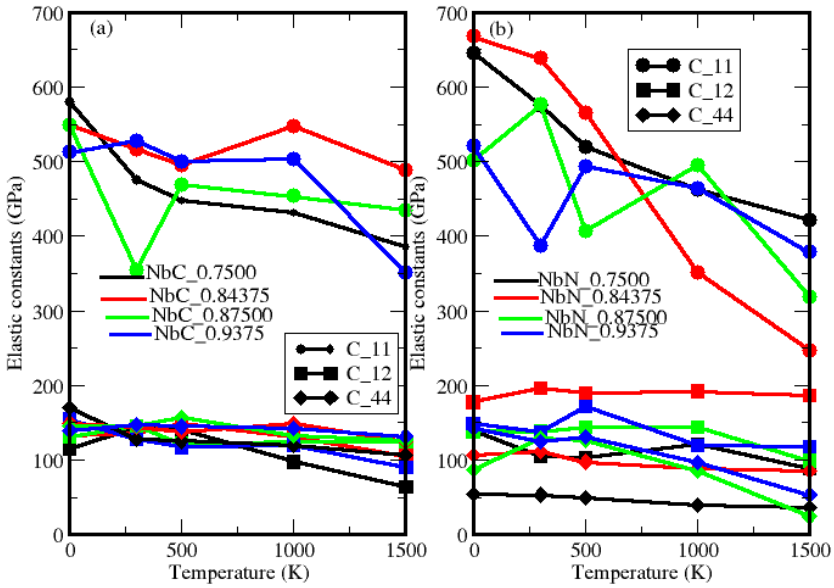

Figure 5.6.1: Calculated elastic constants of (a) Niobium Carbide together with (b) Niobium Nitride in rocksalt crystal structure at different temperatures and defect concentrations.

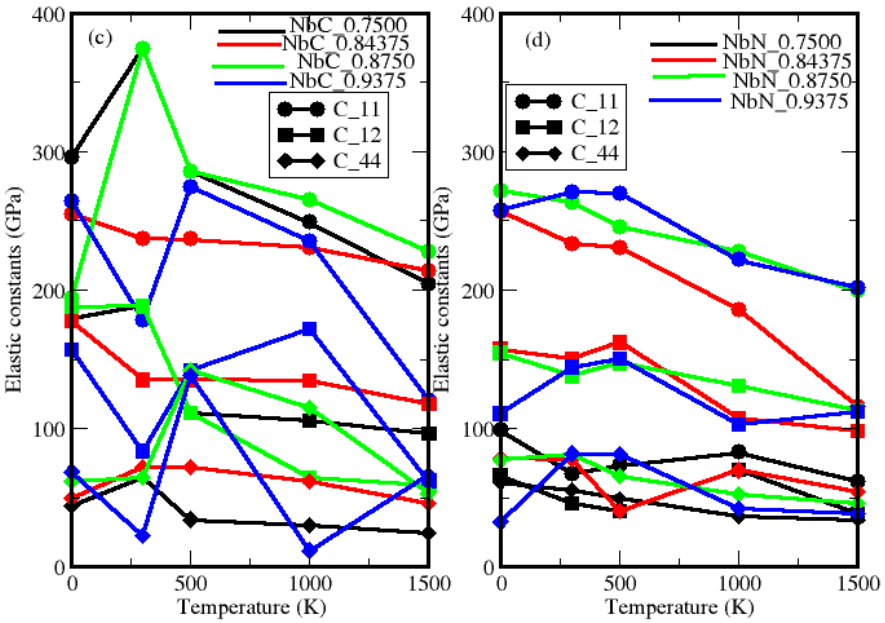

Figure 5.6.2: Calculated elastic constants of (c) Niobium Carbide together with (d) Niobium Nitride in zincblende crystal structure at different temperatures and defect concentrations.

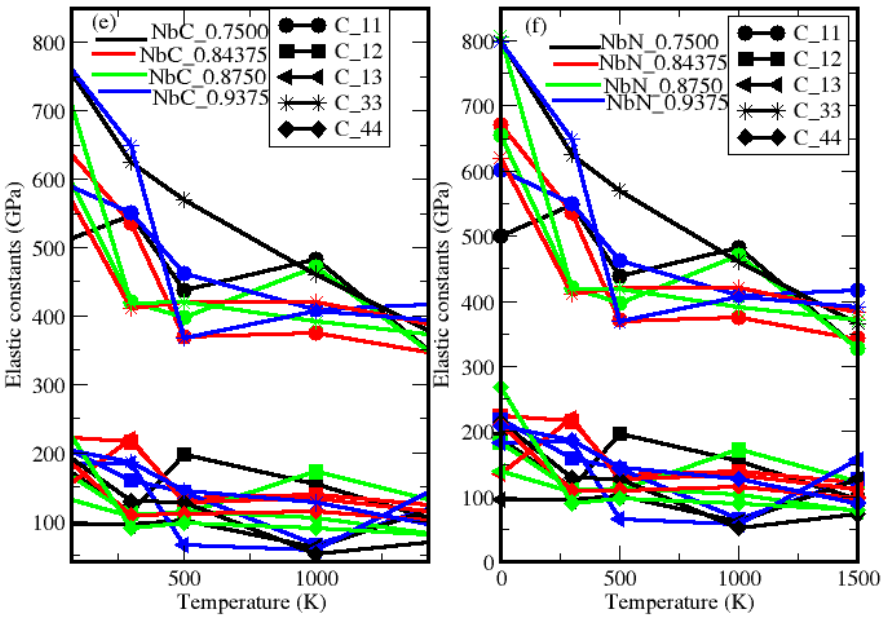

Figure 5.6.3: Calculated elastic constants of (e) Niobium Carbide together with (f) Niobium Nitride in wurzite crystal structure at different temperatures and defect concentrations.

As both the temperature and vacancy concentrations increases, the values of elastic modulus declines nonlinearly, Ruicheng et al. (2018). From 500 K to 1500 K representing the working conditions of these materials the elastic modulus decreases nonlinearly.

It can be hypothesized that the elastic constants reduce due to increase in bonding distance as a result of increased thermal movement of the atoms. In particular, C_{44} and C_{13} in rocksalt as well as wurzite structures as illustrated in Figures 5.6.1 and 5.6.3, respectively, have marginal decrease ranging between 1 % and 20 % as the temperature increases from 0 to 1000 K. Compared to C_{11} and C_{33} one observes that these elastic constants have small values implying that they require less non-directional stress so as to give rise to the corresponding strain. Similarly, C_{11} for Niobium Nitride in rocksalt (Fig. 5.6.1b) and NbC in ZB (Fig. 5.6.2c), C_{33} for NbC in WZ (Fig. 5.6.3e) have significant reduction beween 34 % and 61 % in the values of their elastic constants as the temperature rises from 0 K to 1500 K. For example, there is a decrease in the values of C_{11} for NbC in ZB by 52.28 % and 53.72 % C_{33} for NbC in WZ as the temperature increases.

C_{11} for NbN in RS is greatly affected by change in temperature and defect concentration compared to the carbide. For instance, there is a change in C_{11} by 61.39 % in NbN with RS crystal structure compared to 33 % in NbC (RS) as shown by the decrease in the values presented in Figure 5.6.1. C_{12} for this structure tend to be insensitive to change in temperature inspite of the presence of defects. For the ZB crystal structure, C_{44} was found to be less affected by increase in temperature while C_{11} decreases with increase in temperature by 54 % and 56 % for NbC (Fig. 5.6.2c) and NbN (Fig. 5.6.2d), respectively. For WZ structure, C_{12} for the NbN (Fig. 5.6.3f) decreases with increase in temperature. There is mild effect on the values of other elastic constants with increase in temperature. This is with the exception of C_{33} as mentioned earlier.

5.6.2 Effects of temperature on mechanical properties of Niobium Carbide together with Niobium Nitride

Mechanical properties are very important when determining the applications of different materials. The properties explored in this study as a function of temperature include the bulk modulus (B), Young's modulus (E), and shear modulus (G) as calculated using equations 3.15.12 to 3.15.15. The hardness of the materials was determined using equation 3.15.18 from the already calculated elastic constants. The calculated mechanical properties are as illustrated in Figures 5.6.4 and Figures 5.6.5.

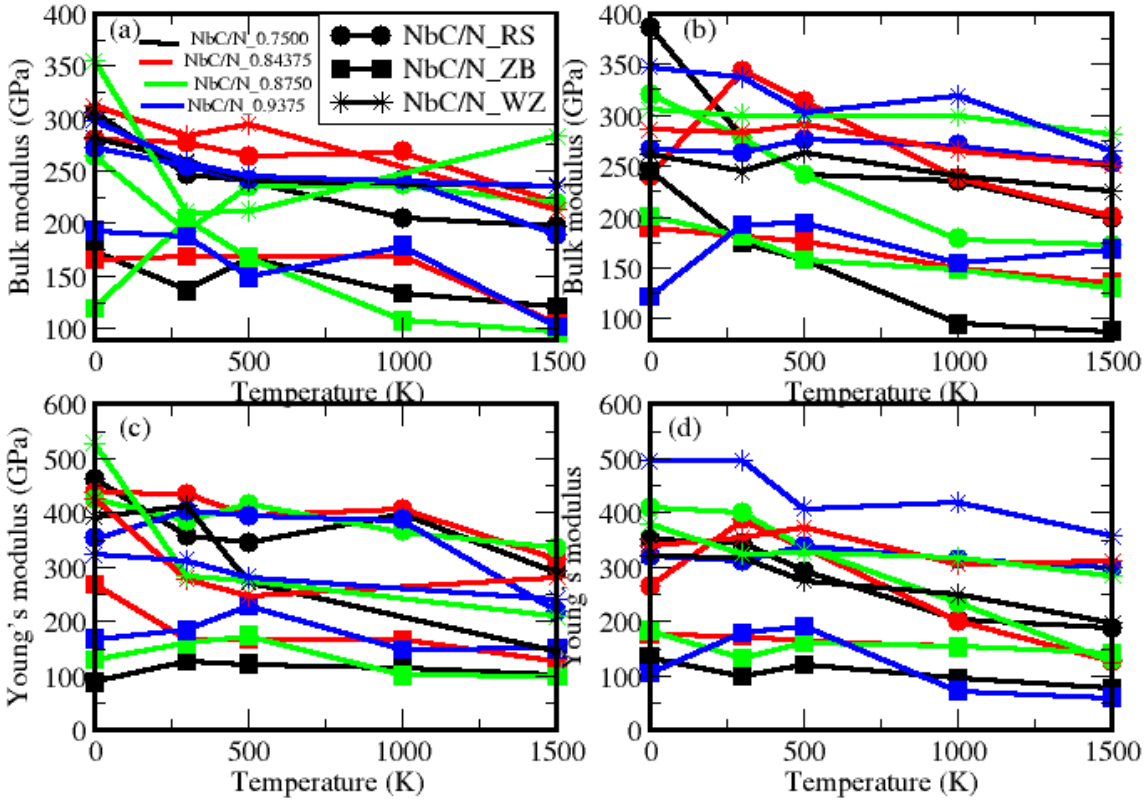

Figure 5.6.4: Calculated bulk modulus for (a-b) Niobium Carbide and Niobium Nitride and Young's modulus for (c-d) Niobium Carbide and Niobium Nitride , respectively, in rocksalt, zincblende and wurzite crystal structures with different defect concentrations and temperature between 0 K and 1500 K.

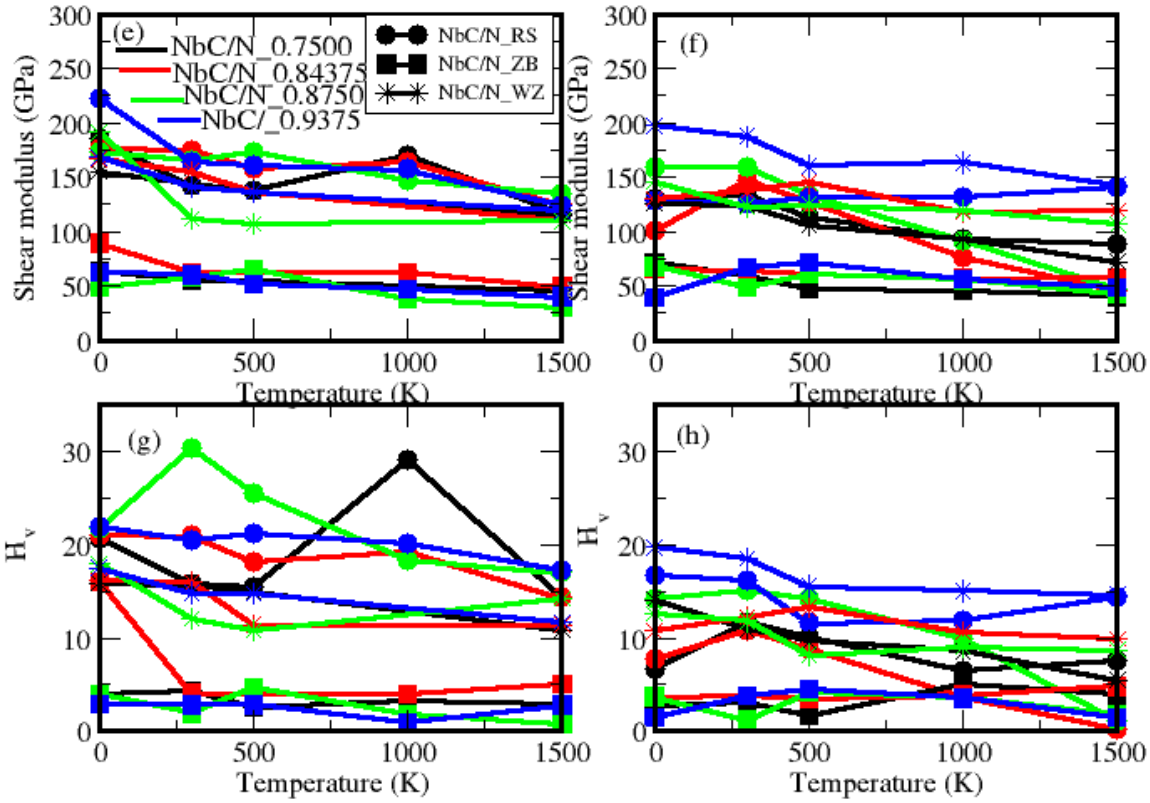

Figure 5.6.5: Calculated shear modulus for (e-f) Niobium Carbide together with Niobium Nitride and Vickers hardness for (g-h) Niobium Carbide and Niobium Nitride , respectively, in rocksalt, zincblende and wurzite crystal structures with different defect concentrations and temperature between 0 K and 1500 K.

Both NbC and NbN have comparable mechanical properties in all structures. A closer look at the plots shows that the values of bulk modulus are slightly higher for NbN compared to those of NbC. This study established that the bulk modulus, Young's modulus and shear modulus decrease with increase in temperature for the two materials in the three structures i.e rocksalt, zincblende and wurzite. This behaviour is attributed to the weakening of the bonds as the temperature is progressively increased. Nonetheless the decrease is only marginal for bulk, shear and Young's moduli. It has already been established that different vacancy concentrations result into different values of strength of the materials, Muchiri et al. (2022). The values of Young's modulus in both systems

and all crystal structures are high compared to other mechanical properties indicating the high rigidity of the materials. According to the results presented in Figures 5.6.4 and 5.6.5, NbC has high values of Young's modulus in cubic structure in comparison with corresponding Niobium Nitride structures across the whole temperature range between 0 to 1500 K. These high values of Young's modulus provide an highlight of the possibility of application of NbC where hardness is necessary. Similarly, temperature also influences the strength of a material. As the temperature rises, the strength of the material reduces and this happens due to the severe thermal motion in the material as the temperature increases and the distance between internal atoms increases leading to reduced mutual attraction and plastic deformation occurs. As the vacancy concentration increases the strength of the material decreases as shown in figures 5.6.4 and 5.6.5. Plastic deformation of a material which describes its ductility is an important parameter when studying materials. This study investigated the toughness of NbC and NbN and classified each structure as either brittle or ductile using Pugh's criteria, Pugh (1954). It reproduces the ductility trends of Niobium Carbide in WZ as well as ZB and Niobium Nitride in all structures. This is obtained from the criteria that $\frac{G}{B} > 0.57$ for brittle materials and $\frac{G}{B} < 0.57$ for ductile materials. The systems become more ductile with increasing temperature as the strength reduces as shown in figure 5.6.6. This becomes very clear when Figure 5.6.6 is compared with Figure 5.5.5 obtained at ground state.

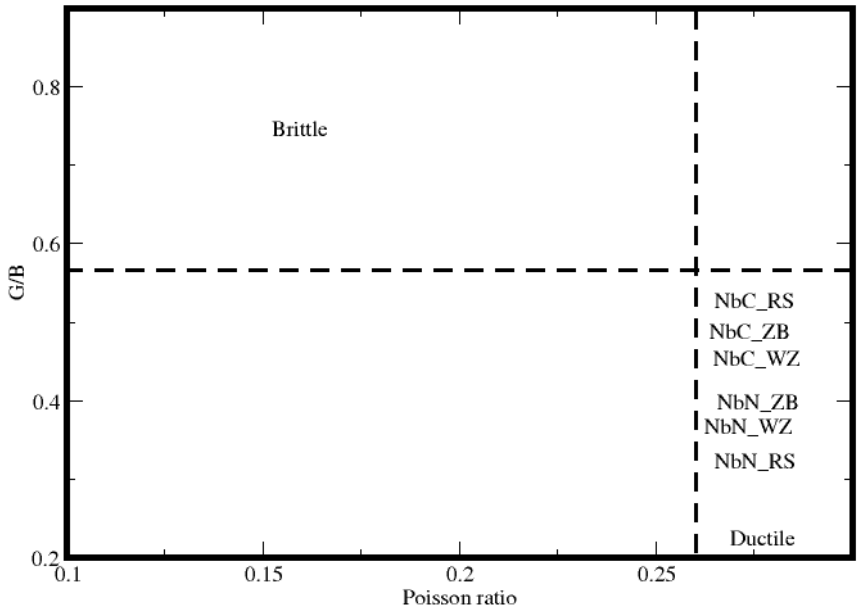

Figure 5.6.6: Maps of ductility and brittleness for Niobium Carbide and Niobium Nitride in different crystal structures with different defect concentrations and temperature ranging between 0 K and 1500 K.

5.6.3 Nudged elastic band calculations

Different processes in materials such as crystalline solids are controlled by ion diffusion through the mechanism of either vacancy mechanism or interstitial mechanism, Angsten et al. (2014). For monoatomic close-packed crystals the atomic diffusion occurs through vacancy mechanism which has been investigated in this study. The vacancy-mediated self-diffusion are thermally activated process and the atoms migrate by passing through an energy barrier by moving from a local energy minimum site to the nearest vacancy site.

The vacancy formation energies of C/N in NbC and NbN have been determined in previous studies, Muchiri et al. (2022). However, limited studies report on the vacancy migration energy barriers of these materials. In this study, the transition states are determined after locating the initial and final positions of the vacancy site in a supercell using the Nudged Elastic Band method. The method is applied to find the minimum energy path of the vacancy between the initial and the final positions for very specific jump and the vacancy migration energy is determined as shown in Figures 5.6.7 to 5.6.9

for the case of NbC and NbN respectively. These figures provide a representation of the transition states of Niobium Carbide and Niobium Nitride from the various defect concentrations considered in this study.

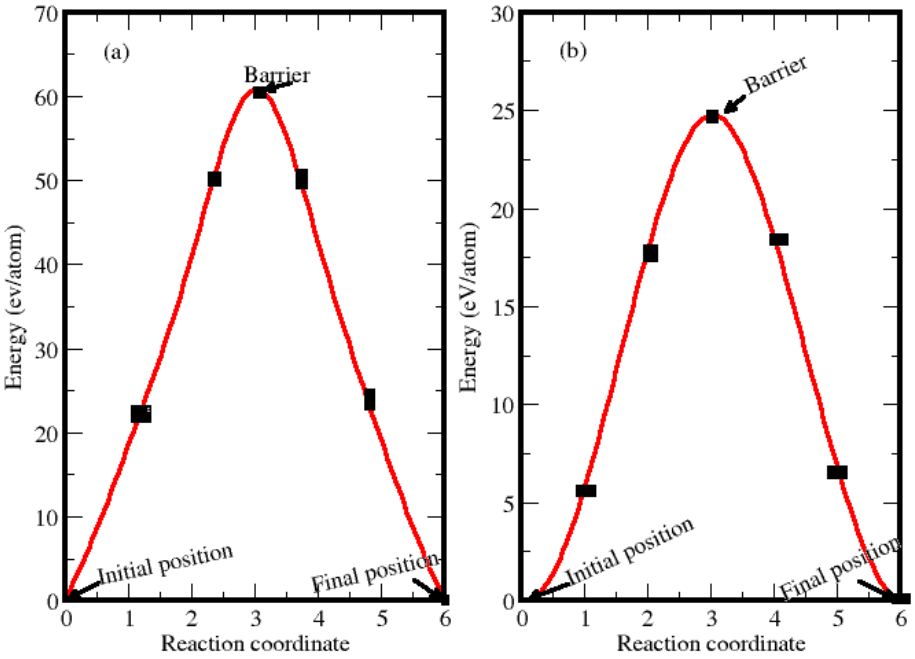

Figure 5.6.7: Vacancy migration energy curve for (a) Niobium Carbide and (b) Niobium Nitride, respectively, in RS with defect concentration of 3%.

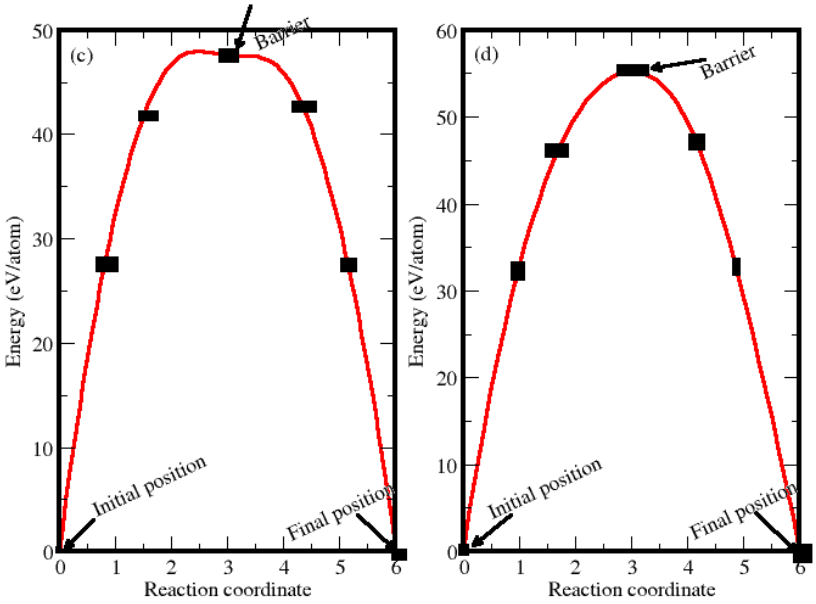

Figure 5.6.8: Vacancy migration energy curve for (c) Niobium Carbide and (d) Niobium Nitride, respectively, in ZB with defect concentration of 2%.

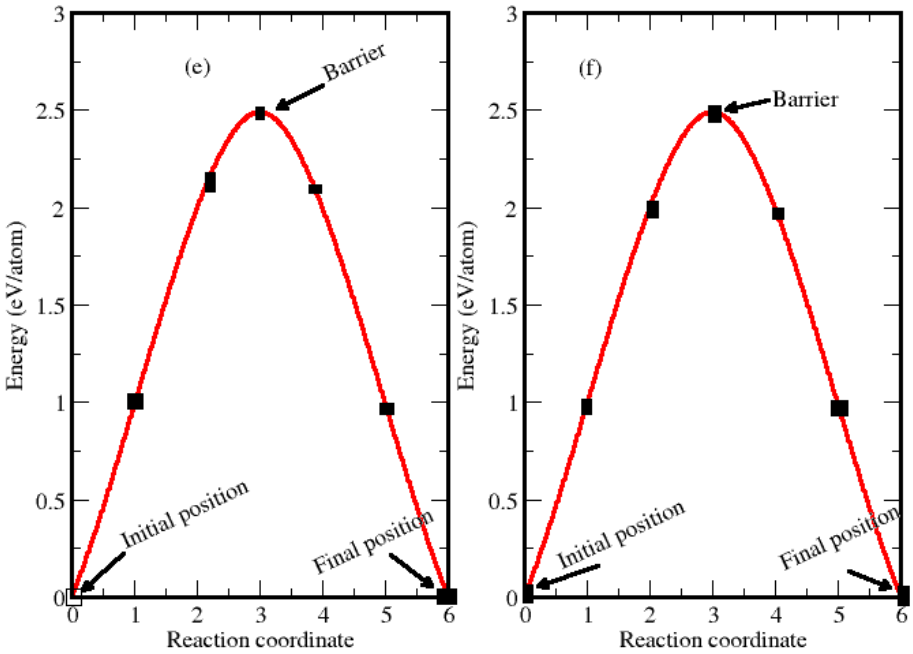

Figure 5.6.9: Vacancy migration energy curve for (e) Niobium Carbide and (f) Niobium Nitride, respectively, in WZ with defect concentration of 8%.

Figure 5.6.10 shows the calculated vacancy migration energies for Niobium Carbide plus Niobium Nitride in RS, ZB as well as WZ with different defect concentrations. Five

discrete images were used along the initial and final states using defect concentrations of 1.56 %, 2.08 %, 3.125 %, 4.160%, 6.25 % and 8.33 %. The migration energies were determined for fixed cell geometries whereby the shape and size of the super-cell were held fixed during NEB minimization. For the fixed cell geometries the migration energies decrease as low carbon concentrations correspond to small lattice constants and bond distances making the migration of the atoms fast. From the results obtained the barriers are located at different levels. The highest value of around 60 eV/atom RS structure, followed by ZB at around 48 eV/atom and the least in WZ at around 2.5 eV/atom. It can be observed that the values of vacancy migration energy for Niobium Carbide as well as Niobium Nitride in identical crystal structure are close to each other due to nearly similarity in size of C and N.

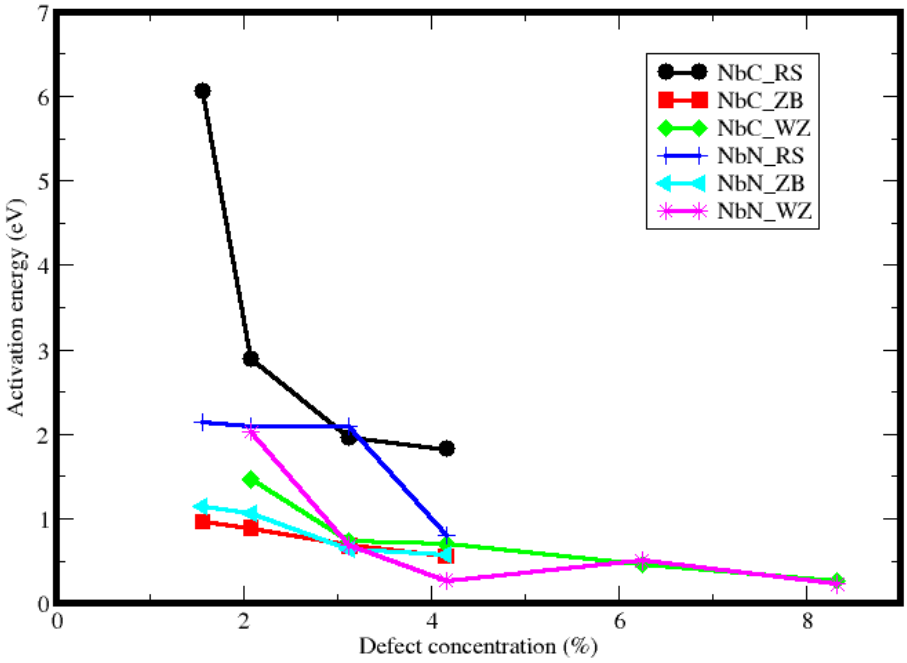

Figure 5.6.10: Calculated vacancy migration energy for Niobium Carbide together with Niobium Nitride in rocksalt, zincblende as well as wurzite crystal structures.

5.7 DYNAMICAL PROPERTIES

Apart from mechanical stability, dynamical stability of Niobium Carbide as well as Niobium Nitride are also very important to the application of the materials, and these

were explored using phonon calculations. From the study, phonon dispersion curves were achieved to represent either the stability or instability of these systems using 3n branches for every crystal lattice containing n number of atoms per unit cell, Lakdja (2014). For instance, the RS structure has 6 normal modes due to the presence of 3 acoustic and 3 optical nodes from the two atoms in the unit cell. A system is dynamically stable when it has real and finite frequencies of the normal modes otherwise it is considered unstable. Figure 5.7.1 shows the phonon spectra of the pristine form of Niobium Carbide as well as Niobium Nitride, in rocksalt, zincblende together with wurzite crystal structures. NbC in the 3 structures as well as NbN in wurzite structure were found to be stable as supported by the absence of imaginary frequencies which is in agreement with other studies, Rathod et al. (2011), Ivashchenko et al. (2010). However, the rocksalt as well as zinclende structures of NbN are unstable as a result of the presence of the imaginary frequencies which is in agreement with the observation made by Isaev et al. (2007). Upon the introduction of anionic vacancies, the dynamically stable structures in the pristine nature retain their stability for defect concentrations ranging 1.56 % and 8 % in the ground state while Niobium Nitride in rocksalt and zincblende structures become dynamically stable as shown in Figure 5.7.2. Thus, low defect concentrations especially below 8 % improves the dynamical stability of the unstable NbN resulting into phonon softening.

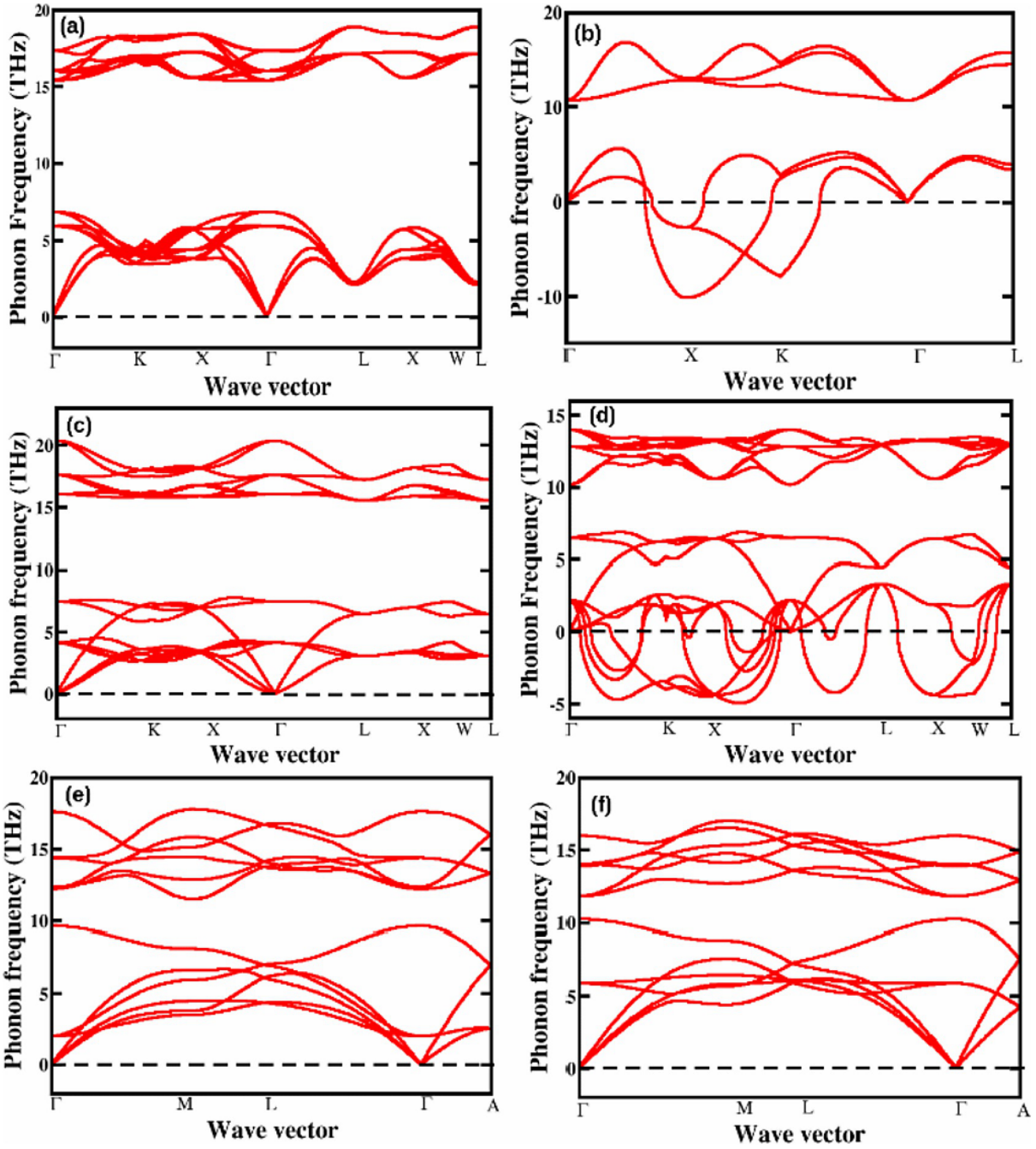

Figure 5.7.1: Phonon dispersion curves for Niobium Carbide in rocksalt, zincblende, wurzite (a), (c) and (e), respectively, and Niobium Nitride in rocksalt, zincblende and wurzite (b), (d) and (f), respectively, in pristine form.

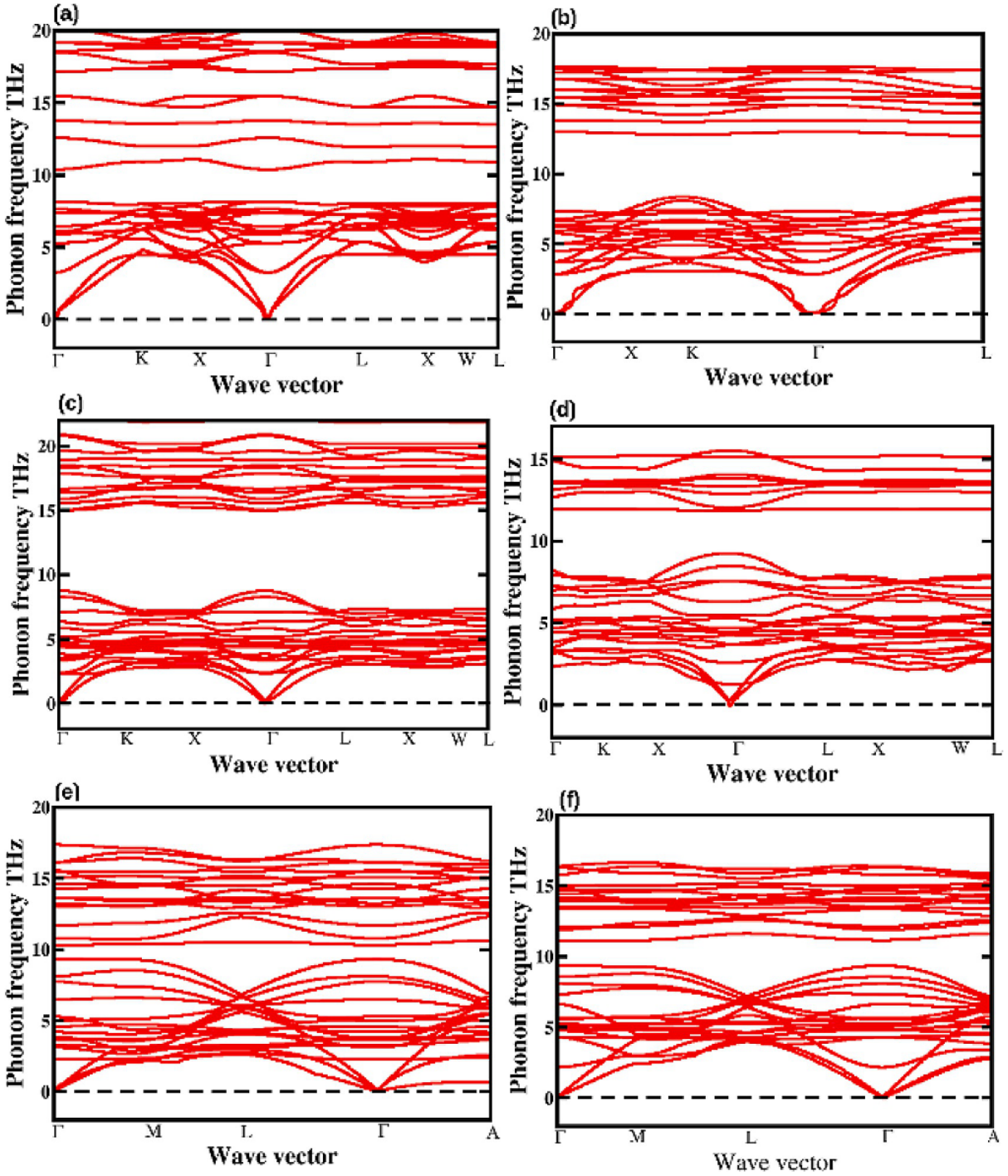

Figure 5.7.2: Phonon dispersion curves for Niobium Carbide in rocksalt, zincblende and wurzite (a), (c) and (e), respectively, and Niobium Nitride in rocksalt, zincblende and wurzite (b), (d) and (f), respectively, with anionic defect concentrations of 4 %.

CHAPTER SIX

CONCLUSION AND RECOMMENDATIONS

6.1 CONCLUSION

This study has used *ab initio* DFT simulations to investigate the physical properties of NbC and NbN in three different structures namely, the rocksalt, Zincblende and Wurzite. Particular emphasis was placed on the determination of the structural properties, elastic constants of the materials, bulk, shear modulus as well as Young's modulus, toughness together with Vicker's hardness under ground state conditions. From the data obtained, the lattice parameters agree well with the experimental values available. The values obtained are 4.49 Å, 4.82 Å for NbC in RS and ZB while 4.38 Å and 4.76 Å were obtained in the cases of NbN in RS and ZB, respectively. For the case of hexagonal crystal structures, the values of the lattice parameters were 3.70 Å and 1.10 Å for NbC in WZ and 3.01 Å and 1.84 Å for NbN in WZ. The deviation of between +4.038 % and -0.2278 % was noted when the obtained values were compared with the available theoretical and experimental data. Present work predicted that NbN is more stronger than NbC as it possesses the highest bulk modulus and least bond length in comparison to the latter. This is supported by the values bond lengths obtained in this work. The Nb-C bond lengths in NbC were 2.25 Å, 2.09 Å and 1.76 Å in RS, ZB and WZ crystal structures, respectively, while in NbN the Nb-N bond lengths were 2.20 Å, 2.06 Å and 1.71 Å in RS, ZB and WZ, respectively.

Based on results obtained in this work, all the structures studied match up to the Born stability criterion which is a prediction that these materials are mechanically stable. Moreover, high values of C_{13} and C_{33} observed in rocksalt structure of Niobium Carbide as well as Niobium Nitride implies such materials would provide reasonable resistance to compressive stress. Amidst the two materials i.e Niobium Carbide together with Niobium Nitride in three different crystal structures, Niobium Carbide in rocksalt structure continually reported high values of shear modulus, Young's modulus as well as

shear Voigt-Reuss-Hill modulus i.e 275.5 GPa, 518.0 GPa, 214.0 GPa, respectively. This suggests that they are potential candidates for applications that require high hardness values. Further, a relationship of toughness along with Vickers hardness is identified amongst the materials considered in this study, whereby systems with $H_V > 20$ GPa were observed to be brittle while on the other hand, those with $H_V < 20$ GPa were ductile. These results play a role in pointing out the suitable hardness related application that suites the considered materials in this study, and may give avenues for engineering intrinsic hardness in such materials so as enhance their performance.

In addition, the study has also considered how the mechanical, elastic, electronic properties as well as dynamical stability of Niobium Carbide together with Niobium Nitride in rocksalt, zincblende as well as wurzite structures are affected by anionic vacancies via *ab initio* density functional theory simulations. The existence of anionic vacancies at low concentrations of between 1 % and 8 % was identified to be supported in NbC, while in NbN the formation energies were positive and this can only be attained under non-equilibrium conditions. The dynamical stability of Niobium Carbide in all the three structures, that is, RS, ZB, and WZ as well as NbN in WZ structure was identified to be insensitive to the presence of both C and N vacancies, while NbN in RS as well as ZB becomes dynamically stable with the introduction of nitrogen vacancies. The findings of this study established that the occurence of Carbon and Nitrogen vacancies in Niobium Carbide together with Niobium nitride, respectively results to an overall deterioration in bulk, shear, Young's moduli, elastic constants as well as Vickers hardness. For instance, the Vickers hardness of Niobium Carbide in RS crystal structure reduced by 36 % with the existence of 8 % C vacancies concentration. In the ZB of NbC the values of C_{11} and C_{12} elastic constants decreased by 54 % and 57 %, respectively. For the NbN in ZB structure, the bulk modulus decreases by 25 % while on the other hand, the shear modulus decreases by 10 % in the WZ structure of NbN with a defect concentration of 12.5 %. The deterioration of the mechanical properties can be accredited to vacancy softening as a result of decrease in the number of covalent bonds, an observation that is consistent with PDOS analysis. Here it was found that C/N vacancies induce metallic

bonding character that can be attributed to the rise in *dd* bonding states between Nb atoms as the contents of C/N decreases. Further, it was observed that anionic vacancies in NbC tend to modify its toughness; in particular, NbC in ZB becomes brittle while NbC in WZ becomes ductile in the presence of C vacancies of up to 6 %. The toughness of NbN was found to be generally insensitive to N vacancies concentrations of up to 8 %. Therefore, in order to achieve optimal mechanical response of NbC and NbN, stringent control of anionic defects is critical.

Molecular dynamics simulations allow accurate calculation of elastic constants at elevated temperature. However, the calculations are time consuming compared to elastic constants calculations of static systems but they are necessary when describing the elastic behaviour of materials at extreme conditions such as high temperature. This is important as the conditions represent modern technological processes. This study reports the elastic properties of Niobium Carbide together with Niobium Nitride in three structures as a function of temperature. The mechanical properties tend to decrease with increase in temperature due to the weakening of the bonds between the crystals. Strong dependence of C_{11} on temperature is noted due to decrease in their values.

6.2 RECOMMENDATIONS

Most industrial working conditions include extreme temperature and pressure. The current study has only considered how temperature affects the mechanical characteristics of materials. Pressure related calculations are recommended to shed light on how the characteristics of these materials would be affected by pressure. It is also important to investigate the effects of other types of defects such as interstitial on the mechanical properties of Niobium Carbide together with Niobium Nitride.

BIBLIOGRAPHY

Ackland, G., Warren, M., & Clark, S. (1997). Practical methods in ab initio lattice dynamics. *Journal of Physics: Condensed Matter*, *9*, 7861.

Ahmed, R., Hashemifar, S. J., Akbarzadeh, H., & M. Ahmed, e. a. (2007). initio study of structural and electronic properties of iii-arsenide binary compounds. *Computational materials science*, *39*, 580–586.

Alexander, P., Oleksandr, B., Gregory, A., Volodymyr, I., Oleg, S., Stefan, J., & Emerson, C. (2016). Structural and mechanical properties of nbn and nb-si-n films: Experiment and molecular dynamics simulations. *Ceramics International*, *42*(10), 11743–11756.

Amriou, T., Bouhafs, B., Aourag, H., Khelifa, B., Bresson, S., & Mathieu, C. (2003). Fp-lapw investigations of electronic structure and bonding mechanism of nbc and nbn compounds. *Physica B*, *325*, 46–56.

Andersen, H. (1980). Molecular dynamics simulations at constant pressure and/or temperature. *Journal of Chemical Physics*, *72*, 2384.

Andrievski, R., Anisimova, I., & Anisimov, V. (1991). Structure and microhardness of tin compositional and alloyed films. *Thin Solid Films*, *205*, 171–175.

Angsten, T., Mayeshiba, T., Wu, H., & Morgan, D. (2014). Elemental vacancy diffusion database from high-throughput first-principles calculations for fcc and hcp structures. *New Journal of Physics*, *16*(1).

Ashby, M., Shercliff, H., & Cebon, D. (2007). Materials: engineering, science, processing, and design (1st ed.).

Balasubramanian, K., Khare, S., & Gall, D. (2018a). Energetics of point defects in rocksalt structure transition metal nitrides: Thermodynamic reasons for deviations from stoichiometry. *Acta Mater.*, *159*, 77–88.

Balasubramanian, K., Khare, S. V., & Gall, D. (2018b). Valence electron concentration as an indicator for mechanical properties in rocksalt structure nitrides, carbides and carbonitrides. *Acta Materialia*, *152*, 175-185.

Baroni, S., Giannozzi, P., & Testa, A. (1987). Elastic constants of crystals from linear response theory. *Physical Review Letters*, *59*(23), 2662–2665.

Benco, L. J. (1997). Metal-to-metal bonding in transition metal monocarbides and mononitrides. *Solid State Chem.*, *128*, 121–129.

Bendavid, A., Martin, P., Kinder, T., & Preston, E. (2003). The deposition of nbn and nbc thin films by filtered vacuum cathodic arc deposition. *Surface and Coatings Technology*, *163*, 347–352.

Benkahoul, M., Martinez, E., Karimi, A., Sanjines, R., & Levy, F. (2004). Structural and mechanical properties of sputtered cubic and hexagonal $\mathrm{nbn}_x thin films. Surf. Coating. Technol., 180–181, 178 - -183$.

Bercegeay, C., & Bernard, S. (2005). First-principles equations of state and elastic properties of seven metals. *Physical Review B*, *72*(21), 214101.

Bloch, F. (1929). Bemerkung zuelektronentheorie des ferromag-netismus und der elektrischen leitfähigkeit. *Z. Phys.*.

Blöchl, P. E. (1994). Projector augmented-wave method. *Physical Review B*, *50*.

Born, M., & Huang, K. (1954). Dynamical theory of crystal lattices. *Oxford University Press, Oxford*.

Born, M., & Oppenheimer, R. (1972). On the quantum theory of molecules. *Annalen der Physik*, *84*(20), 457–484.

Boyer, R. R., Cotton, J. D., Mohaghegh, M., & Schafrik, R. E. (2015). Materials considerations for aerospace applications.

Broser, I., Broser, R., Finkenrath, H., Galazka, R., Gumlich, H., Hoffmann, A., ... et al. (1982). Physics of ii-vi and i-vii compounds, semimagnetic semiconductors, landolt-bornstein. *Numerical Data Funct. Relationships Sci. Technol.*, *17*.

Chaput, L., Togo, A., Tanaka, I., & Hug, G. (2011). Phonon-phonon interactions in transition metals. *Physical Review B*, *84*, 094302.

Chen, J., Boyer, L. L., Krakauer, H., & Mehl, M. J. (1988). Elastic constants of nbc and mon: Instability of B_1-mon. *Phys. Rev. B*, *37*, 3295–3298.

Ching., W., Rulis, P., & Misra, A. (2009). Ab initio elastic properties and tensile strength of crystalline hydroxyapatite. *Acta Biomaterialia*, *5*, 3067—3075.

Chung, D., & Buessem, W. (1967). The voigt-reuss-hill approximation and elastic moduli of polycrystalline mgo, caf2, -zns, znse and cdte. *J. Appl. Phys.*, *38*, 2535–2540.

Classes, B. (2017). Thomson atomic model its limitations | development of atomic model. *Chemistry*.

Cocco, A., & Masin, S. C. (2010). The law of elasticity. *Psicológica*, *31*, 647–657.

Cohen, R. E., Gülseren, O., & Hemley, R. J. (2000). Accuracy of equation-of-state formulations. *American Mineralogist*, *85*, 338–344.

Conklin, J., James, B., & Silversmith, D. J. (1968). Energy-band structure and binding mechanism of tic. *International Journal of Quantum Chemistry*, *2*(S2), 243-255.

Cuevas, J. C., & Scheer, E. (2010). Molecular electronics: An introduction to theory and experiment. *World Scientific*.

Cuppari, M., & Santos, S. (2016). Physical properties of the nbc carbide. *Metals*.

Da Silva, C. R. S., Karki, B. B., Stixrude, L., & Wentzcovitch, R. M. (1999). Ab initio study of the elastic behavior of mgsio3 ilmenite at high pressure. *Geophysical Research Letters*, *26*(7), 943–946.

Desai, A. (2008). Size effect on the mechanical properties in zinc oxide.

Dirac, P. A. M. (1930a). Note on exchange phenomena in the thomas atom. *Math. Proc. Cambridge Philos. Soc*, *26*, 376—385.

Dub, S., Lytvyn, P., Strelchuk, V., Nikolenko, A., Stubrov, Y., Petrusha, I., ... Ivakhnenko, S. (2017). Vickers hardness of diamond and cbn single crystals: Afm approach. *Crystals*, *7*(12).

Dubrovinskaia, N., Dubrovinsky, L., Crichton, W., Langenhorst, F., & Richter, A. (2005). Aggregated diamond nanorods, the densest and least compressible form of carbon. *Applied Physics Letters*, *87*(8), 083106–083106.

Eck, B., Dronskowski, R., Takahashi, M., & Kikkawa, S. (1999). Theoretical calculations on the structures, electronic and magnetic properties of binary 3d transition metal nitrides. *Journal of Materials Chemistry*, *9*, 1527–1537.

Fan, C.-Z., Zeng, S.-Y., Zhan, Z.-J., Liu, R.-P., Wang, W.-K., Zhang, P., & Yao, Y.-G. (2006). Low compressible noble metal carbides with rocksalt structure: Ab initio total energy calculations of the elastic stability. *Applied Physics Letters*, *89*(7), 071913.

Fernandez, A., Haglund, J., & Grimvall, G. (1992). Cohesive properties of 4d- transition-metal carbides and nitrides in the nacl-type structure. *Phys. Rev. B*, *45*, 11557.

Fiolhais, C., Nogueira, F., & Marques, M. A. L. (2003). A primer in density functional theory. *Springer-Verlag Berlin Heidelberg*.

Fontbonne, A., & Gilles, J. (1969). New tantalum nitrides. double nitride and oxynitrides of tantalum and niobium. *CECM, Vitry-sur-Seine, France, Technical Report*.

Friedrich, A., Winkler, B., Juarez-Arellano, E., & Bayarjargal, L. (2011). Synthesis of binary transition metal nitrides, carbides and borides from the elements in the laser-heated diamond anvil cell and their structure-property relations. *Materials*, *4*, 1648–1692.

Fu, T., Peng, X., Zhao, Y., Sun, R., Weng, S., Feng, C., & Wang, Z. (2015). Molecular dynamics simulation of tin (001) thin films under indentation.

Ganeshan, S., Shang, S. L., Wang, Y., & Liu, Z. K. (2009). Effect of alloying elements on the elastic properties of mg from first-principles calculations. *Acta Materialia*, *57*(13), 3876–3884.

Ghose, P., Gafur, M., Das, S. K., Chakraborty, S. R., Mohsin, M., Deb, A., & Qadir, M. (2014). Effects of flux concentrations and sintering temperature on dental poecelain. *The European Physical Journal Applied Physics*.

Giannozzi, P., Baroni, S., Bonini, N., Calandra, M., Car, R., Cavazzoni, C., ... Wentzcovitch, R. (2009). Quantum espresso: a modular and open-source software project for quantum simulations of materials. *Journal of Physics: Condensed Matter*, *21*, 395502.

Gilman, J. (1996). Physical chemistry of intrinsic hardness. *Mater. Sci Eng., A*, *209*, 74–81.

Glass, E. N., & Winicour, J. (1973). A geometric generalization of hooke's law. *Journal of Mathematical Physics*, *14*, 1285–1290.

Goble, R., & Scott, S. (1985). Relationship between mineral hardness and compressibility. *Canadian Mineralogist*, *23*(2), 273–285.

Görling, A. (1996). Density-functional theory for excited states. *Physical Review A*, *54*.

Gou, H., Hou, L., Zhang, J., & Gao, F. (2008). Pressure-induced incompressibility of rec and effect of metallic bonding on its hardness. *Applied Physics Letters*, *92*(24), 241901.

Grüning, M., Marini, A., & Rubio, A. (2006). Density functionals from many-body perturbation theory: The band gap for semiconductors and insulators. *The Journal of Chemical Physics*, *124*.

Gubanov, V., Ivanovsky, A., & Zhukov, V. (2005). Electronic structure of refractory carbides and nitrides. *Cambridge University Press: Cambridge, UK*.

Guerra, F., & Robotti, N. (2008). Ettore majorana's forgotten publication on the thomas-fermi model. *Phys. Perspect.*, *10*, 56—76.

Hafner, J. (2008). Ab-initio simulations of materials using vasp: Density functional theory and beyond. *Journal of Computational Chemistry*, *29*.

Hägg, G. (1931). Regularities in the crystal structure with hydrides, borides, carbides and nitrides of the transition elements. *Journal of Physical and Chemistry. Abt. B*, *12*, 33–56.

Haines, J., Leger, J. M., & Bocquillon, G. (2001). Synthesis and design of superhard materials. *Annu. Rev. Mater. Res.*, *31*, 1–23.

Hamann, D. R., Schlüter, M., & Chiang, C. (1979). Norm-conserving pseudopotentials. *Phys. Rev. Lett.*, *43*, 1494–1497.

Hartree, D. (1928). The wave mechanics of an atom with a non-coulomb central field. part i. theory and methods in mathematical proceedings of the cambridge philosophical society. *Cambridge Univ Press*, *24*, 89–110.

Hendrik, M., & James, P. (1976). Special points for brillouin-zone integrations. *Phys. Rev. B*, *13*, 5188–5192.

Hill, R., Storakers, B., & Zdunek, A. (1989). A theoretical study of the brinell hardness test. *Proceedings of the Royal Society of London. A. Mathematical and Physical Sciences*, *423*(1865), 301—330.

Hohenberg, P., & Kohn, W. (1964). Inhomogeneous electron gas. *Phys. Rev.*, *136*.

Holleck, H. (1986). Material selection for hard coatings. *Journal of Vacuum Science & Technology A*, *4*(6), 2661–2669.

Hones, P., Diserens, M., Sanjin, R., & Levy, F. (1999). Electronic structure and mechanical properties of hard coatings from the chromium-tungsten nitride system. *J. Vac. Sci. Technol. B*, *17*, 1024.

Hugosson, H., Eriksson, O., Jansson, U., & Johansson, B. (2001). Phase stabilities and homogeneity ranges in 4d-transition-metal carbides: A theoretical study. *Phys. Rev. B*, *63*, 134108.

Hull, D., & Bacon, D. J. (1984). Introduction to dislocations. *Pergamon Press, Oxford*.

Ikawa, N., & Tanaka, T. (1971). Thermal aspects of wear of diamond grain in grinding. *Ann CIRP*, *19*, 153–157.

Isaev, E. I., Simak, S. I., Abrikosov, I., Ahuja, R., Vekilov, Y. K., Katsnelson, M., ... Johansson, B. (2007). Phonon related properties of transition metals, their carbides, and nitrides: a first-principles study. *J. Appl. Phys.*, *101*, 123519.

Ivashchenko, V., Turchi, P., & Olifan, E. (2010). Phase stability and mechanical properties of niobium nitrides. *Phys. Rev. B*, *82*(5).

Jaffe, R. L., Henry, J. M., & Anderson, J. B. (1973). Variational theory of reaction rates: Application to f+h2hf+h. *The Journal of Chemical Physics*, *59*(3), 1128–1141.

Jain, A., Ong, S. P., Hautier, G., Chen, W., Richards, W. D., Dacek, S., ... a. Persson, K. (2013). The materials project: A materials genome approach to accelerating materials innovation. *APL Materials*, *1*, 011002.

Jhi, Louie, S., Cohen, M., & Morris, J. J. (2001). Mechanical instability and ideal shear strength of transition metal carbides and nitrides. *Phys Rev Lett.*, *87*.

Jiang, C., Srinivasan, S., Caro, A., & Maloy, S. (2008). Structural, elastic, and electronic properties of fe$_3$c from first principles. *Journal of Applied Physics*, *103*, 043502.

Jonsson, H., Mills, G., & Jacobsen, K. W. (1998). Nudged elastic band method for finding minimum energy paths of transitions. In *Classical and quantum dynamics in condensed phase simulations* (pp. 385–404).

Jun, C., & Shaffer, P. (1970). Elastic moduli of niobium carbide and tantalum carbide at high temperature. *Journal of the less-common metals*, *23*, 367–373.

Karpov, M. I. (2018). Niobium-base refractory alloys with silicide and carbide hardening: current status and prospects. *Metal Sci. Heat Treat.*, *60*.

Karpov, M. I., Vnukov, V. I., Korzhov, V. P., Stro-ganova, T. S., Zheltyakova, I. S., Prokhorov, D. V., ... Nekrasov, A. N. (2012). Structure and mechanical properties of the high-temperature eutectic nb–si alloy obtained by the directional solidification methods. *Deform Razrushenie Mater.*(12), 2–8.

Kerker, G. (1980). Non-singular atomic pseudopotentials for solid state applications. *Journal of Physics C: Solid State Physics*, *13*.

Kim, B.-R., Woo, K.-D., Yoon, J.-K., Doh, J.-M., & Shon, I.-J. (2009). Mechanical properties and rapid consolidation of binderless niobium carbide. *Journal of Alloys and Compounds*, *481*(1–2), 573–576.

Kindlund, H., Sangiovanni, D., de Olcoz, L. M., Lu, J., Jensen, J., Birch, J., ... Hultman, L. (2013). Toughness enhancement in hard ceramic thin films by alloy design. *Apl. Mater.*, *1*, 042104.

Kirchner, B., Di, D. P., & Hutter, J. (2011). Real-world predictions from ab initio molecular dynamics simulations. in: Kirchner b., vrabec j. (eds) multiscale molecular methods in applied chemistry. *Topics in Current Chemistry*, *307*.

Klein, B., Papaconstantopoulos, D., & Boyer, L. (1980). Linear combination of atomic orbitals coherent potential approximation studies of carbon vacancies in the substoichiometric refractory monocarbides $\mathrm{nbc}_x, tac_x, and hfc_x. Phy.\ Rev.\ B, 22, 1946 - 1966.$

Klug, J., Proslier, T., Elam, J., Cook, R., Hiller, J., Claus, H., ... Pellin, M. (2011). Atomic layer deposition of amorphous niobium carbide-based thin film superconductors. *The Journal of Physical Chemistry C*, 25063–25071.

Kohn, W., Becke, A., & Parr, R. (1996). Density functional theory of electronic structure. *The Journal of Physical Chemistry*, *100*.

Kohn, W., & Sham, L. J. (1965). Self-consistent equations including exchange and correlation effects. *Phys. Rev.*, *140*.

Kolkaji, A. (2003). Xcrysden x-window crystalline structure and den-sities. *Computational Mattter. Sci*, *28:155*.

Korir, K., Amolo, G., Makau, N., & Joubert, D. (2011). First-principle calculations of the bulk properties of 4d transition metal carbides and nitrides in the rocksalt, zincblende and wurtzite structures. *Diamond and Related Materials*, *20*(2), 157-164.

Koseki, S., Inoue, K., Morito, S., Ohba, T., & Usuki, H. (2015). Comparison of tin-coated tools using cvd and pvd processes during continuous cutting of ni-based superalloys. *Surf. Coating. Technol.*, *283*, 353–363.

Krajewski, A., D'Alessio, L., & de Maria, G. (1998). Physico-chemical and thermophysical properties of cubic binary carbides. *Cryst. Res. Technol.*, *33*, 341–374.

Kral, C., Lengauer, W., Rafaja, D., & Ettmayer, P. (1998). Critical review on the elastic properties of transition metal carbides, nitrides and carbonitrides. *Journal of Alloys and Compounds*, *265*(1), 215–233.

Kresse, G., & Furthmüller, J. (1996). Efficiency of ab-initio total energy calculations for metals and semiconductors using a plane-wave basis set. *Computational Materials Science*, *6*, 15–50.

Kresse, G., & Furthmüller, J. (2007). Vasp the guide. Retrieved from `http://cms.mpi.univie.ac.at/VASP`

Kresse, G., & Hafner, J. (1993a). Ab initio molecular dynamics for liquid metals. *Physical Review B*, *47*(1), 558–561.

Kresse, G., & Hafner, J. (1993b). Ab initio molecular dynamics for liquid metals. *Physical Review B*, *47*, 558.

Kresse, G., & Joubert, D. (1999a). From ultrasoft pseudopotentials to the projector augmented-wave method. *Physical Review B*, *59*, 1758.

Kresse, G., & Joubert, D. (1999b). From ultrasoft pseudopotentials to the projector augmented-wave method. *Physical Review B*, *59*, 1758.

Kubel, F., Lengauer, W., Yvon, K., Knorr, K., & Junod, A. (1988). Structural phase transition at 205 k in stoichiometric vanadium nitride. *Phys. Rev. B*, *38*, 12908.

Kurakevych, O. (2009). Ultimate metastable solubility of boron in diamond: Synthesis of superhard diamond like bc 5. *Journal of Superhard Materials*, *31*(3), 139–157.

Laidler, K. J. (2022). Transition-state theory. *Encyclopedia Britannica*. Retrieved from `https://www.britannica.com/science/transition-state-theory`

Lailei, W., Yachun, W., Zhigang, Y., Jingwu, Z., Furen, X., & Bo, L. (2013). The phase stability and mechanical properties of nb–c system: Using first-principles calculations and nano-indentation. *Journal of Alloys and Compounds*, *561*, 220–227.

Lakdja, A. (2014). Structural and phonon dynamical stability of the hypothetical rbn and csn compounds. *Comput. Mater. Sci.*, *89*, 1–5.

Lee, T., Ohmori, K., Shin, C., Cahill, D., Petrov, I., & Greene, J. (2005). Elastic constants of single-crystal $\mathrm{tin}_x(001)(0.67 \leq x \leq 1.0)$ determined as a function of x by picosecond ultrasonic measurements. *Phys. Rev. B*, *71*, 144106.

Leung, T., Chan, C. T., & Harmon, B. (1991). Ground-state properties of fe, co, ni, and their monoxides: Results of the generalized gradient approximation. *Physical Review B*, *44*.

Li, & Liu. (2012). First-principles investigations of structural and electronic properties of niobium nitrides under pressures. *J. At. Mol. Sci.*, *3*, 78–88.

Liu, F., Liu, P., Peng, F., & Liu, J. (2017). Hardness and compression behaviour of niobium carbide. *High Pressure Research*, *37*, 244–255.

Llanos, L., Pereda, B., & Lopez, B. (2015). Interaction between recovery, recrystallization, and nbc strain-induced precipitation in high-mn steels. *Metall. Mater. Trans. A*, *46*, 5248–5265.

Lusk, M., & Mattsson, A. (2011). High-performance computing for materials design to advance energy science. *MRS Bulletin*, *36*.

Martin, R. M. (2004). Electronic structure: Basic theory and practical methods. *Cambridge University Press*.

Marvin, C., & Volker, H. (1970). The fitting of pseudopotentials to experimental data and their subsequent application. *In Solid State Physics*, *24*, 37—248.

Matthias, B. T. (1953). Transition temperatures of superconductors. *Phys. Rev.*, *92*, 874–876.

Mayer, I. (2003). Simple theorems, proofs and derivations in quantum chemistry. *Springer*.

McMillan, P. (1999). High pressure synthesis of solids. *Current Opinion in Solid State and Materials Science*, *4*(2), 171–178.

Mehl, M. J., Klein, B. M., & Papaconstantopoulos, D. A. (1994). First principles calculations of elastic properties of metals. , *1*.

Mei, A., Hellman, O., Wireklint, N., Schlepuetz, C., Sangiovanni, D., Alling, B., ... Greene, J. (2015). Dynamic and structural stability of cubic vanadium nitride. *Phys. Rev. B*, *91*, 054101.

Menéndez-Proupin, E., Cervantes-Rodrıǵguez, S., Osorio-Pulgar, R., Franco-Cisterna, M., & Fuentes, M. (2011). Computer simulation of elastic constants of hydrox-yapatite and fluorapatite. *Journal of the Mechanical Behavior of Biomedical Materials*, *4*, 1011—1020.

Mizutani, U. (2001). Introduction to the electron theory of metals (rev. ed.) mizutani, u.(ed.). *Cambridge University Press, Cambridge*.

Mlinar, V. (2007). Electronic structure calculation of single and coupled self-assembled quantum dots.

Mohammed, A.-J., Raed, J., Mahmoud, F., Areej, S., Ahmad, M., Khalid, I., ... Said, A. (2023). Insight into the structural, electronic, optical, and elastic properties of niobium carbide, phase transitions. *A Multinational Journal*, *96*, 337–349.

Monkhorst, H., & Pack, J. D. (1976). Special points for brillouin-zone integrations. *Physical review B*, *13*, 5188.

Mouhat, F., & Coudert, F.-X. (2014). Necessary and sufficient elastic stability conditions in various crystal systems. *Physical Review B*, *90*, 224104.

Muchiri, P., Korir, K., Makau, N., & Amolo, G. (2022). The impact of anionic vacancies on the mechanical properties of nbc and nbn: An ab initio study. *Computational Materials Science*, *203*, 111113.

Muchiri, P., Mwalukuku, V., Korir, K., Amolo, G., & Makau, N. (2019). Hardness characterization parameters of niobium carbide and niobium nitride: A first principles study. *Materials Chemistry and Physics*, *229*(0254), 489–494.

Munir, Z. (1988). Synthesis of high temperature materials by self-propagating combustion methods. *Am Ceram Soc Bull*, *67*.

Murnaghan, F. (1944). The compressibility of media under extreme pressures. *Proc. Natl. Acad. Sci. Unit. States Am.*, *30*, 244–247.

Musil, J. (2000). Hard and superhard nanocomposite coatings. *Surf. Coating. Technol*, *125*, 322–330.

Nambigari, N., Dulapalli, R., Mustyala, K. K., Malkhed, V., Vuruputuri, U., Penumaka, N., & Sirasani, S. (2013). Molecular dynamic simulations of co(iii) and ru(ii) polypyridyl complexes and docking studies with dsdna. *Medicinal Chemistry Research*, *22*, 5557 – 5565.

Nedfors, N., Tengstrand, O., Lewin, E., Furlan, A., Eklund, P., Hultman, L., & Jansso, U. (2011). Structural, mechanical and electrical-contact properties of nanocrystalline-nbc/amorphous-c coatings deposited by magnetron sputtering. *Surface and Coatings Technology*, *206*(2), 354–359.

Nicholls, J. R., Hall, D. J., & Tortorelli, P. F. (1994). Hardness and modulus measurements on oxide scales. *Materials at High Temperatures*, *12*(2-3), 141-150.

Ningthoujam, R., & Gajbhiye, N. (2015). Synthesis, electron transport properties of transition metal nitrides and applications. *Progress in Material Science*, *70*, 50–154.

Nordholm, S. (1987). Analysis of covalent bonding by nonergodic thomas-fermi theory. *J. Chem. Phys.*.

Nosé, S. (1984). A unified formulation of the constant temperature molecular dynamics methods. *J. Chem. Phys.*, *81*, 511–519.

Ortiz, A. U., Boutin, A., Fuchs, A. H., & Coudert, F.-X. (2013). Metal-organic frameworks with wine-rack motif:what determines their flexibility and elastic properties? *The Journal of chemical physics*, *138*, 174703.

Ostlund, N. S., & Szabo, A. (1996). Modern quantum chemistry: Introduction to advanced electronic structure theory. *Dover Publications Inc New edition edn*.

Oyama, S. (1996). The chemistry of transition metal carbides and nitrides. *Springer Science & Business Media*.

Pack, J. D., & Monkhorst, H. J. (1977). Special points for brillouin-zone integrations"—a reply. *Physical Review B*, *16*, 1748.

Pang, X., Yang, J., Li, A., Pang, M., Xiao, Y., Nong, H., ... Liu, C. (2023). Understanding the atomic and electronic structure of the nbc(111)/cu(111) interface via first principles calculation. *Materials Today Communications*, *36*, 106653.

Patricia, G., Rahim, A., & Rodriguez, J. A. (2013). Structural and electronic properties of scc and nbc: a first-principles study. *Solid State Phenomena*, 276–279.

Pauleau, Y. (1995). Solid lubricant coatings produced by physical and chemical vapor deposition techniques, materials and processes for surface and interface engineering. *Springer*, 475–527.

Pauleau, Y. (2012). Materials and processes for surface and interface engineering. *Springer Science Business Media*, *290*.

Payne, M. C., Teter, M. P., Allan, D. C., Arias, T. A., & Joannopoulos, J. D. (1992). Iterative minimization techniques for ab initio total-energy calculations: molecular dynamics and conjugate gradients. *Rev. Mod. Phys.*, *64*, 1045–1097.

Perdew, J. P., Burke, K., & Ernzerhof, M. (1998). Perdew, burke, and ernzerhof reply:. *Phys. Rev. Lett.*, *80*, 891–891.

Perdew, J. P., & Zunger, A. (1981). Self-interaction correction to density-functional approximations for many-electron systems. *Phys. Rev. B*, *23*, 5048–5079.

Pickett, W., Klein, B., & Zeller, R. (1986). Electronic structure of the carbon vacancy in nbc. *Phys. Rev. B*, *34*, 2517–2521.

Polcar, T., & Cavaleiro, A. (2010). Structure, mechanical properties and tribology of wen and weo coatings. *Int. J. Refract. Metals Hard Mater*, *28*, 15–22. doi: https://doi.org/10.1016/j.ijrmhm.2009.07.013

Polcar, T., Parreira, N., & Cavaleiro, A. (2008). Structural and tribological characterization of tungsten nitride coatings at elevated temperature. *Wear*, *265*, 319–326.

Proynov, E., Ruiz, E., Vela, A., & Salahub, D. (1995). Determining and extending the domain of exchange and correlation functionals. *International Journal of Quantum Chemistry*, *56*.

Pugh, S. (1954). Relations between the elastic moduli and the plastic properties of polycrystalline pure metals. *The London, Edinburgh, and Dublin Philosophical Magazine and Journal of Science*, *45*, 823–843.

Qi-Jun, L., Ning-Chao, Z., Fu-Sheng, L., & Zheng-Tang, L. (2014). Structural, electronic, optical, elastic properties and born effective charges of monoclinic hfo2 from first-principles calculations. *Chinese Physics B*, *23*(4), 047101.

Raja, P. M., & Barron, A. R. (2022). Crystal structure. *Rice University*. Retrieved from `https://chem.libretexts.org/@go/page/55904`

Rappe, A., Rabe, K., Kaxiras, E., & Joannopoulos, J. (1990). Optimized pseudopotentials. *Physical. Review B*, *41*, 1227.

Rathod, N., Gupta, S., Gupta, S. K., & Jha, P. K. (2011). First-principles study of structural, electronic, elastic, phonon, and thermodynamical properties of the niobium carbide. *Solid State Phenomena, Trans Tech Publ*, *171*, 67–77.

Ruicheng, F., Hui, C., Haiyan, L., Zhiyuan, R., & Changfeng, Y. (2018). Effects of vacancy concentration and temperature on mechanical properties of single-crystal -tial based on molecular dynamics simulation. *High Temperature Materials and Processes*, *37*(2), 113–120.

Rutherford, P. E. (1911). Lxxix. the scattering of and particles by matter and the structure of the atom. *The London, Edinburgh, and Dublin Philosophical Magazine and Journal of Science*, *21*(125), 669-688.

Samano, E., a. Clemente, a. Díaz, J., & Soto, G. (2010). Mechanical properties optimization of tungsten nitride thin films grown by reactive sputtering and laser ablation. *Vacuum*, *85*, 69–77.

Sangiovanni, D., Hultman, L., Chirita, V., Petrov, I., & Greene, J. (2016). Effects of phase stability, lattice ordering, and electron density on plastic deformation in cubic tiwn pseudobinary transition-metal nitride alloys. *Acta Mater.*, *103*, 823.

Sangiovanni, D., Tasnádi, F., Harrington, T., Odén, M., Vecchio, K., & Abrikosov, I. (2021). Temperature-dependent elastic properties of binary and multicomponent high-entropy refractory carbides. *Materials Design*, *204*, 109634.

Sen, U. (2004). Kinetics of niobium carbide coating produced on aisi 1040 steel by thermo-reactive deposition technique. *Materials Chemistry and Physics*, 189–194.

Seo, H., Lee, T., Wen, J., Petrov, I., Greene, J., & Gall, D. (2004). Growth and physical properties of epitaxial hfn layers on mgo(001). *J. Appl. Phys.*, *96*, 878–884.

Setyawan, W., & Curtarolo, S. (2010). High-throughput electronic band structure calculations: Challenges and tools. *Computational Materials Science*, *49.2*, 299–312.

Seung-Hoon, J., & Jisoon, I. (1997). Electronic structure and structural stability of $\mathrm{tic}_x\mathrm{n}_{1-x}$ alloys. *Phys. Rev. B*, *56*, 13826–13829.

Seung-Hoon, J., Louie, S., Cohen, M., & Jisoon, I. (2001). Vacancy hardening and softening in transition metal carbides and nitrides. *Phys. Rev. Lett.*, *86*, 3348–3351.

Shaffer, P. (1964). Handbook of high temeperature materials. *Materials Index*, *1*.

Shein, I. R., & Ivanovskii, A. L. (2008). Elastic properties of mono-and polycrystalline hexagonal alb_2 -like diborides of s, p and d metals from first-principles calculations. *Journal of Physics: Condensed Matter*, *20*, 415218.

Shih, A. (2000). An experimental investigation of rotary diamond truing and dressing of vitreous bond wheels for ceramic grinding. *International Journal of Machine Tools and Manufacture*, *40*(12), 1755–1774.

Shimada, S., Koyama, T., Kodaira, K., & et al. (1983). Formation of nbc and tac by solid-state reaction. *J Mater Sci.*, *18*, 1291–1296.

Shin, C., Gall, D., Hellgren, N., Patscheider, J., Petrov, I., & Greene, J. (2003). Vacancy hardening in single-crystal $\mathrm{tin}_x(001)layers. J.\ Appl.\ Phys., 93, 6025 - -6028$.

Shin, C., Rudenja, S., Gall, D., Hellgren, N., Lee, T., Petrov, I., & Greene, J. (2004). Growth, surface morphology, and electrical resistivity of fully strained sub- stoichiometric epitaxial tin_x ($0.67 \leq x < 1.0$) layers on mgo (001). *J. Appl. Phys.*, *95*, 356–362.

Shi-Yu, L., Shuoxin, Z., Shiyang, L., De-Jun, L., Zhiqiang, N., Yaping, L., & Sanwu, W. (2022). Stability and mechanical properties of single-phase quinary high-entropy metal carbides: First-principles theory and thermodynamics. *Journal of the European Ceramic Society*, *42*(7), 3089–3098.

Sholl, D., & Steckel, J. A. (2001). Density functional theory: a practical introduction. *John Wiley Sons*.

Simmons, G., & Wang, H. (1971). Single crystal elastic constants and calculated aggregate properties. *A Handbook (MIT Press, Cambridge, MA*.

Singh, D., & Nordström, L. (2006). Planewaves pseudopotentials and the lapw method. *Springer, New York*.

Slater, J. (1951). A simplification of the hartree-fock method. *Physical Review*, *81*(3).

Smith, G., Swift, P., & Bendavid, A. (1999). tin_x films with metallic behavior at high n/ti ratios for better solar control windows. *Appl. Phys. Lett.*, *75*, 630–632.

Smith, R., & Sandly, G. (1922). An accurate method of determining the hardness of metals, with particular reference to those of a high degree of hardness*. *Proceedings of the Institution of Mechanical Engineers*, *102*(1), 623—641.

Soboyejo, . S. T., W. (2006). Advanced structural materials : properties, design optimization, and applications.

Song, W., He, Q., Rao, L., Zhang, S., Wang, J., Ren, X., & Yang, Q. (2022). Heterogeneous nucleation interface between laalo3 and niobium carbide: First-principles calculation. *Applied Surface Science*, *606*, 154731.

Stampfl, C., Mannstadt, W., Ashahi, R., & Freeman, A. (2001). Electronic structure and physical properties of early transition metal mononitrides: Density-functional theory lda, gga and screened-exchange lda-flapw calculations. *Physical Review B*, *63*, 155106.

Staples, L. W. (1964). Friedrich mohs and the scale of hardness. *Journal of Geological Education*, *3*, 98–101.

Steneteg, P., Hellman, O., Vekilova, O. Y., Shulumba, N., Tasnádi, F., & Abrikosov, I. A. (2013). Temperature dependence of tin elastic constants from ab initio molecular dynamics simulations. *Phys. Rev. B*, *87*, 094114.

S̃tich, I., Car, R., Parrinello, M., & Baroni, S. (1989). Conjugate gradient minimization of the energy functional: A new method for electronic structure calculation. *Physical Review B*, *39*, 4997.

Svetlov, I. L., Karpov, M. I., Neiman, A. V., & Stroganova, T. S. (2017). Temperature dependence of the ultimate strength in-situ composites of a multi-component nb–si–x (x = ti, hf, w, cr, al, mo) system. *Deform. Razrushenie Mater.*(10), 17–22.

Tabor, D. (1954). Mohs's hardness scale-a physical interpretation. *Proceedings of the physical Society B*, *67*, 249.

Teter, D. M. (1998). Computational alchemy: The search for new superhard materials. *MRS Bull*, *23*, 22–27.

Thijssen, J. (2007). Computational physics. *Cambridge University Press, Cambridge*.

Thomas, L. H. (1927). The calculation of atomic fields. *Mathematical Proceedings of the Cambridge Philosophical Society*, *23*, 542–54.

Thomson, J. J. (1897). Cathode rays. *Philosophical Magazine*, *44*.

Tian, Y., & Zhao, Z. (2012). Microscopic theory of hardness and design of novel superhard crystals. *International Journal of Refractory Metals and Hard Materials*.

Togo, A., Oba, F., & Tanaka, I. (2008). First-principles calculations of the ferroelastic transition between rutile-type and $cacl_2$-type sio_2 at high pressures. *Phys. Rev. B*, *78*, 134106.

Togo, A., & Tanaka, I. (2015). First principles phonon calculations in materials science. *Scripta Materialia*, *108*, 1–5.

Toth, L. (1971). Transition metal carbides and nitrides. *Academic Press, New York*.

Tsetseris, L., Kalfagiannis, N., Logothetidis, S., & Pantelides, S. (2007). Structure and interaction of point defects in transition-metal nitrides. *Phys. Rev. B*, *76*(22), 22410.

Tsetseris, L., & Pantelides, S. (2008). Vacancies, interstitials and their complexes in titanium carbide. *Acta Mater.*, *56*(12), 2864–2871.

Upadhyaya, G. S. (1996). Nature and properties of refractory carbides.

Valeeva, A. A., & Gusev, A. I. (2021). Effect of nonstoichiometry on elastic properties of niobium carbide nbc_y. *International Journal of Refractory Metals and Hard Materials*, *95*, 105435.

Vanderbilt, D. (1990). Soft self-consistent pseudopotentials in a generalized eigenvalue formalism. *Physical Review B*, *41*.

Veprek, S. (1999). The search for novel, superhard materials. *Journal of Vacuum Science & Technology A: Vacuum, Surfaces, and Films*, *17*(5), 2401–2420.

Vocadlo, L., & Dobson, D. P. (1999). The earth's deep interior: advances in theory and experiment. *Philosophical Transactions of the Royal Society of London. Series A: Mathematical, Physical and Engineering Sciences*, *357*, 3335–3357.

Vojvodic, A., & Ruberto, C. (2010). Trends in bulk electron-structural features of rocksalt early transition-metal carbides. *J. Phys. Condens. Matter*, *22*, 375501.

Voter, A. F., & Doll, J. D. (1985). Dynamical corrections to transition state theory for multistate systems: Surface self-diffusion in the rare-event regime. *The Journal of Chemical Physics*, *82*(1), 80–92.

Wade-Zhu, J., Ghosh, S., Claydon, P., & Wu, H. (2015). Contact damage of silicon carbide ceramics with different grain structures measured by hertzian and vickers indentation. *Journal of the European Ceramic Society*, *35*, 1725–1736.

Wang, Wen, Su, Xu, Qu, Zhang, ... Jiang (2009). First principle calculations on the mechanical properties of niobium nitrides. *Solid State Communication*, *149*, 725–728.

Wang, C.-S. (1992). Derivation of the euler equations in thomas-fermi theories of a hot nuclear system. *Phys. Rev. C*, *45*, 1084–1088.

Weber, W. (1973). Lattice dynamics of transition-metal carbides. *Phys. Rev. B*, *8*, 5082.

Wen, M., Hu, C. Q., Wang, C., An, T., Su, Y. D., Meng, Q. N., & Zheng, W. T. (2008). Effects of substrate bias on the preferred orientation, phase transition and mechanical

properties for nbn films grown by direct current reactive magnetron sputtering. *Journal of Applied Physics*, *104*(2), 023527.

Wen, M., Meng, Q., Hu, C., An, T., Su, Y., Yu, W., & Zheng, W. (2009). Structure and mechanical properties of $\delta - nbn/sin_x and \delta' - nbn/sin_x$ nano-multilayer films deposited by reactive magnetron sputtering. *Surf. Coating. Technol*, *203*, 1702–1708.

Wert, C., & Zener, C. (1949). Interstitial atomic diffusion coefficients. *Phys. Rev.*, *76*, 1169–1175.

William D. Callister, D. G. R. (2013). Materials science and engineering: An introduction. *Wiley*, *9th Edition*.

Williams, W. (1998). The thermal conductivity of metallic ceramics. *JOM*, *50*, 62–66.

Wimmer, E., Krakauer, H., Weinert, M., & Freeman, A. (1981). Full-potential self-consistent linearized-augmented-plane-wave method for calculating the electronic structure of molecules and surfaces: O 2 molecule. *Physical Review B*, *24*.

Woodcock, L. (1971). Isothermal molecular dynamics calculations for liquid salts. *Chemical Physics Letters*, *10*, 257–261.

Woodward, C., Asta, M., Trinkle, D. R., Lill, J., & Angioletti-Uberti, S. (2010). Ab initio simulations of molten ni alloys. *Journal of Applied Physics*, *107*, 113522.

Woydt, M., & Mohrbacher, H. (2015). The use of niobium carbide (nbc) as cutting tools and for wear resistant tribosystems. *Int. J. Refract. Met. Hard Mater*, *49*, 212–218.

Wu, Z., Chen, X.-J., Struzhkin, V. V., & Cohen, R. E. (2005). Trends in elasticity and electronic structure of transition-metal nitrides and carbides from first principles. *Phys. Rev. B*, *71*, 214103.

Wu, Z., & Cohen, R. E. (2006). More accurate generalized gradient approximation for solids. *Phys. Rev. B*, *73*, 235116.

Xiao-Jia, C., Struzhkin, V., Wu, Z., Somayazulu, M., Qian, J., Kung, S., ... Hemley, R. (2005). Hard superconducting nitrides.

Xiao Jia, C., Viktor, S., Zhigang, W., Maddury, S., Jiang, Q., Simon, K., ... HoKwang Mao, e. a. (2005). Hard superconducting nitrides. *Proc. Natl. Acad. Sci. Unit. States Am.*, *102*, 3198–3201.

Xing Qiu, C., Haiyang, N., Dianzhong, L., & Yiyi, L. (2011). Modeling hardness of polycrystalline materials and bulk metallic glasses. *Intermetallics*, *19*, 1275–1281.

Xinyu, W., Longke, B., Yong, W., Ying, W., Yonghua, D., & Mingjun, P. (2021). Explorations of electronic, elastic and thermal properties of tetragonal tm4n3 (tm=v, nb and ta) nitrides. *Materials Today Communications*, *26*, 101723.

Yang, Zhen, L., YeHua, J., Rong, Z., & Feng, J. (2014). First principles study the stability and mechanical properties of mc (m= ti, v, zr, nb, hf and ta) compounds. *J. Alloy. Comp.*, *582*, 500–504.

Yang, Q., Lengauer, W., Koch, T., Scheerer, M., & Smid, I. (2000). Hardness and elastic properties of ti($c_x n_{1x}$), $zr(c_x n_{1x}) and hf(c_x n_{1x}$. *Journal of Alloys Compound.*

Yangsheng, Z., & Gregory, S. (1995). A micromechanistic model of microstructure development during the combustion synthesis process. *Journal of Materials Research*, *10*.

Yao, H., Ouyang, L., & Ching, W.-Y. (2007). Ab initio calculation of elastic constants of ceramic crystals. *Journal of the American Ceramic Society*, *90*, 3194–3204.

Yefei, L., Yimin, G., Bing, X., Ting, M., Ying, Y., Shengqiang, M., & Dawei, Y. (2011). The electronic, mechanical properties and theoretical hardness of chromium carbides by first-principles calculations.

Yu, X.-X., Thompson, G., & Weinberger, C. (2015). Influence of carbon vacancy formation on the elastic constants and hardening mechanisms in transition metal carbides. *J. Eur. Ceram. Soc.*, *35*(1), 95–103.

Zaoui, A., Bouhafs, B., & Ruterana, P. (2005). First-principles calculations on the electronic structure of ticxn1, zrxnb1 - xc and hfcxn1- x alloys. *Mater. Chem. Phys.*, *91*, 108–115.

Zhang, Balasubramanian, Ozsdolay, Mulligan, Khare, Zheng, & Gall. (2015). Epitaxial nbc_xn_{1-x}(001) layers: growth, mechanical properties, and electrical resistivity. *Surf. Coating. Technol.*, *277*, 136–143.

Zhang, Balasubramanian, Ozsdolay, Mulligan, Khare, Zheng, & Gall. (2016). Growth and physical properties of epitaxial nbn(001) films on mgo(001). *Surf. Coating. Technol.*, *288*, 105–114.

Zhang, Sheng, S. H., & Veprek, S. (2007). First principles studies of ideal strength and bonding nature of aln polymorphs in comparison to tin. *Applied Physics Letters*, *91*(3), 031906.

Zhao, X., Togaru, M., Guo, Q., Weinberger, C. R., Lamberson, L., & Thompson, G. B. (2019). Carbon influence on fracture toughness of niobium carbides. *Journal of the European Ceramic Society*, *39*(16), 5167-5173.

Zhen, W., Hirotaka, T., Akira, K., & Yoshinori, U. (1999). Interface and tunneling barrier heights of nbn/aln/nbn tunnel junctions. *Applied Physics Letters*, *75*(5), 701–703.

Zhen-Hua, W., Xiao-Yu, K., Xiao-Fen, H., Peng, L., & Ai-Jie, M. (2011). Pressure-induced structural transition and thermodynamic properties of nbn and effect of metallic bonding on its hardness. *EPL (Europhysics Letters)*, *92*, 56002.

Zhi, X., Xing, J., Fu, H., & Xiao, B. (2008). Effect of niobium on the as-cast microstructure of hypereutectic high chromium cast iron. *Mater. Lett.*, *62*, 857–860.

Zhigang, W., Xiao-Jia, C., Viktor, V., & Ronald, C. (2008). Trends in elasticity structure of transition-metal nitrides and carbides from first principles. *Geophysical Laboratory*, *2*.

Zou, Y., Wang, X., Chen, T., Li, X., Qi, X., Welch, D., ... Li, B. (2015). Hexagonal-structured-nbn:ultra-incompressibility, high shear rigidity, and a possible hard superconducting. *Mater. Scientific Rep.*, *5*, 10811.

Šimůnek, A., & Vackář, J. (2006). Hardness of covalent and ionic crystals: First-principle calculations. *Physical review letters*, *96*(8), 85501.

APPENDIX I

6.3 STRUCTURAL OPTIMIZATION

The structures of both Niobium Carbide as well as Niobium Nitride in rocksalt, zincblende and wurzite crystal structures were optimized. The optimization helped in obtaining an accurate model of the ground state structure. A certain procedure was involved which included optimizing the Monkhorst-Pack grid, the plane wave kinetic energy together with the lattice parameter of the materials in that order.

6.3.1 K-POINT OPTIMIZATION IN ROCKSALT, ZINCBLENDE AND WURZITE

Optimized values of k-points were obtained by selecting the most favourable measurements of the Monkhorst-Pack grid of the k-points Pack & Monkhorst (1977). Here, the accuracy as well as computational tractability acted as the steering factor in the range chosen. Figures A.1-A.6 represent the optimized values of k-point for each compound in the different structures.

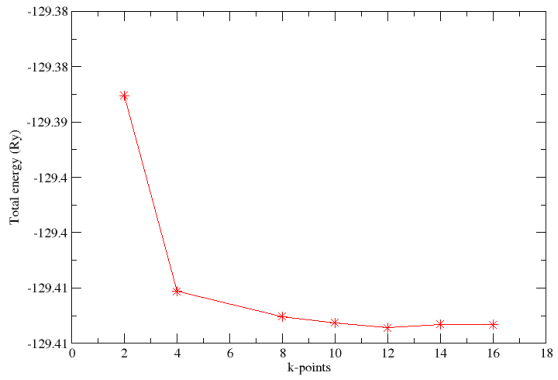

(a) RS crystal structure

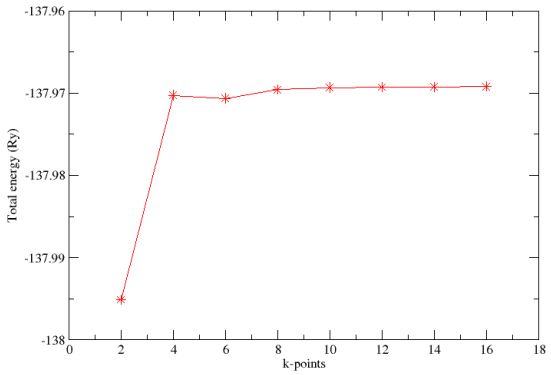

(b) RS crystal structure

Figure 6.3.1: K-point optimization for Niobium Carbide together with Niobium Nitride in rocksalt crystal structure

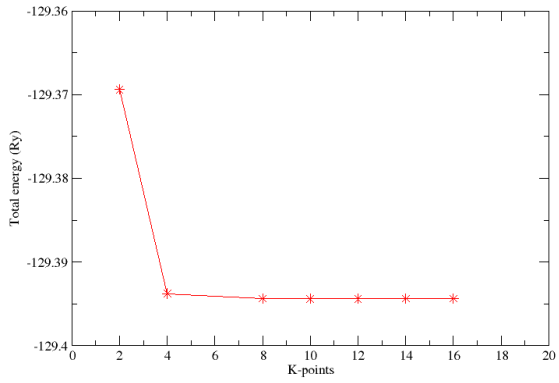

(a) ZB crystal structure

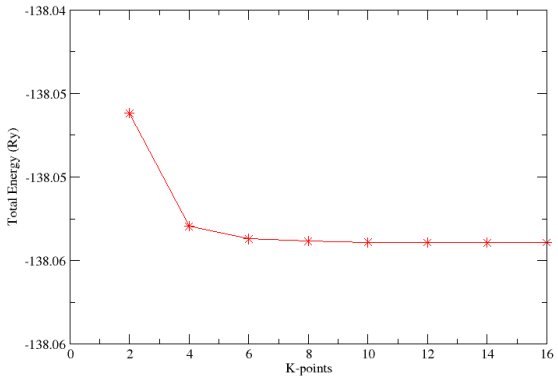

(b) ZB crystal structure

Figure 6.3.2: K-point optimization for Niobium Carbide together with Niobium Nitride in zincblende crystal structure

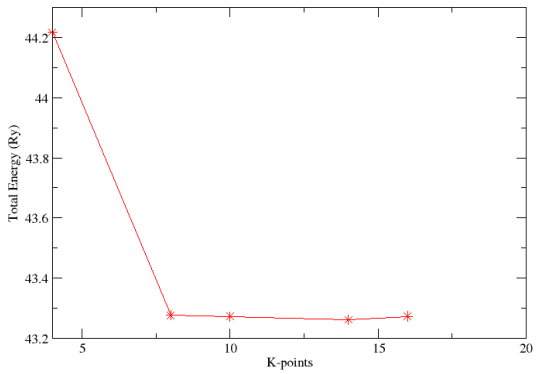

(a) WZ crystal structure

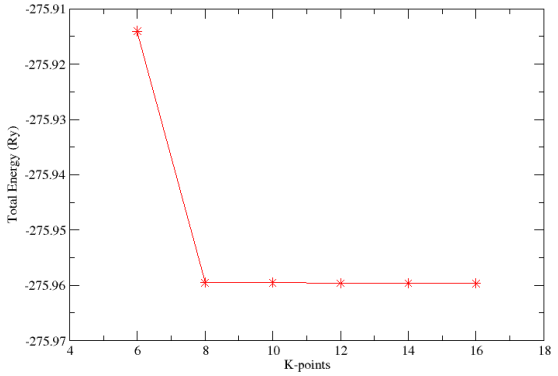

(b) WZ crystal structure

Figure 6.3.3: K-point optimization for Niobium Carbide and Niobium Nitride in wurzite crystal structure

Upon the integration over the Brillouin zone using Monkhorst and Pack mesh Pack & Monkhorst (1977), a grid of 11 x 11x 11 was chosen for RS and ZB crystal structures and a grid of 10 x 10 x 5 for the WZ structures.

6.3.2 PLANE WAVE ENERGY OPTIMIZATION IN ROCKSALT, ZINCBLENDE AND WURZITE

After optimizing the k-points of the two compounds, it was also necessary to obtain the value of the optimized plane wave cut off energy. The representations here show the behavior of the plane wave cut-off energy with total energy of the system.

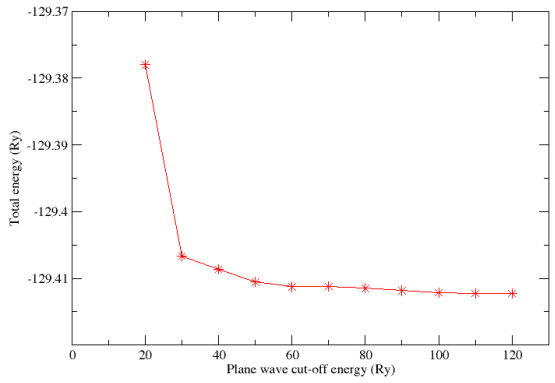

(a) RS crystal structure

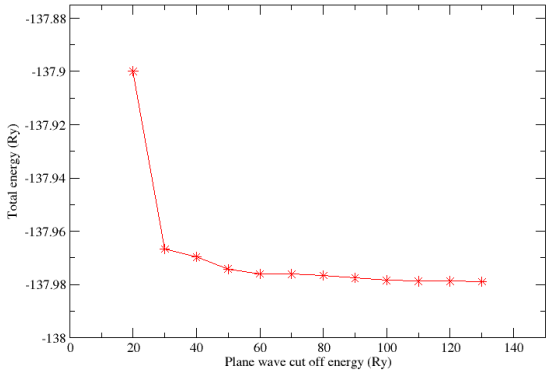

(b) RS crystal structure

Figure 6.3.4: Plane wave energy cut-off optimization for Niobium Carbide together with Niobium Nitride in rocksalt crystal structure

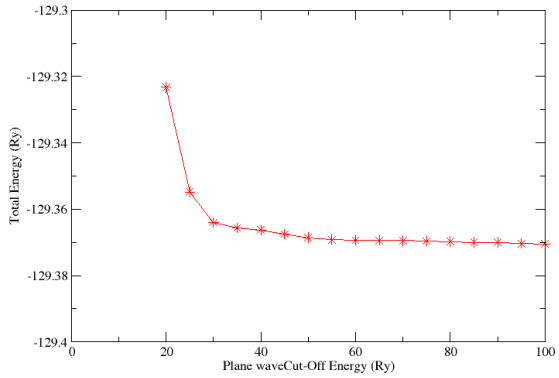

(a) ZB crystal structure

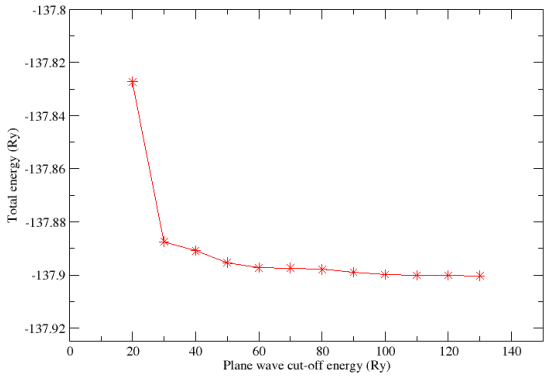

(b) ZB crystal structure

Figure 6.3.5: Plane wave energy cut-off optimization for Niobium Carbide together with Niobium Nitride in zincblende crystal structure

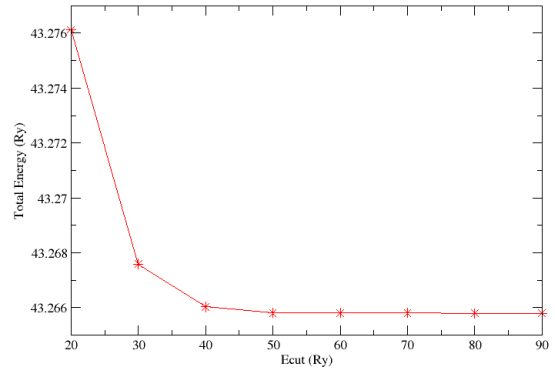

(a) WZ crystal structure

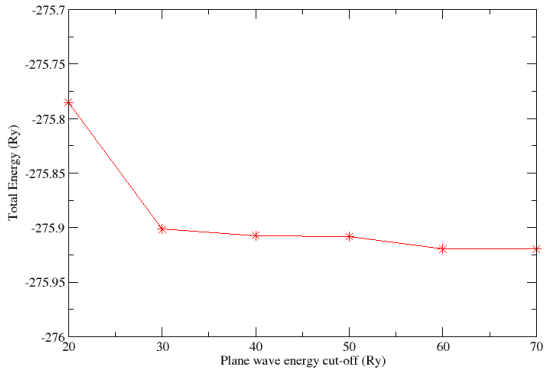

(b) WZ crystal structure

Figure 6.3.6: Plane wave energy cut-off optimization for Niobium Carbide together with Niobium Nitride in wurzite crystal structure

The optimization of the kinetic energy of the plane wave gave an optimized value of 60 Rydberg for both NbC as well as NbN.

6.3.3 LATTICE PARAMETER OPTIMIZATION IN ROCKSALT AND ZINCBLENDE

Optimization of the lattice parameter was performed with an aim of finding the equilibrium value. The calculations were performed in the ground state for Niobium Carbide and Nibium Nitride.

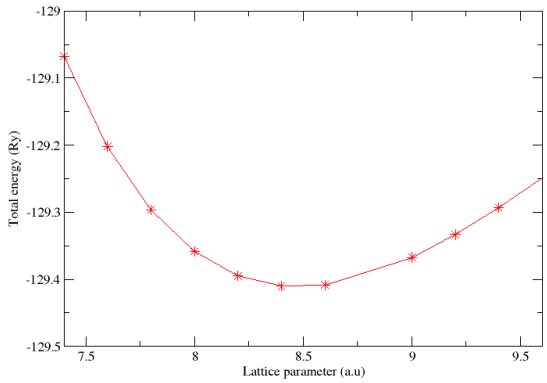

(a) RS crystal structure

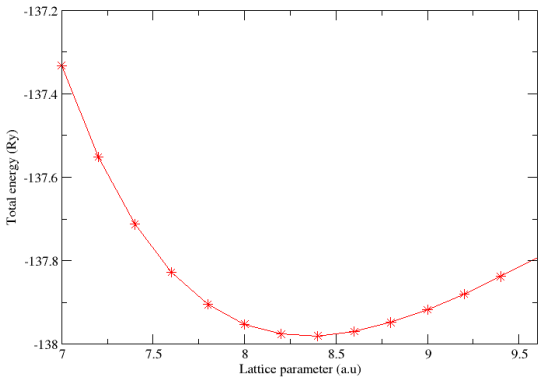

(b) RS crystal structure

Figure 6.3.7: Lattice parameter optimization for Niobium Carbide together with Niobium Nitride in rocksalt crystal structure

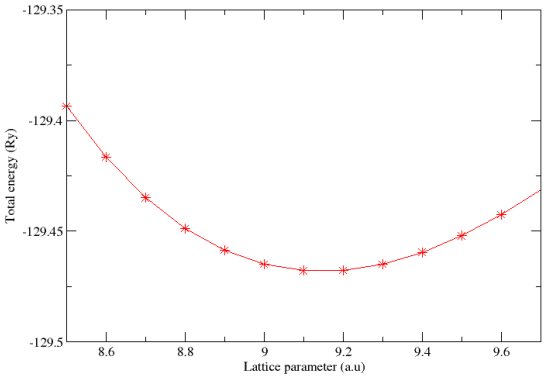

(a) ZB crystal structure

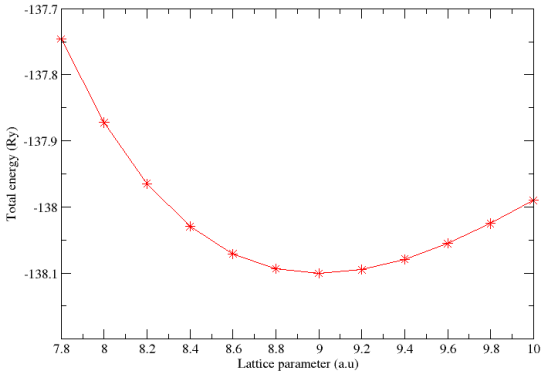

(b) ZB crystal structure

Figure 6.3.8: Lattice parameter optimization for Niobium Carbide as well as Niobium Nitride in zincblende crystal structure

APPENDIX II

6.4 EFFECTS OF TEMPERATURE ON THE MECHANICAL PROPERTIES OF NIOBIUM CARBIDE AND NIOBIUM NITRIDE

6.4.1 Elastic constants of Niobium Carbide together with Niobium Nitride at high temperature

Table 6.1: Calculated elastic constants of Niobium Carbide in rocksalt, zincblende and wurzite crystal structures between zero and 1500 K

Structure	Temperature K	$C_{11} GPa$	$C_{12} GPa$	$C_{13} GPa$	$C_{33} GPa$	$C_{44} GPa$
$NbC_{0.75}(RS)$	0	580.25	114.65			170.50
	300	475.84	144.89			128.31
	500	447.37	140.65			125.43
	1000	430.92	97.83			119.90
	1500	385.16	64.25			107.12
$NbC_{0.84375}(RS)$	0	549.80	132.79			149.68
	300	516.23	136.27			144.14
	500	494.92	149.82			137.93
	1000	547.62	130.29			149.23
	1500	489.13	105.60			124.12
$NbC_{0.875}(RS)$	0	549.33	131.71			146.32
	300	355.21	145.31			145.46
	500	469.06	121.97			156.81
	1000	453.60	124.21			133.22
	1500	434.81	124.52			125.56
$NbC_{0.9375}(RS)$	0	512.47	154.49			139.96
	300	527.94	127.43			147.74
	500	499.81	117.47			144.96
	1000	503.22	120.23			142.05
	1500	351.08	90.26			131.71
$NbC_{0.75}(ZB)$	0	296.30	179.04			44.53
	300	374.23	188.34			64.39
	500	285.99	111.10			34.22
	1000	249.00	105.53			30.04
	1500	204.24	96.49			24.18
$NbC_{0.84375}(ZB)$	0	255.21	178.03			49.91
	300	236.95	135.13			71.91

	500	236.85	135.20			71.93
	1000	230.79	134.90			61.81
	1500	213.59	117.60			45.62
$NbC_{0.875}(ZB)$	0	193.96	87.66			62.05
	300	374.23	188.34			64.39
	500	285.99	111.10			142.16
	1000	265.25	64.60			115.28
	1500	227.75	58.87			53.051
$NbC_{0.9375}(ZB)$	0	264.26	157.24			68.80
	300	178.58	83.69			22.40
	500	274.96	141.82			138.36
	1000	235.58	172.23			11.77
	1500	120.28	62.12			66.41
$NbC_{0.75}(WZ)$	0	500.57	189.45	95.39	799.52	214.12
	300	548.04	113.35	94.84	624.68	128.92
	500	438.23	197.29	101.85	570.39	127.49
	1000	483.21	154.99	63.58	461.23	51.48
	1500	328.48	95.74	127.03	365.53	73.03
$NbC_{0.84375}(WZ)$	0	670.35	224.71	135.19	620.31	210.46
	300	535.65	215.94	219.97	411.73	109.23
	500	370.30	132.71	127.13	420.31	110.46
	1000	375.29	138.95	133.41	420.09	115.06
	1500	342.43	121.44	110.7	382.45	98.45
$NbC_{0.875}(WZ)$	0	654.87	183.19	139.17	906.51	268.80
	300	420.07	111.58	107.79	419.52	90.54
	500	397.68	110.38	114.05	419.77	97.03
	1000	471.20	172.27	104.36	391.69	90.45
	1500	327.98	124.31	78.24	370.94	79.23
$NbC_{0.9375}(WZ)$	0	602.30	218.53	83.69	798.12	209.23
	300	550.41	159.63	184.22	648.54	186.25
	500	462.44	143.33	65.43	368.71	144.43
	1000	409.20	65.68	57.20	407.57	126.97
	1500	417.68	127.11	157.25	391.59	90.55

Table 6.2: Calculated elastic constants of Niobium Nitride in rocksalt, zincblende and wurzite crystal structures between zero and 1500 K

Structure	Temperature K	$C_{11} GPa$	$C_{12} GPa$	$C_{13} GPa$	$C_{33} GPa$	C_{44}
$NbN_{0.75}(RS)$	0	645.60	138.62			53.96
	300	575.15	104.58			53.43
	500	520.54	102.82			48.98
	1000	463.20	120.82			40.07
	1500	422.12	88.44			36.08
$NbN_{0.84375}(RS)$	0	667.80	177.70			106.08
	300	638.31	196.00			111.94
	500	564.87	189.70			97.47
	1000	351.10	192.06			88.85
	1500	246.42	186.56			85.06
$NbN_{0.875}(RS)$	0	501.21	138.71			86.891
	300	576.15	138.39			129.20
	500	407.08	144.35			126.31
	1000	495.55	144.46			85.53
	1500	318.14	99.08			24.06
$NbN_{0.9375}(RS)$	0	520.59	149.37			42.15
	300	387.40	137.05			124.38
	500	493.88	171.72			131.37
	1000	464.95	120.06			96.75
	1500	378.47	118.30			53.33
$NbN_{0.75}(ZB)$	0	98.61	65.86			60.68
	300	67.33	46.21			55.53
	500	73.48	40.30			49.54
	1000	82.76	70.39			36.39
	1500	61.49	38.53			34.19
$NbN_{0.84375}(ZB)$	0	256.85	157.42			78.18
	300	233.18	150.70			77.33
	500	231.06	162.20			40.62
	1000	185.84	107.21			69.83
	1500	115.59	98.38			54.27
$NbN_{0.875}(ZB)$	0	271.58	154.66			77.32
	300	263.06	138.01			81.33
	500	245.42	147.26			65.60
	1000	228.36	130.74			52.52
	1500	199.48	112.90			45.84

$NbN_{0.9375}(ZB)$	0	258.01	110.92			32.46
	300	270.59	144.34			81.84
	500	269.99	150.60			81.20
	1000	221.84	103.04			41.93
	1500	201.46	112.38			38.17
$NbN_{0.75}(WZ)$	0	381.81	217.71	155.50	534.70	84.66
	300	436.94	207.47	124.15	481.89	76.38
	500	419.88	194.47	166.63	534.32	110.09
	1000	400.43	181.28	143.52	465.56	109.96
	1500	387.49	91.04	130.47	500.65	112.96
$NbN_{0.84375}(WZ)$	0	439.40	223.74	170.40	607.82	105.98
	300	432.29	204.87	174.32	599.79	115.00
	500	453.38	216.45	173.03	618.53	116.90
	1000	385.86	175.92	159.68	525.88	105.60
	1500	388.59	83.00	196.95	611.42	101.86
$NbN_{0.875}(WZ)$	0	435.10	237.34	162.83	621.63	90.02
	300	411.97	225.55	147.34	621.70	101.20
	500	444.17	253.58	162.68	634.71	94.32
	1000	447.45	249.31	162.49	636.37	100.47
	1500	443.25	255.27	163.29	640.57	95.44
$NbN_{0.9375}(WZ)$	0	517.86	273.06	167.62	805.47	115.52
	300	515.62	273.73	167.14	811.27	117.74
	500	468.80	240.82	153.71	697.00	121.40
	1000	488.38	264.48	161.86	731.80	103.36
	1500	369.57	104.40	84.15	490.55	107.86

6.4.2 Vacancy migration energies

Table 6.3: Calculated vacancy migration energies (eV/atom) of C/N for NbC as well as NbN in three crystal structures namely, rocksalt, zincblende and wurzite with different vacancy concentrations

Defect concentration %	NbC RS	NbC ZB	NbC WZ	NbN RS	NbN ZB	NbN WZ
1.560	2.8876	0.97041		2.09250	1.14119	
2.080	6.0708	0.89066	1.4673	2.08907	1.06925	2.03192
3.125	1.9639	0.68216	0.6994	0.79959	0.64569	0.68256
4.160	1.8249	0.56164	0.45875	2.14876	0.57699	0.27081
6.250			0.73988			0.50216
8.330			0.25922			0.22495

APPENDIX III

6.4.3 PSEUDOPOTENTIALS

```
<PP_INFO>
Generated using Vanderbilt code, version   7  3  4
Author: unknown    Generation date:    4    3    5
Automatically converted from original format
    0        The Pseudo was generated with a Non-Relativistic Calculation
  1.00000000000E+00    Local Potential cutoff radius
nl pn  l   occ               Rcut            Rcut US             E pseu
2S  2  0  2.00     10.00000000000      1.10000000000     -1.00978244769
2P  2  1  2.00     10.00000000000      1.10000000000     -0.38870429969
</PP_INFO>


<PP_HEADER>
   0                  Version Number
  C                   Element
   US                 Ultrasoft pseudopotential
    F                 Nonlinear Core Correction
 SLA  PW   PBE  PBE    PBE  Exchange-Correlation functional
   4.00000000000      Z valence
  -10.72515811861     Total energy
  0.0000000  0.0000000 Suggested cutoff for wfc and rho
    1                 Max angular momentum component
  721                 Number of points in mesh
    2    4            Number of Wavefunctions, Number of Projectors
 Wavefunctions        nl  l   occ
                      2S  0  2.00
                      2P  1  2.00
</PP_HEADER>


<PP_MESH>
  <PP_R>
  0.00000000000E+00  7.06180151333E-06  1.42443146680E-05  2.15496028610E-05
  2.89797647603E-05  3.65369349077E-05  4.42232843318E-05  5.20410211722E-05
  5.99923913133E-05  6.80796790299E-05  7.63052076433E-05  8.46713401887E-05
```

Figure 6.4.1: Carbon Pseudopotential

```
<PP_INFO>
Generated using Vanderbilt code, version   7  3  5
Author: unknown    Generation date:    9    6 2004
Automatically converted from original format
    1        The Pseudo was generated with a Scalar-Relativistic Calculation
  1.80000000000E+00    Local Potential cutoff radius
nl pn  l   occ               Rcut            Rcut US             E pseu
4S  4  0  2.00     10.00000000000      1.80000000000     -4.29170630695
4P  4  1  6.00     10.00000000000      2.00000000000     -2.53726946229
4D  4  2  4.00     10.00000000000      2.20000000000     -0.22346874833
5S  5  0  1.00     10.00000000000      1.80000000000     -0.29266359077
5P  5  1  0.00     10.00000000000      2.00000000000     -0.08163975362
</PP_INFO>


<PP_HEADER>
   0                  Version Number
  Nb                  Element
   US                 Ultrasoft pseudopotential
    T                 Nonlinear Core Correction
 SLA  PW   PBE  PBE    PBE  Exchange-Correlation functional
   13.00000000000     Z valence
 -117.18509514438     Total energy
  0.0000000  0.0000000 Suggested cutoff for wfc and rho
    2                 Max angular momentum component
  887                 Number of points in mesh
    5    6            Number of Wavefunctions, Number of Projectors
 Wavefunctions        nl  l   occ
                      4S  0  2.00
                      4P  1  6.00
                      4D  2  4.00
                      5S  0  1.00
                      5P  1  0.00
</PP_HEADER>
```

Figure 6.4.2: Niobium Pseudopotential

```
<PP_INFO>
Generated using Vanderbilt code, version   7  3  4
Author: unknown    Generation date:    4    3    5
Automatically converted from original format
    0        The Pseudo was generated with a Non-Relativistic Calculation
  1.00000000000E+00    Local Potential cutoff radius
nl pn  l   occ               Rcut            Rcut US             E pseu
2S  2  0  2.00     10.00000000000      1.10000000000     -1.36393068723
2P  2  1  3.00     10.00000000000      1.10000000000     -0.52143879723
</PP_INFO>


<PP_HEADER>
   0                  Version Number
  N                   Element
   US                 Ultrasoft pseudopotential
    F                 Nonlinear Core Correction
 SLA  PW   PBE  PBE    PBE  Exchange-Correlation functional
    5.00000000000     Z valence
  -19.30116713812     Total energy
  0.0000000  0.0000000 Suggested cutoff for wfc and rho
    1                 Max angular momentum component
  729                 Number of points in mesh
    2    4            Number of Wavefunctions, Number of Projectors
 Wavefunctions        nl  l   occ
                      2S  0  2.00
                      2P  1  3.00
</PP_HEADER>


<PP_MESH>
  <PP_R>
  0.00000000000E+00  6.05297272571E-06  1.22094125726E-05  1.84710881666E-05
  2.48397983660E-05  3.13173727780E-05  3.79056722844E-05  4.46065895761E-05
  5.14220496971E-05  5.83540105970E-05  6.54044636943E-05  7.25754344475E-05
```

Figure 6.4.3: Nitrogen Pseudopotential

APPENDIX IV

6.5 PUBLICATIONS, CONFERENCE PRESENTATIONS AND SCHOOLS ATTENDED

6.5.1 Publications

1. Muchiri, P.W., Mwalukuku, V.M., Korir, K.K., Amolo, G.O., & Makau, N.W. (2019). Hardness characterization parameters of Niobium Carbide and Niobium Nitride: A first principles study. *Materials Chemistry and Physics, 229,* 489-494.

2. Muchiri, P., Korir, K., Makau, N., Amolo, G. (2022). The impact of an-ionic vacancies on the mechanical properties of NbC and NbN:*An ab initio* study. Computational Materials Science, 203 , 111113.

6.5.2 Conferences and Schools Attended

1. African Physical Society (AfPS) International Conference, online, 18^{th}-20^{th}, Nov, 2020. 2. 20th International Workshop on Computational Physics and Materials Science: Total Energy and Force Methods, online, 23^{rd}-25^{th} Feb, 2021.

3. MaX School on Advanced Materials and Molecular Modelling with Quantum ESPRESSO, online, 17^{th}-28^{th} May, 2021.

6.5.3 Poster presentations

1. P.W. Muchiri, K.K. Korir, G.O.Amolo & N.W. Makau, poster titled: Comprehensive study on the mechanical and structural properties of Niobium Carbide and Niobium Nitride. Poster presented during the US-Africa Initiative Workshop, online, 14^{th}-18^{th} June, 2021.